L-Università ta' Malta
Faculty of Engineering

MASTER OF SCIENCE IN ENGINEERING DISSERTATION

Exploitation of EEG-Extracted Eye Movement for a Hybrid SSVEP Home Automation System

JEANLUC MANGION

Supervised by:

PROF. ING. KENNETH CAMILLERI

Co-supervised by:

DR TRACEY CAMILLERI

A dissertation submitted in partial fulfilment of the requirements for the degree of Master of Science in Engineering

by the

Faculty of Engineering

October 2020

L-Università ta' Malta
Faculty of Engineering

Copyright Notice

1) Copyright in text of this dissertation rests with the Author. Copies (by any process) either in full, or of extracts may be made only in accordance with regulations held by the Library of the University of Malta. Details may be obtained from the Librarian. This page must form part of any such copies made. Further copies (by any process) made in accordance with such instructions may not be made without the permission (in writing) of the Author.

2) Ownership of the right over any original intellectual property which may be contained in or derived from this dissertation is vested in the University of Malta and may not be made available for use by third parties without the written permission of the University, which will prescribe the terms and conditions of any such agreement.

3) Publication rights over the academic and/or research results presented in this dissertation are vested jointly in both the Author and his/her academic Supervisor(s), and unless such rights are explicitly waived in writing, both parties must be listed among the authors in any academic publication that is derived substantially from this work. Furthermore, any other public communication / disclosure of any form that focuses on the project must acknowledge that this work has been carried out by the Author and the Supervisor(s) (named explicitly) through the University of Malta.

Dedicated to my parents, my brother and my love.

Their patience and love knows no bounds.

Abstract

Brain-computer interface (BCI) systems allow a direct communication between a user and a computer using only brain activity. BCIs convert electrical neurosignals, recorded through electroencephalography (EEG), into actual commands to operate a software application or a device. Among the various neurophysiological phenomena that can be used to drive BCI systems, steady state visual evoked potentials (SSVEPs) have demonstrated the highest performance for BCI systems. The flickering stimuli required by these systems tend to be annoying for the user and the accuracy of SSVEP-based BCIs tends to also decrease as the number of flickering stimuli increases. To address these issues, the project aims to extract EEG potentials related to eye movements to estimate the point of gaze of the user when looking at the stimuli and hence obtain a broad idea of the stimulus the user is focusing on. This information will be used such that stimuli which are far from the user's point of gaze can be switched off prior to the flickering of the stimuli. This reduces the number of simultaneously flickering stimuli which should improve both the annoyance factor and the classification accuracy.

To test out this hypothesis, an offline study is conducted to investigate what type of eye-movement can be reliably detected from EEG and how the number of frontal channels considered and size of the training set influences the detection of eye-movements. Results have shown that a 99% accuracy is achieved when discriminating between horizontal and vertical eye-movements with three frontal channels and with 16 training trials. Subsequently a real-time hybrid BCI (hBCI) which fuses SSVEPs with EEG-based eye-movement potentials is developed. A smart home system is designed and integrated with an SSVEP-based BCI and also with the developed hBCI. A comparative analysis is conducted to evaluate the differences between the two systems and significant differences in accuracy and efficiency were found between the two. A 72.8% accuracy, an 82.4% efficiency and an ITR of 28.6bpm are achieved by the proposed hBCI whereas a 61.5% accuracy, a 74% efficiency and an ITR of 27.6bpm are achieved by the SSVEP-based BCI.

Acknowledgements

First and foremost, I would like to express my sincere gratitude to my supervisor Prof. Ing. Kenneth Camilleri for his continuous support, patience and encouragement. His enthusiasm, expertise and motivations has inspired me and helped me overcome all the challenges encountered throughout the process of this dissertation.

I also wish to extend my appreciation to my co-supervisor Dr.Tracey Camilleri for her suggestions. Her expertise and immense knowledge within the field of signal processing has helped me to overcome the numerous obstacles faced during this project.

I am also grateful to those individuals who dedicated a portion of their time to participate in this study.

Finally, I would like to thank my parents, my brother and Denise, who unconditionally believed in me even when I myself failed to do so. They stood by me through thick and thin and their continuous words of encouragement inspired me to hold on until the end.

Contents

List of Figures

List of Tables

List of Abbreviations

AC Air conditioning

API Application Programming Interface

AR Autoregressive

BCI Brain Computer Interface

BMI Brain Machine Interface

bpm bits per minute

CCA Canonical Correlation Analysis

CI Conceptual Imagery

CSP Common Spatial Patterns

CWT Continuous Wavelet Transform

DC Direct Current

EEG Electroencephalogram

EMD Extended Moving Difference

EMG Electromyography

EOG Electrooculography

ERD Event Related Desynchronisation

ERP Event Related Potential

FBCCA Filter Bank Canonical Correlation Analysis

fMRI functional Magnetic Resonance Imaging

fNIRS functional Near-Infrared Spectroscopy

FoA Focus of Foveal Attention

GUI Graphical User Interface

hBCI hybrid Brain Computer Interface

HCI Human Computer Interface

HMM Hidden Markov Model

ICA Independent Component Analysis

IEEE Institute of Electrical and Electronic Engineers

IIR Infinite Impulse Response

IOT Internet of Things

IR Infrared

ITR Information Transfer Rate

LAN Local Area Network

LCD Liquid Crystal Display

LED Light Emitting Diode

MEG Magnetoencephalography

MI Motor Imagery

MRI Magnetic Resonance Imaging

NN Neural Network

PC Personal Computer

PET Positron Emission Tomography

QR Quick Response

RF Radio Frequency

SDRAM Synchronous Dynamic Random Access Memory

SSVEP Steady State Visually Evoked Potential

SVM Support Vector Machine

TCP Transmission Control Protocol

TV Television

UDP User Diagram Protocol

VOG Videooculography

VR Virtual Reality

1 Introduction

1.1 Background

Smart homes offer its occupants an alternative way of living. This is because, in contrast with traditional homes, they typically include a home automation system that encompasses a centralised environment where devices are connected to a central component, referred to as the hub. Generally a microcomputer or a mini network server acts as the central hub within such a system. Personal computers, tablets or even smartphones act as access points on the smart home network.

These electronic devices do not handle the back-end operations ongoing behind the screen of a smart home network. They merely act as front-end devices presenting the user with an interface to control the smart home environment. Hence this enables the occupants of the smart home to control every device connected to the home network from a single point, making every device operable from the grasp of their hands. Despite offering comfort to its users, home automation systems can offer more independence to patients with severe mobility impairment. However, even with a home automation system, users might still encounter issues to operate the system, should they lack fine motor skills as a consequence of their medical condition. This interface might not be suitable for everyone so an alternative means of control is necessary.

Brain Computer Interfaces (BCIs), also referred to as Brain Machine Interfaces (BMIs), is a growing research area which offers an alternative way to operate an electronic device. BCIs enhance the interaction with the computer as they allow human neural activity to act as a control signal and directly control electronic devices such as personal computers and tablets. Several studies over the past years have shown that non-invasive neural activity can actually replace traditional and conventional means of computer interaction, allowing users to re-

frain from using any muscular activity.

The main purpose behind BCI research is to provide an alternative means of communication for patients with severe mobility impairment. Such an interface can help in improving the quality of life of such patients. Moreover it can ease the emotional pain and frustration, caused by the inability to interact with others through conventional means. BCIs rely on the continuous monitoring of one's brain activity typically using electroencephalography.

Since they are both advantageous to patients with severe neuromuscular disability, smart homes and BCIs can be integrated with each other, offering the opportunity of a partially independent lifestyle for these individuals. A smart home caters for a direct link between a single computer and the rest of the home network environment, while a BCI provides a direct link between the computer and the human brain. Hence, a smart home BCI allows the direct control of the smart devices in a home using brain signals

Among the various neurophysiological phenomena that can be used to drive BCI systems, the most reliable type of BCI is that based on steady-state visually evoked potentials (SSVEPs). SSVEPs are a reaction within one's neural activity, caused by exposure of one's visual system to stimuli flickering at a specific frequency. This reaction exhibits an oscillatory activity, mainly in the occipital region, matching the frequency of the flickering stimuli and its harmonics. In an SSVEP-based BCI, various stimuli flickering at specific frequencies, are presented to the user, with each stimulus corresponding to a particular command. The user selects a command by focusing on the corresponding stimulus. Further stimuli within a BCI interface provides the user with more control options, however this also increases the annoyance factor of the system. To address this problem, it is hypothesized that EEG potentials related to eye-movements can be extracted to estimate the user's point of gaze, which information can then be used to simplify the BCI menu by flickering only those stimuli in the area enclosing the user's

point of gaze.

1.2 Objectives of the Dissertation

The aim of this dissertation is to design and implement a smart home BCI. The BCI will be of a hybrid architecture and will employ a system based on Steady State Visual Evoked Potentials (SSVEPs) fused with EEG-based eye-movement potentials. Thus signal processing algorithms that can reliably classify eye-movement EEG potentials must be identified. The complete smart home hybrid BCI should be practical, efficient and provide a reliable performance. On completion of the development of the smart home hybrid BCI system, experimental sessions are to be conducted on several subjects. These will be used to compare between a smart home SSVEP-based BCI and a smart home hybrid BCI. In view of these aims, the specific objectives of this work can be summarised as follows:

1. Investigate the extent to which eye-movements may be classified reliably using EEG electrodes. As part of this investigation, the following particular questions are addressed:
    - How many directional eye-movements can be reliably classified?
    - To what extent can eye-movements be detected from the occipital region and from the frontal brain region?
    - To what extent can eye-movements in the same direction but different visual angles, be distinguished?
    - How does the classification accuracy vary with the number of EEG frontal channels used?
    - How does the classification accuracy vary with the size of the training set?

2. Design and implement a real-time smart home BCI application based on two different architectures: a standard SSVEP-based architecture and a hybrid one which fuses SSVEPs with EEG-based eye-movement potentials. These two architectures are to be tested with several subjects to assess whether the hybrid BCI approach provides any benefits over and above the standard SSVEP approach typically found in the literature [90] [27].

1.3 Layout of the Dissertation

Chapter 2 presents an overview on home automation systems and on the neuroimaging technologies used for brain signal acquisition. It also gives an introduction to various EEG-based BCI systems.

Chapter 3 presents a comprehensive literature review which was carried out to explore the various signal processing techniques used to extract eye-movement information from EEG data. Furthermore it gives a thorough review on smart home BCIs which have been implemented so far.

Chapter 4 describes the methodology used for the EEG-based eye-gaze offline analysis. It also gives a detailed explanation of the signal processing algorithms used. The experimental protocols for the data acquisition session are also presented. Furthermore, the chapter presents the results which were obtained from the analysis and discusses them while highlighting the conclusions drawn.

Chapter 5 describes the design and implementation of a real-time smart home BCI for an SSVEP-based and hybrid architectures. The experimental procedures by which the comparative analysis between the different systems was carried out, are also described. Furthermore, the chapter presents the results of the comparative analysis which compared the the smart home hybrid BCI with the smart home SSVEP-based BCI. A discussion of the results then follows highlighting the conclusions drawn from the results.

Chapter 6 summarizes the work done and the main results obtained during this project. It concludes the dissertation and gives suggestions for future work.

2 A General Overview of Home Automation Systems and BCIs

This chapter gives an overview on home automation systems. It describes the main components which make up a typical system and the various communication protocols used. It also discusses the interfaces employed within home automation systems to engage with the user and how BCIs can aid motor-impaired smart home users. This is followed by an overview on BCIs describing the various neuroimaging techniques which can be used to record brain activity. The chapter subsequently focuses on EEG-based systems describing the various modalities for brain signal acquisition.

2.1 Home Automation Systems

Many may think that the concept of a smart home is quite recent. However early forms of home automation were conceived in the early 20^{th} century. Home automation began with labour-saving machines consisting of gas or electrically powered home appliances. These were introduced to the market as soon as homes started to be connected to the electrical power distribution network [31]. Home automatons were then incorporated into a system by the development of the first home automation network communication protocol in 1975 [81]. Since then, home automation systems, or domotic systems, have been developed into various forms and can be categorised into three generations in accordance with Li *et al.*[61]:

- 1^{st} Generation: Devices communicating with a network server acting as a central hub
- 2^{nd} Generation: Artificial intelligence integrated with the smart home technology
- 3^{rd} Generation: 'Personification' of domotic artificial intelligence through the integration of service robots

Despite the numerous forms that a domotic system can take today, a home automation system makes use of various sensors and actuators to automatically monitor and operate home appliances. Such a system facilitates the operation of such appliances, making life comfortable for the occupants in the smart home. Sensors and actuators are vital components in a domotic system [39]. Sensors receive information about the current status of devices or climate conditions and send this information to the central hub. This hub acts as the processing unit of the smart home, catering for all the decision-making and instruction handling. Such a hub may take the form of a network server or a computer. Acting accordingly on the information received from the sensors, the hubs sends relevant instructions to the actuators which in turn execute them [100].

Communication between the smart home devices may take place on different media. Early domotic systems made use of wiring systems in order to convey the message from a device to the hub [49]. Although a small portion of current smart homes still make use of wires to carry information, most domotic systems today utilise wireless communication protocols to transmit information from one place to another [7]. Information may be transmitted along infrared signals, radio-frequency bands and also WiFi communication links.

Another important aspect of communication within a home automation system is the interaction between the user and the system. The user interface is the central feature of any home automation system allowing the user to control numerous different devices from a centralised location. User interfaces vary in complexity according to the variety of devices or appliances controllable by the system. [91]. In some environments, a more complicated interface is required to provide a wide range of commands to the user, possibly including BCI technology to provide the motor-impaired user with a suitable means of communication.

2.2 Brain Computer Interfaces

As the name implies, a Brain-Computer-Interface (BCI) is a system in which a user can communicate with a computer using only his brain signals. A BCI can be implemented in various ways but in general it always involves three steps. First, brain signals are acquired from the subject. They are then processed and interpreted by the processing unit of the BCI. Lastly, commands are executed according to the interpretation of the brain signals.

BCIs can either be non-invasive or invasive [69]. Invasive BCIs require a neurosurgery, during which electrodes are implanted directly into the brain. This ensures a high signal quality at the expense of a complex procedure with possible contingencies, like for instance, the formation of scar tissues. As the body reacts to the alien objects within, it forms a scar around the electrodes reducing the signal quality [83]. On the other hand, non-invasive BCIs detect neural activity without the need of any surgical intervention. The next sections will discuss the different modalities for brain signal acquisition, electroencephalography (EEG) and its standard electrode placement, and EEG-based BCI systems.

2.2.1 Neuroimaging Technologies for Brain Signal Acquisition

Neural activity may be detected from its electric, magnetic or metabolic nature. The magnetic effect of neural activity can be detected with magnetoencephalography (MEG) by recording the magnetic fields induced by the electric currents occurring in the brain [67] [19]. The magnetic fields are recorded with highly sensitive magnetometers [84].

The metabolic effect of neural activity is captured by positron emission tomography (PET), a nuclear imaging technique. A radio-tracer, that is, a minuscule amount of radioactive material, is injected into the bloodstream [15]. As the radio-tracer reaches the brain, it attaches itself to the glucose. As the glucose is

consumed by the brain, different glucose levels within the cerebral region, may be captured by a PET scan.

Another neuroimaging technique is functional magnetic resonance imaging (fMRI). It has been shown that neural activity affects the cerebral blood flow. Neurons require oxygen which is delivered by haemoglobin in red blood cells [8]. As neural activity within an area increases, a greater demand for oxygen is created, hence increasing the blood flow to that area. The magnetic characteristics of the haemoglobin is changed according to the oxygen levels within it. This change is detected by an MRI machine [32]. Similar to fMRI, oxygen levels are also detected with functional Near-Infrared Spectroscopy (fNIRS) which detects how much oxygen is present within the area through the use of infra-red light [43].

Electrical neural activity is recorded with electroencephalography (EEG). Electrodes are placed on the scalp to measure the electric potential induced by the neurons. A neuron consists of an axon and dendrites, which can be considered as the sending and receiving parts of a neuron respectively [11]. Neurons transmit information by means of electrical charges. An axon induces a charge and transmits it to the nearest dendrite. Potential differences are induced between the synapses and the axon due to ions distribution in the membrane of the neuron[94]. The synapse is the gap between the axon and the dendrite. Only when a group of neurons fire together can the effect be detected by EEG equipment [50].

2.2.2 EEG Electrode Layout

EEG electrodes are positioned on the scalp according to the International 10/20 system [1], which is an internationally recognised standard to illustrate the position of scalp electrodes used within an EEG context. The 10/20 system, shown in Figure 1, provides a uniform framework by which EEG scientists can document their studies.

Scalp positions within this system are designated according to their locations with respect to the four lobes which make up the cerebral cortex [88]. The electrodes on the frontal lobe, which is responsible for reasoning, motor action, cognitive skills and speech, all start with the letter 'F'. The parietal lobe, which processes all sensory information, is located in the central to posterior section of the brain. Electrode positions that are located centrally within this region are designated with the letter 'C' whereas those electrode positions that are located posteriorly within this region are designated with the letter 'P'. The two temporal lobes, associated with the interpretation of sounds, is found at the bottom and to the sides of the brain. Due to its location, the accessibility to the temporal lobe through the International 10/20 system is quite limited, and in fact there are only few electrode positions on the temporal lobes, which are designated with the letter 'T'. Lastly, the occipital lobe, which processes all the visual information [70], is at the back of the head. Electrodes on the occipital lobe are designated with the letter 'O'. Some positions which lie between two lobes are designated with the two corresponding letters.

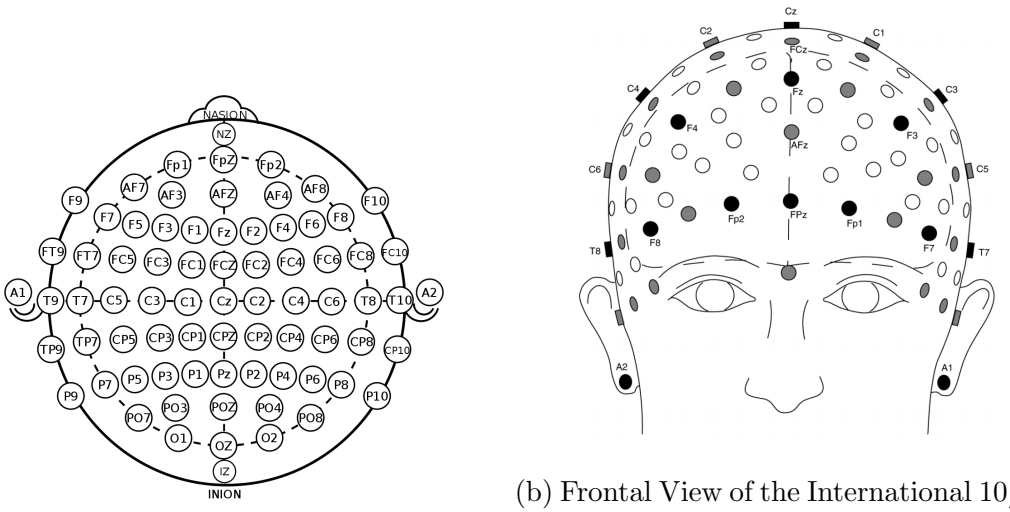

(a) International 10/20 System [1]

(b) Frontal View of the International 10/20 System [71]

Figure 1: Frontal and Top View of the International 10/20 System

2.2.3 Various EEG-based BCI systems

A large majority of the BCIs use EEG since it is the most portable and most cost-effective neuroimaging technique, relative to the other brain recording modalities mentioned in Section 2.2.1. EEG also has an excellent temporal resolution though a relatively poor, spatial resolution. Various types of EEG-based BCI systems exist, all of which use different techniques and different EEG channels for acquisition. However all EEG-based BCIs can be divided into two categories: evoked and spontaneous, or as sometimes also referred to, exogenous and endogenous, respectively [98].

Evoked-type BCIs heavily depend on external stimulation which can be of auditory, visual or sensory nature. The stimuli evoke certain potentials within the brain, which are recognised by the BCI and interpreted as commands [3]. Spontaneous systems require no external stimuli as the mental activity within a specified region is interpreted as a control input.

The P300 system is an evoked BCI. In such a system, event-related potentials (ERPs) are utilised. ERPs are computed by averaging epochs of data related to a specific event. Users are exposed to an oddball paradigm where presentations of sequences of repetitive stimuli are infrequently interrupted by a deviant stimulus. The infrequent event evokes the P300 component. The name of the component refers to a peak within the ERP that occurs around 300ms after the infrequent stimulus is presented [28].

Another evoked-type BCI is one based on steady-state visually evoked potentials (SSVEPs). SSVEP-based BCIs make use of visually evoked potentials which are electrical potentials, most prominent within the visual cortex, occurring in response to a visual flickering stimulus. It is known that a visual stimulus flickering at a constant frequency will generate a corresponding visually evoked potential with a frequency equal to that stimulus frequency [80]. Since a stimulus flickering at a specific frequency evokes an SSVEP signal that includes the flick-

ering frequency, signals may be analysed in the frequency domain, facilitating the recognition of SSVEPs. SSVEP spectra exhibit a peak at their respective fundamental frequency and subsequent harmonics.

Motor-Imagery based BCIs are of the spontaneous type. Motor Imagery (MI) refers to an imagined movement or an action that is mentally executed. Prominent changes within the brain rhythms are observed within the motor cortex when the user is planning or executing a voluntary movement [101]. This allows for the detection of imagined body movements as motor imagery produces quasi-identical effects on the brain rhythm as the real movement performed. Upon this basis, several BCIs have been developed to control the movement of a mouse cursor for instance by imagining left or right hand movement [56].

Another spontaneous BCI is the Conceptual Imagery (CI)-based BCIs. Such BCIs are a recent development. Research has shown that the link between the EEG patterns of a user and the conceptual objects that a subject thinks about is quite consistent [59]. Such BCIs can lead to more natural interactions with the system. With an adequate and personally-customised training, users can for instance imagine a lamp in order to switch it on or off.

Hybrid systems have also been developed by researchers in order to improve BCI systems in three aspects: (i) improve BCI classification accuracy, (ii) increase number of user options within the application, and (iii) reduce brain-command detection time. A hybrid BCI (hBCI) can either: (i) integrate a neural data acquisition device with another biosignal acquisition method like electroculography (EOG), or (ii) combine two or more brain activities within a singular unit. A typical example of the first type of hBCIs would be a combination of video-oculography (VOG) and EEG to extract the ocular artifact and remove it from the EEG signal [85]. As for the second type of hBCIs, a typical example would be utilising both P300 and SSVEP components, to gain from the advantages of both techniques [44].

2.3 Chapter Summary

This chapter provided an introduction to home automation systems and brain computer interfaces. It started out with an overview of the components which make up a home automation system, discussing the typical hardware devices used and the communication technologies generally utilised. The overview was concluded with a discussion on the user interfaces of such systems and how BCIs can aid motor-impaired users. The second part of the chapter focused on BCIs starting with an overview on the various neuroimaging devices available, followed by a generic description of EEG-based systems and the EEG electrode layout.

3 Review of Smart Home BCIs and EEG-based Eye-Movement Extraction

This chapter starts with a focus on the smart home BCIs reported in literature. It discusses the smart home BCIs from different perspectives. As the goal of the project is to design a smart home hBCI which fuses SSVEPs with EEG-based eye-movement potentials, the second part of the chapter focuses on the most commonly used techniques for processing EEG-based eye-movement signals. It explains briefly the algorithms used for each technique and concludes with a performance comparison between the different techniques used.

3.1 A Review of the BCI Systems Implemented within a Smart Home Environment

The independence of persons with mobility impairment has always been an important concern. One critical factor for such individuals is their dependency on their families or carers to carry out basic tasks within their own home. This inspired a lot of effort in the last couple of years to incorporate the use of BCI systems within a smart home environment. In this section, literature related to BCIs in smart homes will be reviewed and analysed, to help understand the state of the art and identify any gaps in this field.

3.1.1 Nature of BCI Systems Used

Several ways exist to establish a communication link between the human brain and the computer. This can be done through visually evoked potentials [37], motor [16] or conceptual imagery [93], facial expressions and cognitive state assessment [65]. P300-based smart home BCIs [37], [45], [24] were implemented in various ways, each having different menu layouts as described in Section 3.1.2.

An SSVEP-based system was implemented by Saboor *et al.* [82]. All stimuli

were presented on Epson Moverio BT-200 augmented reality glasses. QR codes were included within the system to identify the controllable devices within the smart home environment. Once a device is detected, a maximum of four flickering stimuli were presented according to the device selected. Another SSVEP-based system was implemented by Adams *et al.* [2], where the flickering stimuli were distributed across three different screens dispersed around the home environment.

Corralejo *et al.* and Cho *et al.* implemented MI-based smart home BCIs. In the system implemented by Corralejo *et al.* [45], users were instructed to imagine the movement of either their left or their right hand to move the cursor in one-dimension; either left or right. The cursor was then used to operate the home automation system. In the other system implemented by Cho *et al.* [16], a VR BCI system was presented. Apart from being implemented in a real environment, the home automation system was also emulated in a virtual environment. MI brain signals were acquired with an EEG headset to allow the user to navigate to the left or right within the virtual space and to control devices within the virtual environment. Objects controlled within the virtual environment, trigger the corresponding events in the real home automation system.

CI-based smart home BCIs were developed by Kosmyna *et al.* [58] and Suleri [93]. Kosmyna *et al.* [58] suggested a BCI operating on conceptual imagery, in which mental imagery was used to execute mental commands. Subjects were instructed to imagine an image or concept in connection with the device to be controlled. Template matching algorithms were used to train and classify the EEG data. Suleri [93] implemented a BCI system which functions on a combination of motor and conceptual imagery. Black curtains and noise-cancelling headphones were included in the setup in order to enhance the effectiveness of the conceptual imagery.

Various smart home BCIs depending on cognitive state assessment were implemented and utilised facial muscles as switches [65], [51], [63], [33]. Double or

triple blinks, detected from frontal channels, were interpreted either to select a particular device or to prompt the BCI into active mode. Algorithms were used to observe the activity within the EEG frequency bands. The attention and meditation levels of the users were computed, monitored and assessed to operate the selected device.

Each BCI system discussed above has its own advantages and disadvantages. Some systems may be easy to set up at the expense of performance whereas others may be more robust but lack practicality. A thorough discussion of the techniques mentioned above is presented later in Section 3.1.4.

3.1.2 Menu Layouts

The layout of the menus differed according to the nature of the BCI systems used and the number of options available to the user. For instance, Guger *et al.* [37] and Corralejo et al. [45], both opted for cascaded menus within their respective smart home P300-based BCI systems. With regards to the system implemented by Guger *et al.* [37], seven menus were drawn to include all the options available to the user. Six of these menus allowed the user to control devices directly while the other menu allowed the user to access a specific device or a position within the house, as shown in Figure 2. Corralejo *et al.* [45] opted for a principal menu which consisted of a 3×4 matrix where most of the tiles represented a controllable device. Three of the tiles were assigned the function to either pause, stop or resume the application. The secondary menu was formed according to whatever the user chose in the principal menu. For instance, should the user choose to control the TV, a 5×5 matrix would appear as a secondary menu. On the other hand, DeVenuto *et al.* [24] designed a P300-based BCI which utilised a single menu since only four options were available to the user. The icons in the menu are flashed one after the other to evoke the P300 component within the user's brain signals.

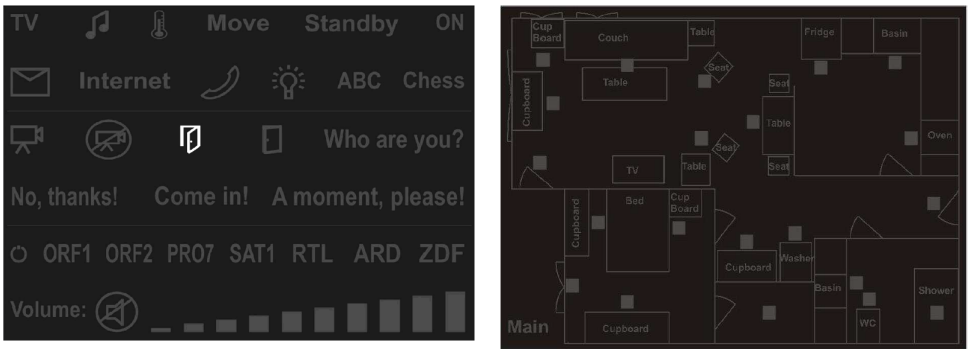

Figure 2: User Interface of the P300-Based BCI System implemented by Guger *et al.* [37]

For the MI-based smart home BCI [21] implemented by Corralejo *et al.*, a different menu layout was applied. As shown in Figure 3, the screen was divided into two menus one of which was consistent and present, throughout the operation of the BCI. The other menu was of a hierarchical structure. The green cursor was operated through motor imagery. Scrolling through the menu was permitted by moving the cursor to the right, while in order to select an option, one had to move the cursor to the left. Secondary menus were designed for each device.

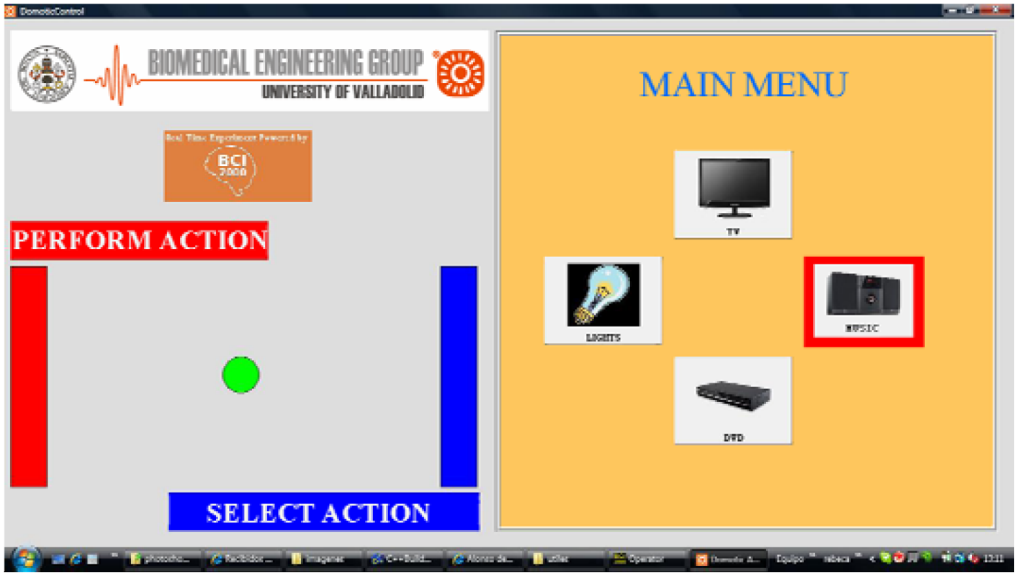

Figure 3: User Interface of the MI-Based BCI System implemented by Corralejo *et al.* [21]

In general, icons were preferred over textual descriptions, where this was possible [63] [45]. This attributes to the fact that an image conveys a message much more efficiently than text [23]. Moreover, with regards to visuals, icons take less space than text and give the menu a more organised and aesthetically-pleasing look. Except for P300-based systems, BCIs have between four to eight icons on the menu. P300-based systems on the other hand could easily include more options, and hence more icons, within one menu, as can be seen in Figure 2.

3.1.3 Hardware Used in Smart Home BCIs

All the hardware used in smart home BCIs can be categorised in two: (i) the EEG data acquisition device and (ii) the components used to control or compose the home automation system itself. EEG headsets can either be laboratory grade or consumer EEG systems [79]. Low-end EEG headsets are cheaper and more portable than laboratory grade EEG equipment, however the use of such equipment comes at the expense of accuracy.

With regards to the hardware of the home automation system itself, from the review conducted in this study, it was observed that the systems implemented can be roughly categorised into three so-called generations. In first generation systems, a virtual home was created and no physical devices were required as was the case in several studies [37], [25], [93]. This allowed the designers to focus more on the BCI part of the smart home and hence refrained themselves from actually implementing the smart home and dealing with its problematics.

Second generation systems utilised relays to control and operate actual, physical devices. However such operation is limited to solely a toggle operation, that is an on-off switch operation, as was the case in various studies [65], [51], [63], [33]. Devices included computers, monitors, routers, kettles, medical devices, lights, fans and locks.

Third generation systems went a step further and offered more flexibility within their menus, as users were given much further options than simply switching a device on and off. Corralejo *et al.* implemented such a system [45], [21] where the user could modify the volume or temperature of the TV or AC unit respectively, instead of just switching them on and off. Such systems made use of IR blasters in order to provide this flexibility.

Second and third generation systems included a microcontroller within their architecture which acted as the central hub within the home automation system. Various microcontrollers were used. Some studies included an Arduino [63] or a Raspberry Pi board while others opted for an ESP32 [82] or ARM7 [33] development board. Communication between the devices and the central hub was done on wireless technology like Bluetooth [65] or WiFi [4].

3.1.4 Discussion

A comparative analysis of different smart home BCI systems was carried out. BCI systems that rely on the observation of activity within the EEG bands and compute the user's attention and meditation levels accordingly, are the most easy to implement as two or three electrodes may suffice to develop such a system. This enables researchers to use a commercial grade EEG system. However, a BCI based on a commercial grade EEG acquistion device, will be time-consuming should the user interface be complex with a menu that includes several options. As a result, the operation of several devices was limited to just a toggle operation.

Imagery-based BCIs are endogenous and hence require no external stimuli. However it is difficult to navigate a complex smart home menu with motor imagery . Specifically, users must first control a cursor with motor imagery which in turn operates the menu of the home automation system. A VR system as implemented by Cho *et al.* [16], would imply more direct results, but still motor imagery requires a high level of focus in order to function smoothly. On the other hand, conceptual imagery seems to have the most direct approach when control-

ling devices. The subject is first trained to think of an image or imagined action in relation to the action that the subject wishes to execute. Then during the real-time running of the BCI, the subject must rethink the same exact thing that the subject thought during the training stage in order to execute the required action. However, such a technique requires an even higher level of focus from the user. CI-based BCI systems need to be implemented in an environment which is free of distractions, which is not always possible, especially for people with mobility impairment [59].

A lower level of focus is needed for the P300 and SSVEP based BCIs, which are the most reliable of all the mentioned BCI techniques. Since P300 and SSVEP-based BCI are exogenous, the subject just needs to attend to the target and the evoked potential is generated. A P300-based system tends to be slower than an SSVEP-based system, since one has to wait until the desired target is flashed. This can take some time especially when there are lot of options available, as in the case of home automation systems. On the other hand, SSVEP-based BCIs tend to be limited with the number of options, as increasing the number of options would increase the number of flickering stimuli, increasing the distractions and the annoyance factor of the system. However, SSVEP-based BCIs have a more direct approach than the P300-based systems as one does not have to wait for the target to flash or appear. The limitation on the number of unique flickering frequencies may be overcome by including different phase differences for different stimuli and by re-structuring the user-interface into hierarchical menus. According to Amiri *et al.* [5], SSVEP-based BCI system have more accuracy and better information transfer rates (ITR) than the P300-based BCI systems. This makes the SSVEPs a suitable choice for designing a BCI to control a home automation system.

From the review on smart home BCIs, one can notice that there is a lack in development of third generation BCIs. Third generation smart homes are more complex to implement but offer much more flexibility in return. To the best of

our knowledge, two such systems [45] [22] have been developed, one of which was based on motor imagery while the other utilised the P300 component. Since it was concluded that SSVEP is most suitable choice for a smart home BCI, this project will address this gap by designing and implementing a third generation smart home SSVEP-based BCI.

3.2 A Review on the Extraction of Eye-Movement Information from EEG data

Despite being the most suitable choice for a smart home BCI, the limitations of SSVEP-based BCIs still need to be addressed. Since smart home BCIs may require several user options within the menu, this will lead to several flickering stimuli within a smart home SSVEP-based BCI. Although the user may focus on a single stimulus, all the stimuli within the visual field are processed by the brain. Studies has shown that multiple stimuli presented at the same instant will compete for neural representation in the visual cortex [57]. Should the stimuli be located spatially close to each other, this would attribute to a far more intense competing effect, as in accordance with the Stiles-Crawford effect, which states that light entering the pupil through the centre is perceived to be stronger and brighter than that light entering at the boundaries of the pupil [92].

The recognition of SSVEPs is hindered by such a competing effect, as the fundamental frequencies of the SSVEPs start to interfere with each other and spatial resolution is lost. Besides frequency encoding the stimuli, phase encoding [52] and dual frequency coding [104] have been used as alternative encoding methods to address the issue of the competing effect.

Other studies tried to include other technologies and form a hybrid BCI in order to improve the BCI performance, some of which acquiring biological signals from another source apart from neural activity. EEG signals have been combined mostly with electrooculographic (EOG) signals [72]. EOG signals are utilised to predict the eye-gaze direction and estimate the focus of foveal attention (FoA).

However such hybrid systems require the user to have EOG electrodes attached to the face in addition to the EEG headset. Studies have also combined EEG with video-oculography (VOG), employing an eye tracker to determine the FoA [86], however such hybrid systems require the use of multiple instruments, namely the VOG device and the EEG device, working in synchrony. Hence, the question of whether the eye-movement data can be obtained from just EEG electrodes, is relevant to such hybrid BCIs. This allows BCI designers to predict eye movement using just an EEG cap, rendering a hybrid BCI system which is of less discomfort to the user and simpler.

3.2.1 Types of Eye-Movements Identified

There are various studies that have shown that eye-gaze movement may be extracted from EEG. Although most of the works are concerned only with horizontal eye-movements, other works [10], [41] also discriminate vertical eye movements.

3.2.2 Electrodes Position

Belkacem *et al.* [9] applied electrodes mostly on the frontal lobe but few of them were even placed on the temporal lobe. Data was acquired from the following scalp positions: $AF_7, AF_8, F_7, F_8, FT_7, FT_8, T_7$ and T_8. From Figures 1a and 1b it can be seen that these electrodes cover the region just above and beside the eyes, making them ideal to gather eye-movement data. Other researchers used a smaller combination of the aforementioned locations along with additional adjacent scalp positions. For instance, Gupta *et al.* [38] acquired data from F_7 and F_8 and from AF_3 and AF_4, while Hai *et al.* [40] also used FP_1 along with F_7 and F_8. On the other hand, Belkacem *et al.* [10] acquired eye-movement-related EEG data from just two scalp position T_9 and T_{10} from the temporal lobe.

3.2.3 Signal Pre-Processing

Once acquired, EEG data is pre-processed in order to prepare it for feature extraction. Data is initially filtered to remove any unwanted noise, which typically includes the powerline frequency and any activity outside the frequency band of

interest. A notch filter is applied at the power line frequency to remove associated components. An additional filter is applied to filter out frequency components larger than 10Hz. Belkacem *et al.* [10] and Hsieh *et al.* [46] both implemented a lowpass filter Butterworth filter with a cut-off at 10Hz and 7Hz, respectively, as frequency components larger than this are not associated with eye movements. Gupta *et al.* [38] on the other hand used a 5^{th} order Butterworth filter operating between 0.5Hz and 3Hz.

Removal of the baseline and normalisation may also be carried out. Belkacem *et al.* [9], also applied a least-squared polynomial of the 10^{th} degree to smoothen the signals. Others implemented a Hamming filter followed by an Extended Moving Difference (EMD) filter to reject voltage drift noise [40].

3.2.4 Eye Movement Feature Extraction

After the pre-processing stage, feature extraction algorithms are applied to the data to extract features that characterise the data and also reduce its dimension. These are fed to the classifier. The outcome of the studies mentioned in this section will be discussed in Section 3.2.6.

One typical feature extraction method is the Independent Component Analysis (ICA) technique used by Samadi [41] and Hsieh *et al.* [46]. ICA allows the multichannel EEG data to be decomposed into independent signal sources. This allows the artifacts to be distinguished from true EEG data. The ICA algorithm works on the general assumption that all the observed signals are a combination of linearly mixed signal sources. Figure 4 illustrates the concept behind the ICA technique.

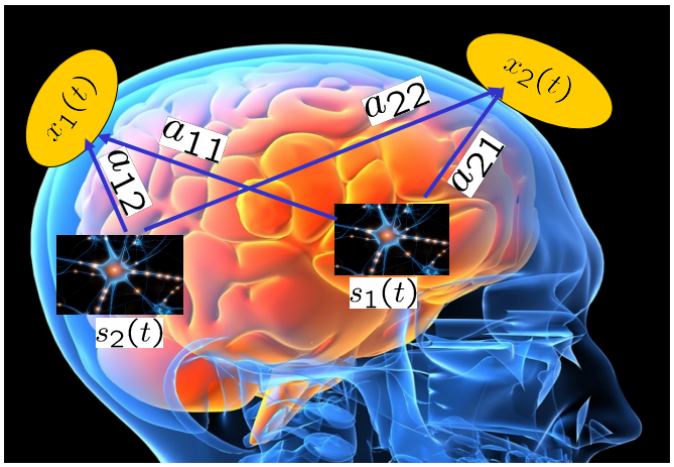

Figure 4: Graphical Illustration of ICA [76]

The ICA can be represented mathematically by the following equations:

$$\begin{aligned} x_1(t) &= a_{11}s_1(t) + a_{12}s_2(t) \\ x_2(t) &= a_{21}s_1(t) + a_{22}s_2(t) \\ x &= As \end{aligned} \tag{1}$$

where x denotes the observed EEG data acquired from different channels while s represents two sources within the brain. The matrix A denotes the mixing matrix which is responsible for modifying the original signal sources into the observations. The ICA solves for s and A by maximising the statistical independence between the components of the signal sources themselves.

After the ICA was implemented, Samadi segmented the ICA-derived source signals into epochs. Epochs were composed of 400ms temporal windows with 50% overlap. Features were extracted from each windows by computing the mean, variance, maximum and minimum amplitude. These features were then fed to a Support Vector Machine (SVM) classifier, which will be explained in Section 3.2.5.

A different approach for feature extraction used by Gupta *et al.* [38], is the Common Spatial Pattern (CSP) filter. CSP maximises the variance within one class while minimising the variance within the other classes. Once the spatial fil-

ters are obtained, the common logarithm is applied on the variance of the product of the spatial filter with the data. These were taken as features and fed to the classifier.

All of the above can be explained mathematically by the pair of equations below:

$$\begin{aligned} F_a &= log(var(S_F X_a)) \\ F_{Ra} &= log(var(S_F X_{Ra})) \end{aligned} \tag{2}$$

where F_a represents the features for class a. Class a represents a particular class such as a leftwards glance. S_F and X_a represent the spatial filter and signal data. On the other hand F_{Ra} and X_{Ra} denote the features and signal data for all other classes other than class a. These features are then used to train an SVM classifier.

Belkacem *et al.* [9] carried out basic arithmetic operations to determine the features. Utilising eight electrodes, they subtracted the summation of four channels belonging to the right hemisphere from the corresponding sum of the left hemisphere. This can be expressed mathematically through the equation below:

$$X_{new}(n) = \sum_{i \in L} X_i(n) - \sum_{j \in R} X_j(n) \tag{3}$$

where n represents the sample data at a specific timing, i denotes the channel while L and R represent the set of channels used within the left and right hemisphere respectively. The channels used were $AF_7, F_7, FT_7, T_7, AF_8, F_8, FT_8$ and T_8. This expression was used to distinguish between the left and right and vertical glances. A further expression was used to distinguish between upward and downward glances, which sums all eight channels.

$$Y = \sum_{m=1}^{8} X_m(n) \tag{4}$$

where m denotes the channel number. It was observed that these two signals include a peak occurring at a specific time. The area of these peaks was deter-

mined using a simple trapezoidal integral method and used as a feature.

In an additional study [10], the Continuous Wavelet Transform (CWT) was applied to the signals X_{new} and Y. The corresponding scalogram, a quantifiable representation of the energy of the coefficients, was generated and the peak-to-peak amplitude of the signals as well as the gradient of the peaks were calculated. These four quantities (amplitude, gradient, energy and area of the peak) were used as features for the classification process. Data was segmented within one second temporal windows. The amplitude was measured by calculating the difference between the minimum and the maximum values of the samples within the window. The gradient was computed by dividing the amplitude by the window length, which in this case was one second. The area was measured with the same procedure as described in the paragraph above.

In contrast to other studies, Hai *et al.* [40] implemented a univariate Autoregressive (AR) model to extract the features from their data. They opted for a second order AR model as shown in the equation below.

$$y(n) = a_1 y(n-1) + a_2 y(n-2) \tag{5}$$

where $y(n)$ is the filtered EEG signal. EEG data was acquired from three electrodes positioned at *FP1, F7* and *F8* resulting in a total of 6 AR coefficients for all three channels. During the experiment, data was acquired for blinking, fixation and bi-directional horizontal glances. Hence four sets of feature vectors, each consisting of six AR coefficients, were created, one for each class. The AR coefficients were inputted into a neural network for classification. The neural network will be discussed in the next section.

3.2.5 Classification of Eye Movements

After features are extracted from the data, they are fed to a classifier so that the eye movement may be predicted. Support Vector Machines (SVM) are the most commonly used classification method for EEG-based eye-movement predic-

tion.

SVM classifiers aim to find the ideal hyperplane that separates two classes of data, maximising the margin between them. For non-linear separable data, this requires a non-linear transformation such that it would be possible to linearly separate the data in the transformed space [73] [66]. Figure 5 illustrates the concept behind non-linear SVMs.

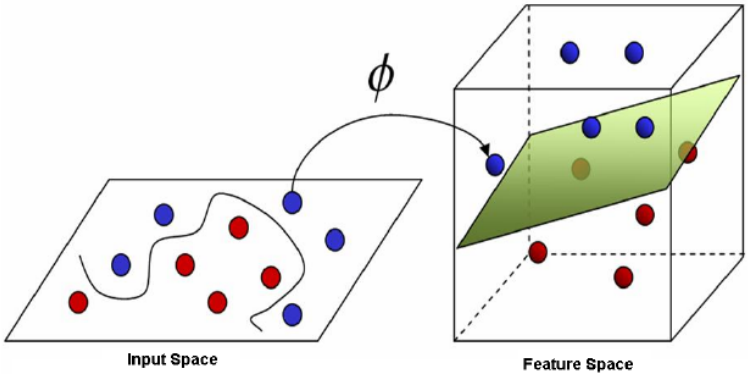

Figure 5: Graphical Illustration of the Non-Linear SVM Concept [13]

Alternatively, Hsieh *et al.* [46] use a Hidden Markov Model (HMM) for eye movement classification. An HMM is a way to model sequential data where the processes that are generating the data are hidden but represented in the model using latent variables.. The model is defined by the number of states and by three matrices and vectors: (i) the transition probability matrix which consists of all the probabilities of all the transitions between the states, (ii) the initial state distribution vector which consists of the probabilities of an observation initially occurring in any of the defined states, and (iii) the observation probability matrix which includes the probability of a particular observation occurring.

Hsieh *et al.* [46] defined three states within their model: left, right and centre. The model was based on the assumption that the user would start gazing at the centre. Another assumption was that the user could not glance directly from left to right, but rather glances to the centre prior to glancing to the left. A similar assumption was taken when glancing from left to right. The probability of a

state continuation was assigned to be 0.5, while glancing to the left or right was assigned to be 0.25. Glancing back to the centre had to be given a probability of 0.5 since glancing from left to right and vice-versa was defined to be impossible. Figure 6 illustrates the three-state machine implemented by Hsieh *et al.*

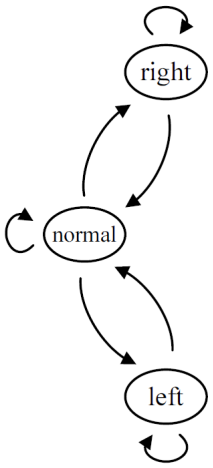

Figure 6: 3-State Machine implemented by Hsieh *et al.* [46]

Multi-layer perceptrons have also been used for eye movement classification [40]. Multi-layer perceptrons are made up of multiple layers of perceptrons where each perceptron uses the weighted sum of its inputs to provide an activation. Multi-layer perceptrons are trained in a supervised manner to classify an input vector into one of a number of classes at its output. As mentioned in Section 3.2.4, Hai *et al.* used the AR coefficients as eye movement features; these features were used in a multi-layer perceptron with two hidden layers to output four Boolean values, each of which representing a class, namely blinks, fixations, rightwards and leftwards glances.

3.2.6 Performance Comparison

A comparison between all papers was carried out in order to assess the accuracy results. Table 1 describes the feature extraction algorithms and classification methods implemented by the various authors and the results they achieved for horizontal glances and vertical glances. Table 1 also includes the various electrodes positions utilised.

Reference	Electrode Positions	Feature Extraction Method	Classifier	Horizontal Glances Percentage Accuracy	Vertical Glances Percentage Accuracy
Belkacem *et al.*, 2013 [9]	*AF7, AF8, F7, F8, FT7, FT8, T7 and T8*	Arithmetic Combinations of Channel Signal Values	Thresholds	69.73%	55.0%
Gupta *et al.*, 2012 [38]	*AF3, AF4, F7* and *F8*	CSP Filter	SVM	95%	/
Hsieh *et al.*, 2014 [46]	*AF3, AF4, F7* and *F8*	ICA	HMM	88.6%	/
Hai *et al.*, 2013 [40]	*Fp1, F7, F8*	AR Model	NN	94%	/
Belkacem *et al.*, 2015 [10]	*T9* and *T10*	CWT	Thresholds	98%	46%

Table 1: Performance Comparison Table

As can be observed, the studies carried out by Gupta *et al.* and Hai *et al.* achieved a highly accurate result despite making use of only four and three electrodes respectively. Both studies were limited to distinguishing between left and right glances. Belkacem *et al.* [10] achieved a high accuracy rate despite having gathered EEG data from only two temporal scalp positions. Specifically, an ac-

curacy rate of 98% was obtained for detecting horizontal glances, while vertical glances were detected with only 46% accuracy.

These results suggest that a mere electrode signal comparison, as done by Belkacem *et al.* [9], is not sufficient, and that some spectral signal decomposition helps to provide better features.

3.2.7 Conclusion

Nearly all algorithms discussed can be or have been implemented in a real-time scenario. Applications varied from playing a simple game [46] [10] to controlling a mouse cursor on the screen [20]. It is noteworthy that, to the best of our knowledge, there are no studies which investigated whether eye-movement information can be obtained from electrodes placed on the occipital region alone. This would be beneficial should the detection of eye-movements be combined with an SSVEP-based BCI which utilises occipital channels for acquisition. Also, to the best of our knowldege, there are no studies that investigate whether one can recognise glances at different visual angles but in the same direction. Finally, there also appears to be no study that seeks to combine the EEG-based eye-movement detection with a BCI. This project will address these issues by conducting a study to determine to what extent can eye-movement information be extracted from the occipital lobe and whether one can classify a glance at specific visual angles. Finally, the EEG-based eye-movement detection will be incorporated within an SSVEP-based BCI and two fusion methods will be compared to study whether and which hybrid BCI performed better than the non-hybrid SSVEP-based BCI.

4 EEG-based Eye Movement Detection

In the previous chapter, a general overview of the techniques used to extract ocular information from EEG was presented. This chapter is divided into two sections where the first covers the methods used to carry out the EEG-based eye-gaze analysis and the methodology by which this analysis is carried out. In the second section of the chapter, the results of the EEG-based eye-gaze analysis are presented and discussed.

4.1 Methods and Methodology

Following the overview of the EEG-based eye-movement-potential extraction techniques presented in the previous chapter, the feature extraction and classification algorithms which were most appropriate for the purpose of this project were investigated. The mathematical theory behind these signal processing techniques is discussed in detail in the first part of this section. Subsequently, the experimental paradigms and the methodologies used for the EEG-based eye-gaze analysis are also explained in this section.

4.1.1 System Architecture

A computer system with a 22 inch monitor, a resolution of 1920×1080 pixels and a refresh rate of 60Hz, was used for this project. The g.USBamp from g.tec [36] and the RED500 eye-tracker from SensoMotoric Instruments [47] were used for EEG and eye-movement data acquisition respectively. SIMULINK was used to acquire the data from the g.USBamp while all the processing was carried out in Python. The visual stimuli were designed using PsychoPy [74], an open-source Python toolbox, which permits control of the timing of the stimuli with very high precision.

4.1.1.1 Hardware Description

The equipment used for EEG data acquisition was composed of an EEG cap, EEG active electrodes, two 16-channel bio-signal amplifiers along with their re-

spective driver interface boxes and power supplies.

A g.GAMMA cap [36] was used for an EEG cap. The g.GAMMA cap allows the researcher to acquire EEG data from several different positions distributed on the scalp according to the extended international 10-20 electrode placement system. g.SCARABEO electrodes were used. These are active EEG electrodes with a small physical form (10×16 mm) which are inserted into the holder rings of the g.GAMMA cap. Highly conductive electrode gel was applied to the scalp through the opening within the electrode itself, to ensure optimal electrode-skin contact. The g.USBAMP bio-signal amplifier was used to amplify the EEG signal acquired from the scalp with a high precision and accuracy. Each amplifier allows a maximum of 16 input sources with a 256Hz sampling rate.

In parallel with the EEG data acquisition system, an eye-gaze tracker was used to record the eye-gaze of the subject in order to provide a ground truth for analytic purposes. A RED500 eye-gaze tracker was used. With a sampling rate of 500Hz, it uses infrared (IR) technology to track the pupil of the user as he/she looks at the computer screen. The output of the eye-tracker is given in screen pixel coordinates which reflects upon the user's point of gaze on the computer screen.

4.1.1.2 Software Description

The EEG acquisition process was developed within SIMULINK, interfacing the physical EEG equipment with the Python processing algorithms. A SIMULINK API was provided by g.tec as part of their firmware suite. The API was then integrated within the SIMULINK model.

Similarly, a Python API for the eye-gaze tracker was provided by SMI. This was integrated directly with the Python processing program as they were in the same programming language. To counter for the different languages of the APIs,

a UDP protocol was implemented to integrate the two APIs together.

The visual stimuli, which are described in Section 4.1.3, were designed using PsychoPy, which inherently provides an access to a vast library of stimuli having different shapes and sizes. Apart from that, PsychoPy allows the timings of the stimuli to be controlled with a frame-by-frame precision.

With a double-buffered system, stimuli are initially placed on the 'back buffer' while the 'front buffer' is presented on the screen. On each cycle, the 'back buffer' is initially blank and stimuli are rendered, that is, gradually added to the back buffer. At a point in time, when all stimuli have been rendered on the 'back buffer', the buffers are flipped such that the stimuli drawn at the back are now presented at the front, that is, on the screen. The flipping of these buffers is synchronised with the refresh rate of the monitor. It is this fact which exactly gives the software designer precise control over the stimuli timings.

4.1.2 Participating Subjects and Experimental Setup

Five healthy subjects participated in this study. The research study was approved by the University Research Ethics Committee (UREC) of the University of Malta (UREC Code:1905). Every participant was seated in front of an LCD monitor which was placed approximately at eye-level with the subject. Participants were also advised to limit their physical movement to avoid the coupling of EMG artifacts with the recorded data. A chin rest was provided to restrict head movement.

EEG data was recorded at a sampling frequency of 256 Hz from a total of 19 channels. Eight of these channels were in the occipital region while the rest were in the frontal area and temporal areas. The EEG channels selected were O_1, O_z, O_2, PO_7, PO_3, PO_z, PO_4, PO_8, T_7, FT_7, F_7, AF_7, Fp_1, Fp_z, Fp_2, AF_8, F_8, FT_8 and T_8. This set of electrodes was chosen in order to carry out a thorough analysis of which combination of frontal channels is best to extract eye-movement

related EEG and to determine to what extent is the occipital region capable of providing such information. In parallel with the EEG data, video-oculography was recorded at a sampling frequency of 500Hz to provide a ground truth for analysis, specifically to determine the exact point of gaze of the subject on the computer screen.

4.1.3 Data Acquisition Session: Experimental Paradigm

The purpose of the data acquisition session was to gather EEG-based eye-gaze data for offline-analysis. The session consisted of 5 sessions, with 80 trials each. In a trial, the subject was instructed to glance from the center to one of eight directions as shown in Figure 7, and back to the center.

Throughout the sessions, participants were instructed to follow a target presented on screen, with their eyes, as per the protocol illustrated in Figure 8. Subjects were instructed not to blink during the session except during rest periods which were indicated by a red stimulus. In each session, 10 trials were allocated for each position hence amounting to the total of 80 trials. Each session started with the stimulus fixated at the center of the screen for 5 seconds. Trials followed immediately after. In each trial the stimulus was presented at the center for 1 second and was then shifted to one of the designated 8 positions for another second. The trial concludes by re-centering the stimulus for the next second. A rest period of 1.5 seconds was allocated after each trial. Figure 8 illustrates the timings of the experiment. In this work a cross shape was selected for targets as it helps the subject to focus the gaze at a singular point, which is the centre of the cross itself.

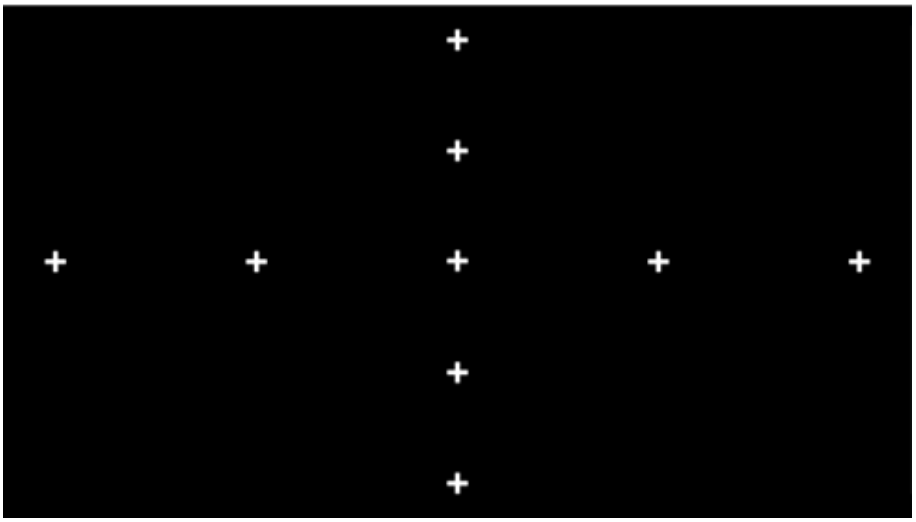

Figure 7: Possible Positions taken by Stimuli during EEG-Based Eye-Gaze Data Acquisition Session

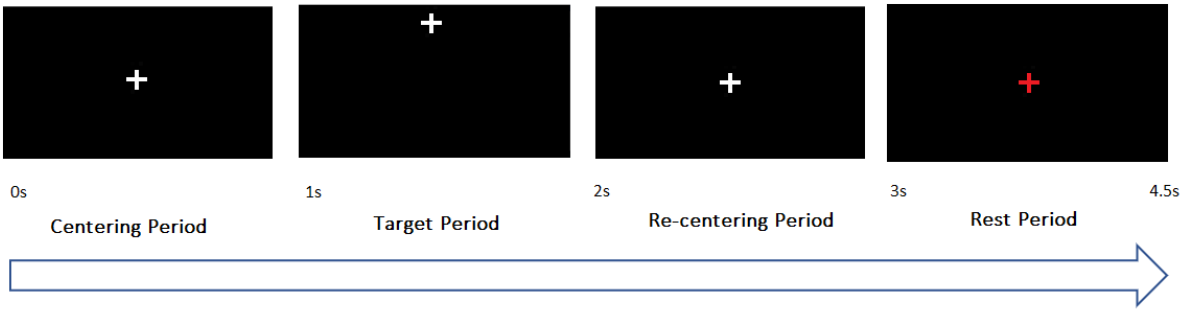

Figure 8: Timing Protocol of a Single Trial for EEG-Based Eye-Gaze Data Acquisition Session

4.1.4 Signal Pre-Processing, Feature Extraction and Classification

This section describes the algorithms used to filter the data in the pre-processing stage. It also elaborates upon the feature extraction techniques used and the classification methods.

4.1.4.1 Pre-Processing

EEG data gathered from the data acquisition sessions were organised into epochs as per the structures required by the code implemented in the MNE Python library [35] [34]. The MNE library is an open source package which fa-

cilitates the processing, analysis and visualisation of both MEG and EEG data. Epochs were then filtered with a 4^{th} order Infinite Impulse Response (IIR) band-pass filter having cut-off frequencies at 0.5 and 7Hz [62]. The EEG data was also organised into custom-made files, which was used to integrate the EEG data with the VOG data, allowing us to visualise both data types simultaneously as shown in Figure 9.

As per the data collection protocol described in Section 4.1.3, each trial lasted three seconds. In each trial the stimulus was presented at the center for 1 second and was then shifted to one of the designated eight positions for another second. The stimulus was then re-centered for the last second of the trial. Hence the data within the trial which was relevant to this study was found in that one second when the stimulus was off-centre. A frame of 0.5s after the target is shifted off-centre, was sufficient to capture the eye-gaze signal. The frame also catered for the visual reaction time which on average amounts to 0.25 seconds [54] [97] .

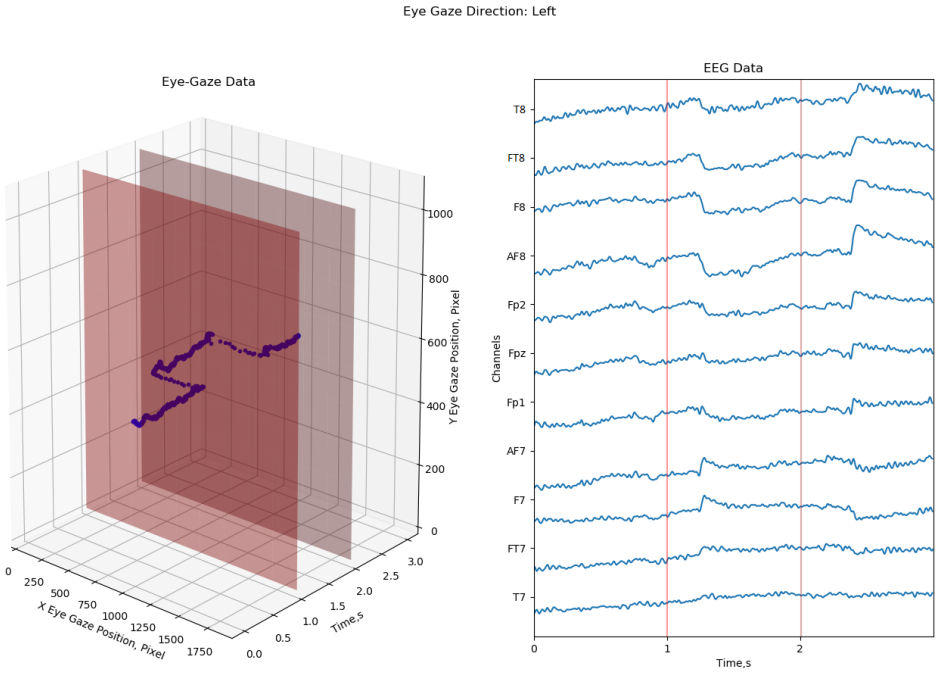

Figure 9: Simultaneous Visualisation of Eye-Gaze Data Captured Through VOG and EEG Data

4.1.4.2 Feature Extraction

As part of the machine-learning process, features need to be extracted from the EEG data in order to be fed into the classifiers in the following stage. The technique of common spatial patterns (CSP) [77] was utilised in order to decompose two multi-variate signals pertaining to two different classes into two sets of components. Significant differences lies in the variances between the two sets of components facilitating discrimination between the two classes.

The data of each epoch, E_c, was shaped into an N×T matrix, where N represents the number of EEG channels making up the data and T denotes the number of samples within the epoch. An N×N covariance matrix, S, was calculated for each epoch pertaining to a specific class. Covariance matrices were normalised by their trace as shown in Equation 6. The covariance matrix indicates a degree of how the EEG channels are linearly associated with each other. $cls1$ and $cls2$ represent the two different classes [38].

$$S_c = \frac{E_c E_c^T}{trace(E_c E_c^T)}, c \in [cls1, cls2] \tag{6}$$

Covariance matrices pertaining to a specific class were averaged in order to obtain a single and averaged covariance matrix for each class, as can be seen in Equation 7:

$$\overline{S_c} = \frac{\sum_{i=1}^{n} S_{c_i}}{n}, c \in [cls1, cls2] \tag{7}$$

The averaged covariance matrices of the two classes were summed up to obtain the Composite Covariance Matrix, S_{cmp} as observed in Equation 8 [38]:

$$S_{cmp} = \overline{S_{cls1}} + \overline{S_{cls2}} \tag{8}$$

Eigenvalue decomposition follows next, as the composite covariance matrix was factored as in Equation 9. The largest eigenvector of the composite covariance

matrix points in the direction of the largest spread in variance within the matrix. The magnitude of such vectors are numerically represented by their respective eigenvalues. Eigenvectors were sorted in descending order according to their eigenvalues.

$$S_{cmp} = V\lambda V^T \tag{9}$$

The whitening transformation matrix, W, was then found as in Equation 10, and this was applied to the average covariance matrix of each class as seen in Equation 11. This linearly transforms the data into a form where the new covariance matrix is identical to the identity matrix. Hence $S_{W_{cls1}}$ and $S_{W_{cls2}}$ share the same common eigenvectors U [77].

$$W = \lambda^{-\frac{1}{2}} V^T \tag{10}$$

$$S_{W_c} = W\overline{S_c}W^T, c \in [cls1, cls2] \tag{11}$$

The whitened covariance matrix, S_{W_c} is once again factored into its eigenvectors as shown in Equation 12 [77]:

$$S_{W_c} = U\gamma_c U^T, c \in [cls1, cls2] \tag{12}$$

$$\sum_c \gamma_c = I, c \in [cls1, cls2] \tag{13}$$

Since as shown in Equation 13, two corresponding eigenvalues within γ_{cls1} and γ_{cls2} sum up to one, the eigenvector with the largest magnitude for S_{W_1} is the same eigenvector but with smallest magnitude for S_{W_2}. This property makes the eigenvectors U useful for discriminating between the two classes. A projection matrix was calculated as shown in Equation 14. One may consider only the first and last eigenvectors within U as they carry the most information, however other eigenvectors can also be taken into consideration. Hence U can be reduced to U_k where k denotes the sets of eigenvectors used. Applying the projection matrix to

the epoch E, as per Equation 15, maps the epoch into the CSP space, denoted by Z.

$$P = U_k^T W \tag{14}$$

$$Z = PE \tag{15}$$

The natural logarithm was applied on the variance of the resulting epoch Z and considered as a feature for classification.

4.1.4.3 Classification

Classification is the final part of the machine-learning process. Feature vectors are fed into the classifier to assign them a label. A Support Vector Machine (SVM) was opted for in this work [18]. The theory behind such a classifier is described in this section. It is explained for feature vectors which are in a two-dimensional space. However the mathematics can easily be extrapolated to higher dimensional data.

As per Figure 10, the objective of the SVM is to find lines to discriminate between two classes. Furthermore, the SVM tends to find the optimal line to maximise the margin between the support vectors pertaining to each class. Support vectors are the data points which are closest to the discriminating plane.

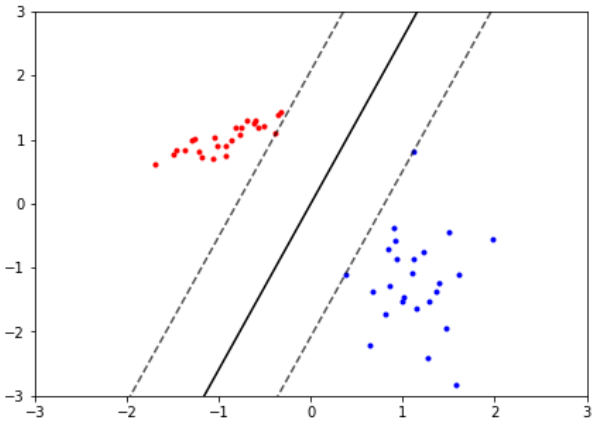

Figure 10: Illustration of SVM Division Line and Support Vectors [6]

The analysis of SVM starts from the classical binary classification problem given by the linear model in Equation 16:

$$y(x) = w^T \Phi(x) + b \tag{16}$$

$\Phi(x)$ denotes the feature-space transformation which in this research study was the CSP algorithm. w^T and b represent the gradient and intercept of the line respectively. The training data set consists of N input feature vector $x_1, x_2, ...x_N$ with corresponding labels or target values $t_1, t_2, ...t_N$ where $t_n \in -1, 1$. Testing data is classified according to the sign of $y(x)$. Assuming that the training data set is linearly separable, such that there exists a value of w and b which guarantees that $y(x_n)$ is greater than 0 for data points having a positive label and otherwise, for data points having a negative label, then $t_n y(x_n)$ is greater than 0 for all training data points.

The margin, which needs to be maximised, can be computed by finding the distance from a data point x_n to the line. This is given by Equation 17 [18]:

$$margin = \frac{t_n y(x_n)}{||w||} = \frac{t_n(w^T \Phi(x_n) + b)}{||w||} \tag{17}$$

It is desired to maximise the margin by solving Equation 18:

$$max(margin) = \arg\max_{w,b} \frac{1}{||w||} \min_n [t_n(w^T \Phi(x_n) + b)] \tag{18}$$

To bypass the minimisation problem, we can assume that w and b are rescaled such that $t_n y(x_n) >= 1$ for all training data points. This simplifies Equation 18, requiring only the maximisation of $\frac{1}{||w||}$. This is equivalent to minimising $||w^2||$.

Hence the optimisation function is shown in Equation 19 while the constraint function is shown in Equation 20 [18].

$$\arg\min_{w,b} \frac{1}{2}||w^2|| \tag{19}$$

$$t_n(w^T\Phi(x_n) + b) >= 1 \tag{20}$$

Lagrange multipliers are used to solve the constrained optimisation problem introducing the Lagrange multipliers a_n such that $a_n >= 0$. The Lagrangian function is given by Equation 21 [18]:

$$L(w, b, a) = \frac{1}{2}||w^2|| - \sum_{n=1}^{N} a_n t_n(w^T\Phi(x_n) + b) - 1 \tag{21}$$

As part of the Lagrangian solution, equating the derivatives of $L(w, b, a)$ to zero, Equations 22 is obtained:

$$w = \sum_{n=1}^{N} a_n t_n \Phi(x_n) \tag{22}$$

Plugging this into Equation 16 we obtain Equation 23 which is used to classify new data points.

$$y(x) = \Phi(x) \sum_{n=1}^{N} a_n t_n \Phi(x_n) + b \tag{23}$$

4.1.5 Methodology for the Offline Analysis of EEG-based Eye-Gaze Data

As stated in Section 3.2.7, one of the objectives of this study on eye-movement-related EEG, was to analyse and determine the extent of utilising EEG channels recorded from the occipital region for eye-movement detection. Another objective was to explore the classification between two saccades in the same direction having different visual angles. Five analytical approaches, which will be described later on in this section, were taken to extract as much information as possible from the offline analysis.

As both the CSP and SVM algorithm require training, the gathered data was divided in three batches. One batch was used to train the CSP algorithm, another batch to train the SVM classifier while the last batch was used as testing data. A three-fold cross-validation method was employed to facilitate the implementation. The use of two training batches of data to estimate parameters for CSP and SVM respectively, improves the generalisation of the system.

4.1.5.1 Classifying Eye-Movements

This section describes the process taken to classify an eye movement into one of eight possible classes. Specifically, a hierarchical system was carried out within the classification process. The hierarchy consists of three tiers as shown in Figure 11. At the first tier, epochs are classified as either horizontal or vertical saccadic eye movements. Once labeled, epochs are passed down to the second tier of the hierarchical classifier which consists of the 'L vs R vs O' and the 'U vs D vs O' classifiers. Epochs labeled as 'Horizontal' are passed to the 'L vs R vs O' classifier while epochs labeled as 'Vertical' are passed to the 'U vs D vs O' classifier. Epochs labeled as 'Others' by the 'L vs R vs O' classifier are handed to its sibling class within the tier, which in this case is a 'U vs D' classifier. Similarly, epochs labeled as 'Others' by the 'U vs D vs O' classifier are handed to an 'L vs R' classifier for classification. Epochs labeled at the second tier are then handed down to the third and final tier. At the final tier, epochs are classified according to the visual angle extent of the horizontal or vertical eye movement performed. Epochs were categorised either into trials with a 23.9 ° visual angle, which will be referred to as 'normal' within this text, or into trials with a 12.5 ° visual angle, which will be referred to as 'small' within this text. Epochs labeled as 'Left' from the second tier of the hierachical classifier are passed to an 'NL vs SL vs O' classifier. Similarly, epochs labeled as 'Right', 'Up' or 'Down' from the second tier are passed to their respective classifiers at the third tier. Similar to classifiers at the second tier of the hierarchy, epochs classified as 'Others' by a classifier are passed to its sibling classifier within that branch. Epochs labeled as 'Others' by the 'NL vs SL vs O' classifier are passed to an 'NR vs SR' classifier

and conversely, epochs labeled as 'Others' by the 'NR vs SR vs O' classifier are passed to a 'NL vs SL' classifier . Similarly, epochs labeled as 'Others' by the 'NU vs SU vs O' classifier are passed to an 'ND vs SD' classifier and conversely, epochs labeled as 'Others' by the 'ND vs SD vs O' classifier are passed to an 'NU vs SU' classifier. The 'Others' class was introduced from the second tier downwards for each classifier to compensate for misclassification. The 'Others' class consisted of epochs pertaining to the other classifier within the same tier. For instance, the 'Others' class of the 'Up vs Down vs Others' classifier was assumed to consist of epochs pertaining to the 'Left' or 'Right' class and hence these epochs are passed to a 'Left vs Right' classifier. Although three classes were present at the second tier downwards, both the CSP algorithm and SVM classifier were executed with a 'One vs One' approach. Taking the 'Up vs Down vs Others' classifier again as an example, first the 'Up' class and the 'Down' class were considered; then the 'Up' class and the 'Others' were considered and lastly, the 'Down' class and the 'Others' class were considered. Since, due to the 'Others' class, each binary classifier produced three results, majority voting was then applied to declare the winner of the three outcomes. In the case of a tie, arbitrarily, the outcome from the first pair was chosen. The CSP and SVM algorithms were executed in a binary mode as they were actually designed for binary feature extraction and classification.

4.1.5.2 Determining the Optimal Number of Components for CSP

As stated in Section 4.1.4.2, the CSP algorithm offers the possibility of using a different number of components to build up the feature set. This number of components is limited by the number of EEG channels used in the recording. To find the optimal number of components to use for highest possible classification, the offline classification process was carried out several times, each time increasing the number of components used in the CSP algorithm. Components were were added by two taking the next eigenvector from the top and bottom of the eigenvector matrix.

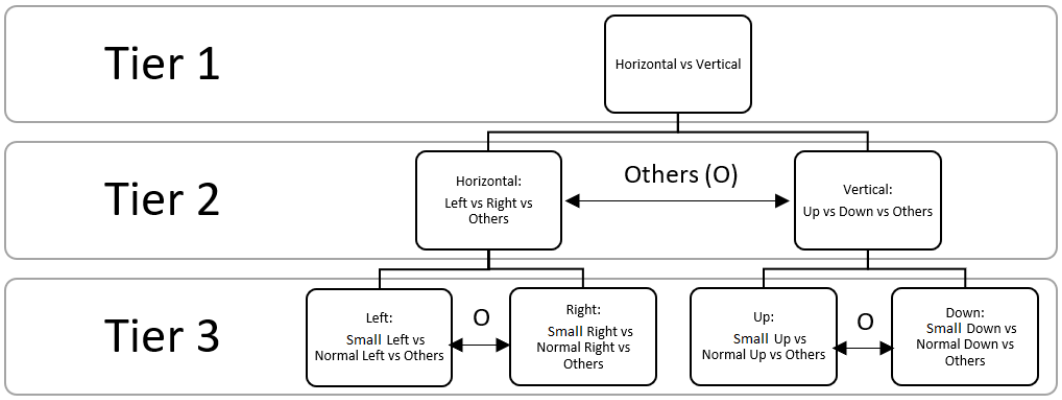

Figure 11: 3-Tiered Hierarchical Classifier used to classify EEG-based Eye Movement Potentials into one of Eight Classes

4.1.5.3 Analysis of Different Scalp Regions

As the purpose of the project, at a later stage, is to fuse EEG-based eye-movement potentials with an SSVEP-based BCI, a system dependent on electrodes placed at the occipital region, then, naturally, the question of whether eye-movement information can be derived from signals recorded from this brain region, arises. To address this question, the offline data analysis was carried out three times: i) using only the frontal channels, ii) using only occipital channels and finally using all the channels in the frontal and occipital regions. This was done to investigate whether channels from the occipital region can aid or replace channels from the frontal region in extracting eye-movement related information. It was noted that the maximum number of CSP components varied from one test to the other as different regions had a different number of EEG channels.

4.1.5.4 Analysis of Frontal Channels

During acquisition, eleven channels were recorded from the frontal region. An analysis was then carried out to identify how classification performance varies with the number of frontal channels used. In this case, 11, 7, 5 and 3 electrodes were considered as listed in Table 2.

Number of Frontal Channels	Frontal Channels
11	*T7, FT7, F7, AF7, Fp1, Fpz, Fp2, AF8, F8, FT8 T8*
7	*F7, AF7, Fp1, Fpz, Fp2, AF8 F8*
5	*AF7, Fp1, Fpz, Fp2 AF8*
3	*AF7, Fpz, AF8*

Table 2: Frontal Channels Considered for Each Case

4.1.5.5 Training Data Requirements

The goal of this analysis was to identify how classification performance varies as the number of trials used for training the CSP and the SVM algorithms is reduced. This analysis was carried out three times, starting with 64 training epochs and halving the amount for each test down to 16 epochs. Since each epoch takes 4.5 seconds, this analysis seeks to reduce the training time from 288 seconds to 72 seconds while determining how this reduction in training time affects the classifcation performance.

4.2 Results and Discussion

This section presents the results of the EEG-based eye-gaze analysis carried out on the data acquired as described earlier in Section 4.1.3. Numerical values corresponding to the bar graphs presented in this section are tabulated and presented for completeness in Appendix A. Except for when indicated otherwise, all tables portray the results averaged over the five subjects from which data was acquired. As described earlier, this analysis is composed of five analyses. Subsequently a discussion of the results follows.

4.2.1 Analysis of Determining the Optimal Number of Components for CSP

As stated in Section 4.1.5.2, an analysis of components was carried out to determine the optimal number of components for transforming the EEG data to CSP space. Table 3 shows the accuracy results obtained using different number of CSP components across the various individual classifiers. For Table 3, all the EEG channels were considered. As can be seen, the optimal number of CSP components varies between 2 and 8 for the different individual classifiers.

	CSP Components								
	2	4	6	8	10	12	14	16	18
H vs V	99.61%	98.82%	98.61%	98.19%	98.13%	97.99%	97.92%	97.78%	97.50%
L vs R vs O	88.96%	89.93%	88.33%	89.31%	88.96%	88.54%	88.40%	86.88%	87.43%
U vs D vs O	74.44%	76.81%	77.36%	78.26%	77.50%	77.85%	77.85%	77.57%	77.29%
NL vs SL vs O	64.17%	67.64%	67.99%	67.78%	67.78%	65.42%	64.44%	64.65%	63.26%
NR vs SR vs O	65.42%	70.42%	71.74%	70.07%	69.10%	68.47%	67.92%	67.85%	66.60%
NU vs SU vs O	49.24%	55.42%	52.71%	53.40%	54.24%	53.68%	51.60%	53.61%	52.43%
ND vs SD vs O	47.78%	50.97%	51.25%	51.04%	50.14%	49.17%	48.96%	50.90%	49.93%

Table 3: Results of the Analysis of Determining the Optimal Number of Components for CSP

As seen from Table 3, the accuracy is not substantially affected by the number of CSP components used. For this reason it would be sufficient to use just two CSP components for each classifier. This results in a feature set made up of only

two elements, allowing the SVM to operate within a two-dimensional space.

4.2.2 Classification of Eye Movements Results

In this analysis, two approaches were taken. One approach analysed the individual classifiers making up each tier of the hierarchical system. The other approach analysed the results when the classifiers of the whole hierarchical system were taken into consideration. The results of the two approaches are shown in the tables presented in Appendix A, all of which are two-dimensional. Classifiers lie on the rows, while the different scalp regions used are distributed across the columns.

4.2.2.1 Individual Classifiers

In this section, the individual classifiers were compared. Figure 12 illustrates the performance of the classifiers and contrasts them with each other. It also shows how the performance changes when different scalp regions are used. As can be seen from Figure 12, the 'H vs V' classifier produces the best results, achieving approximately 98% score. There is however a substantial drop in the accuracy from the 'H vs V' to the 'L vs R vs O' classifier.

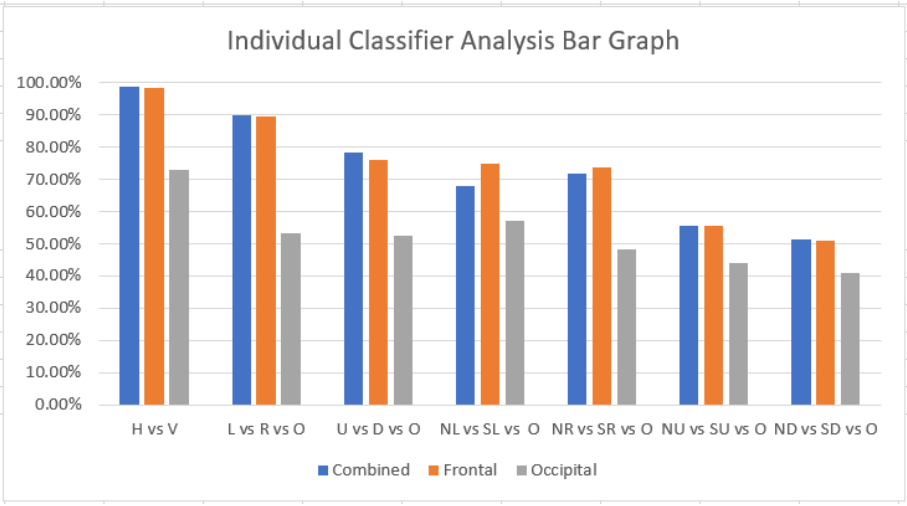

Figure 12: Classification Accuracies of the Individual Classifiers

As shown by the scatter plots in Figures 13, and 14, the CSP features for the 'H vs V' classifier are more linearly separable than the features for the 'L vs R vs O' classifier, especially that of the 'L vs R' classifier. The different levels of linear separability of the CSP features for the 'H vs V' and 'L vs R vs O' classifiers contribute to the difference in the accuracy of these two classifiers.

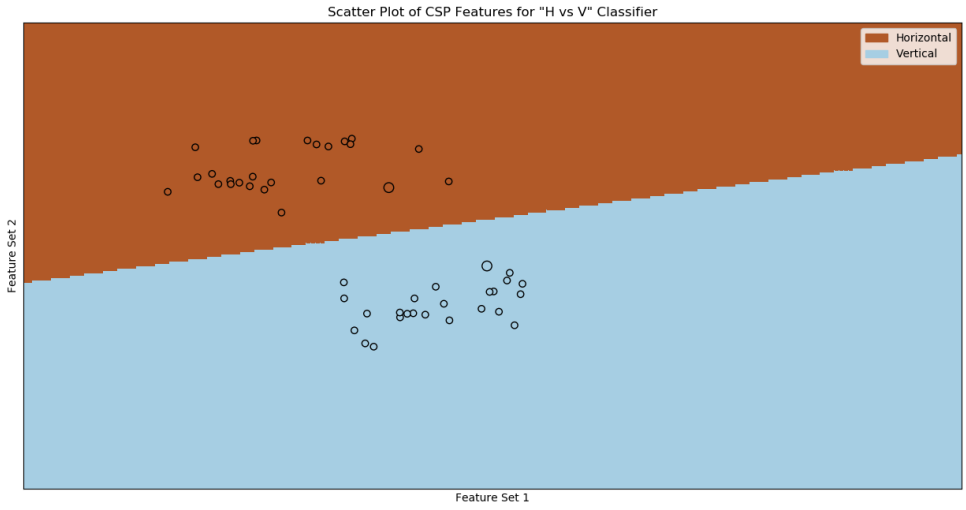

Figure 13: Scatter Plot of CSP Features for 'H vs V' Classifier

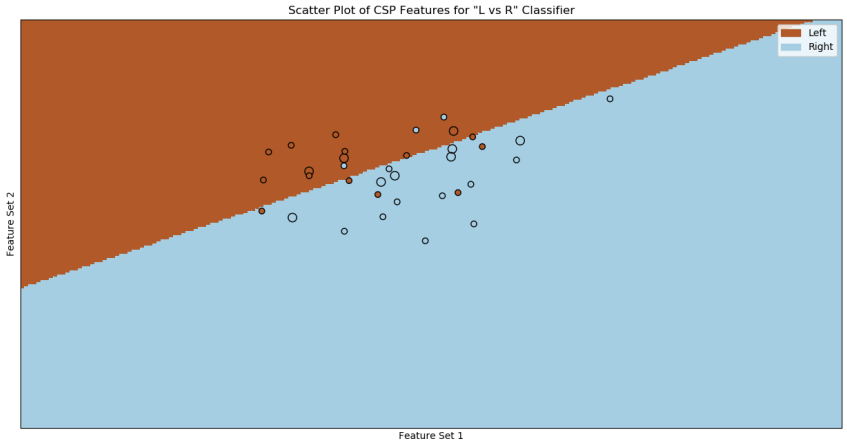

(a) Scatter Plot of CSP Features for 'L vs R' Classifier

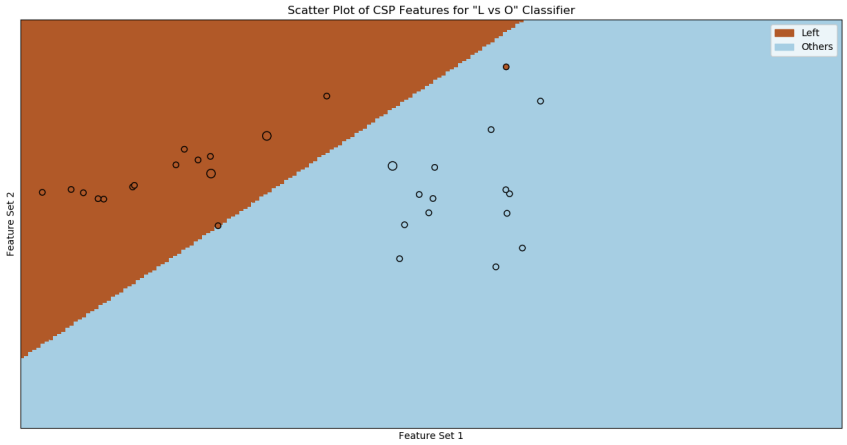

(b) Scatter Plot of CSP Features for 'L vs O' Classifier

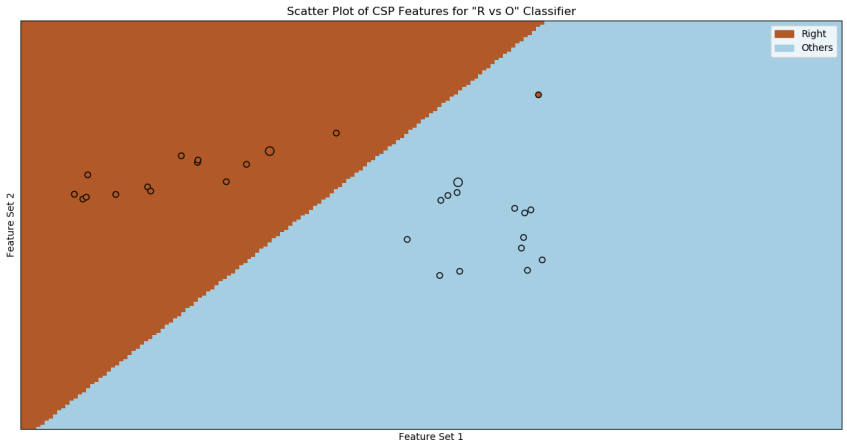

(c) Scatter Plot of CSP Features for 'R vs O' Classifier

Figure 14: Scatter Plots of CSP Features for 'L vs R vs O' Classifier

From the bar graph it is also evident that there is a substantial drop in the accuracy from the 'L vs R vs O' to the 'U vs D vs O' classifier considering the combined and frontal scalp regions. This can be explained by Figures 15a and 15b. One can observe that the signals at the channels *FT8, F8, AF8, AF7, F7, FT7* are inverted when comparing the Left glance to the Right glance. This spatial difference across the channels contributes towards a more effective CSP transformation and more discriminable features. On the other hand, for vertical glances the case is different. Figures 16a and 16b illustrate the EEG plots of an upward and downward eye movement respectively where it can be seen that only the central channels above the forehead are mostly affected. In relation to horizontal eye movements, vertical eye movements do not constitute much of spatial difference across the 'Up' and 'Down' classes, contributing to the drop with the classifiers accuracy mentioned above.

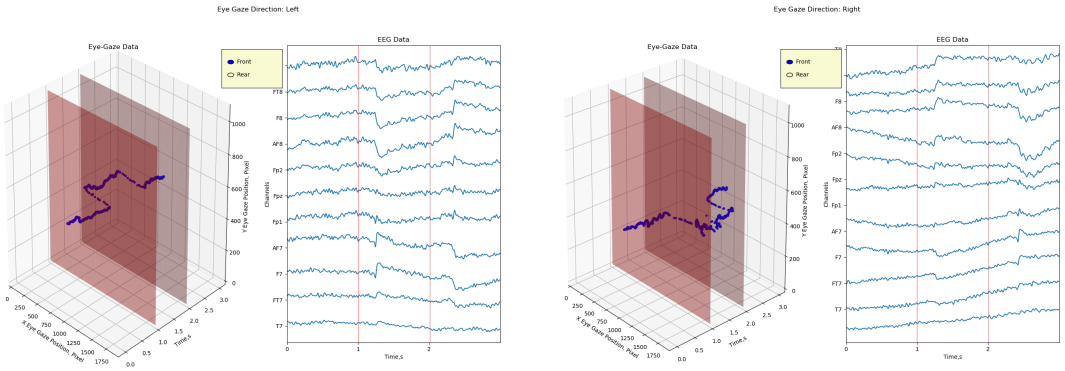

(a) EEG and Eye-Gaze Plot of a Leftward Glance

(b) EEG and Eye-Gaze Plot of a Rightward Glance

Figure 15: EEG and Eye-Gaze Plots for Horizontal Glances

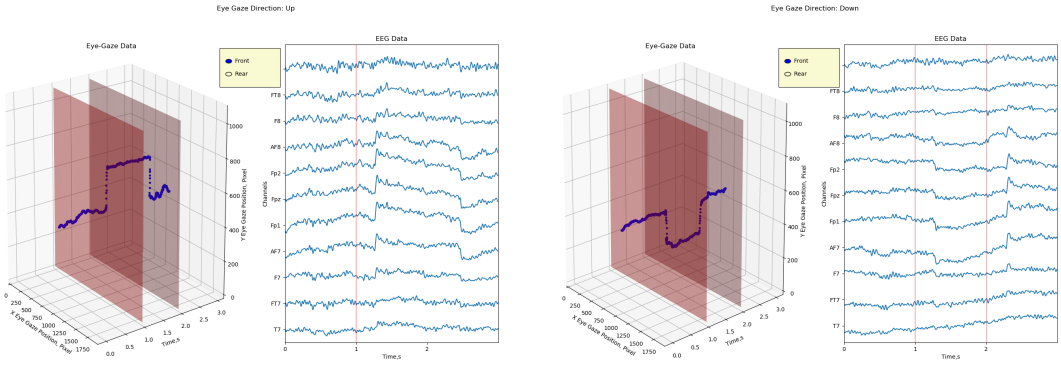

(a) EEG and Eye-Gaze Plot of an Upward Eye Movement

(b) EEG and Eye-Gaze Plot of a Downward Eye Movement

Figure 16: EEG and Eye-Gaze Plots for Vertical Eye Movements

Such a spatial difference is not clearly visible within the occipital channels, leading to the low classification rate shown in Figure 12. As can be seen from Figures 17a and 17b, which show the EEG plots of horizontal glances obtained from occipital channels, there is only a weak indication of spatial contrast between the two classes. This contributes to the significant drop in the accuracy of the classifiers from when frontal channels are considered to when occipital channels are considered.

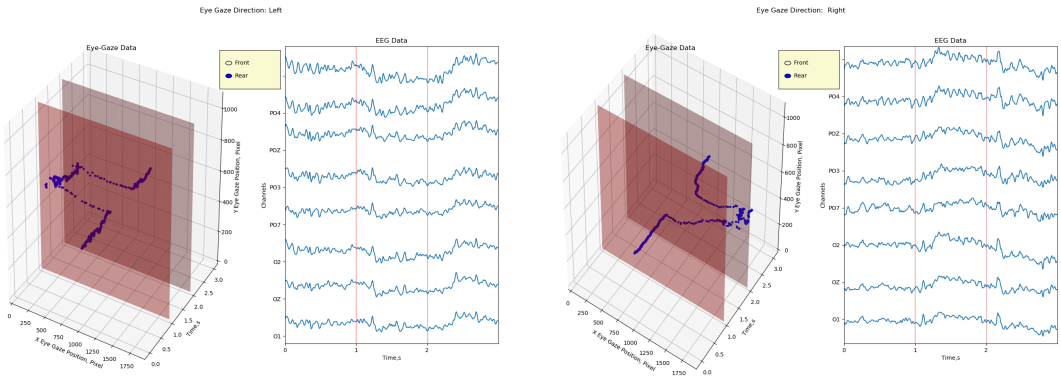

(a) EEG and Eye-Gaze Plot of a Leftward Eye Movement

(b) EEG and Eye-Gaze Plot of a Rightward Eye Movement

Figure 17: EEG and Eye-Gaze Plots for Horizontal Eye Movements Acquired from Occipital Channels

A similar argument can be applied for the low classification rates within the 3rd Tier classifiers ('L vs SL vs O', 'R vs SR vs O', 'U vs SU vs O' and 'D vs SD vs O'). Figures 18a and 18b portray the EEG plots of leftward glances. One can observe that there is no evident spatial contrast between the two plots.

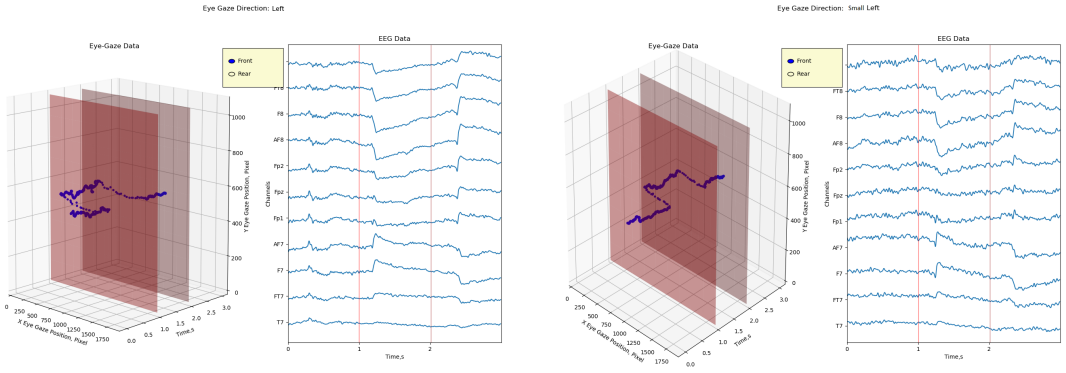

(a) EEG and Eye-Gaze Plot of a Leftward Eye Movement with Large Visual Angle

(b) EEG and Eye-Gaze Plot of a Leftward Eye Movement with Small Visual Angle

Figure 18: EEG and Eye-Gaze Plots for Leftward Eye Movements

4.2.2.2 Hierarchical Classifier

The hierarchical classifier system was tested as a whole unit. As tabulated in Table 9 found in Appendix A, accuracy scores were computed at each tier, determining how many trials were classified correctly in: i) one of either two classes ('Horizontal' or 'Vertical') at the first tier, ii) one of either four classes ('Up', 'Down', 'Left' or 'Right') at the second tier, and iii) one of either eight classes ('Normal Up', 'Small Up', 'Normal Down', 'Small Down', 'Normal Left', 'Small Left', 'Normal Right' and 'Small Right') at the third tier. Figure 19 shows the accuracy scores of the hierarchical system at various tiers for the various scalp regions while Table 8 shows the accuracy scores obtained by the individual classifiers which make up the hierarchical classifier. Both frontal and combined regions achieve close to 100% accuracy at the 1st tier, whereas this drops to 73% for the occipital region. At the second tier, the classification accuracy drops to 75% for both the combined and frontal regions, whereas the occipital region barely reaches 44%. At the third tier, the classification accuracy drops to 55% for the combined

and frontal regions while the occipital region only reached 26% accuracy rating.

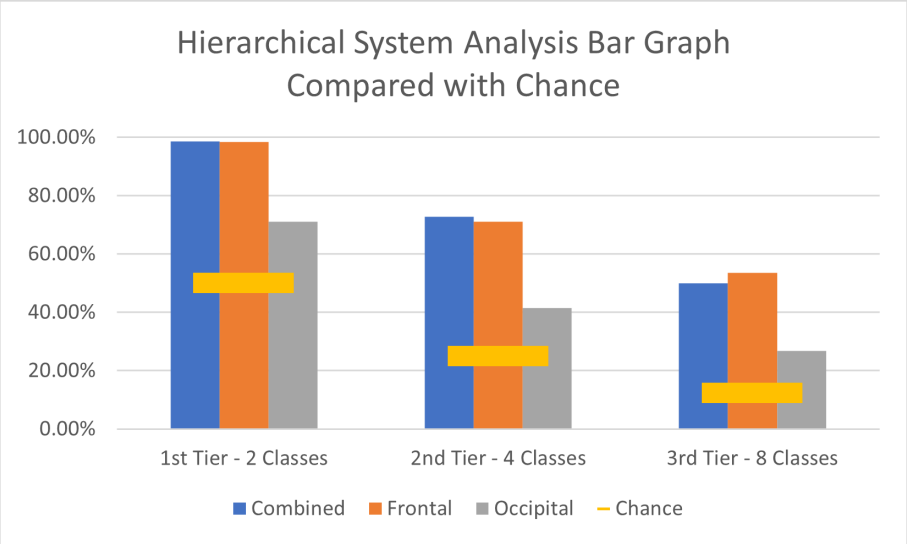

Figure 19: Hierarchical System Analysis Bar Graph Compared with Chance Levels

	Scalp Region Used		
	Combined	**Frontal**	**Occipital**
H vs V	98.9%	99.1%	76.3%
L vs R vs O	91.2%	89.0%	51.5%
U vs D vs O	75.5%	68.5%	49.6%
NL vs SL vs O	64.4%	72.8%	41.6%
NR vs SR vs O	65.4%	69.8%	34.0%
NU vs SU vs O	53.2%	53.3%	34.03%
ND vs SD vs O	46.9%	45.8%	33.5%

Table 4: Table of Results for Individual Classifiers making up the Hierarchical Classifier

Although the classification rates seem low at the lowest tier, they are still above chance level. Trials are first passed through the first tier of the hierarchical classifier which only consists of the 'H vs V' classifier. Since the output classes of the first tier consists of only the 'Horizontal' and the 'Vertical' class the probability by chance at this level would be 50%. Trials are then passed to the second tier of the hierarchical classifier which consists of the 'L vs R vs O' and the 'U vs D vs O' classifiers. Trials labeled as 'Others' by the 'L vs R vs O' classifier are handed to its sibling class within the tier, which in this case is a 'U vs D' classifier. Similarly, trials labeled as 'Others' by the 'U vs D vs O' classifier are handed to an 'L vs R' classifier for classification. Hence the output classes of the second tier amount to four classes which are the 'Up', 'Down', 'Left' and 'Right' classes, resulting in a probability by chance of 25% at the second tier. Trials are then passed to the third and final tier of the hierarchical classifier which consists of the 'NL vs SL vs O', the 'NR vs SR vs O', 'the 'NU vs SU vs O' and the 'ND vs SD vs O' classifiers. Similar to classifiers at the second tier of the hierarchy, trials classified as 'Others' by a classifier are passed to its sibling classifier within that branch. Trials labeled as 'Others' by the 'NL vs SL vs O' classifier are passed to a 'NR vs SR' classifier and conversely, trials labeled as 'Others' by the 'NR vs SR vs O' classifier are passed to a 'NL vs SL' classifier . Similarly, the same principle applies for trials labeled as 'Others' by the 'NU vs SU vs O' and 'ND vs SD vs O' classifiers. Hence the output classes of the third tier amount to eight classes which are 'Normal Up', 'Small Up', 'Normal Down', 'Small Down', 'Normal Left', 'Small Left', 'Normal Right' and 'Small Right', resulting in a probability by chance of 12.5% at the third tier. Even the occipital region, which seems to contribute towards the low classification rates, can at least double the chance for a correct prediction at the third tier. Meanwhile the frontal and combined regions managed to quadruple the chance for a correct prediction at the lowest tier.

Figure 20 portrays the confusion matrix at the 3rd tier for the combined region case. The confusion matrix shows that the trials with large visual angles were

classified better than their counterparts with a small visual angle. The confusion matrix also shows that most misclassifications occur within the third tier. In the case of the 'Small Down' class (7th row), 38.1% of the 'Small Down' trials were classified correctly as ' Small Down' but a significant 30.8% were misclassified as 'Normal Down'. The rest of the trials were misclassified as upward glances. Very few trials were misclassified as horizontal glances, attributing to the high classification rate of the 'H vs V' classifier which is shown in Figure 21a.

Figure 21a to Figure 21g show the confusion matrices of the individual classifiers making up the hierarchical classifier. Figures 21b and 21c show that for the 'L vs R vs O' and ' U vs D vs O' classifiers, few trials were misclassified as 'Others' in comparison with the classifiers in the third tier of the hierarchy, whose confusion matrices are shown in Figures 21d, 21e, 21f and 21g.

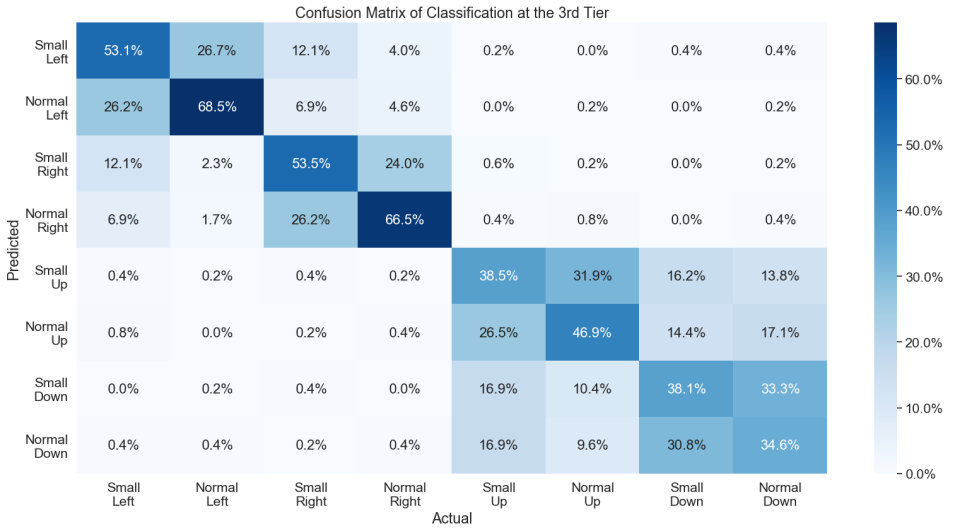

Figure 20: Confusion Matrix of Hierarchical Classifier at the 3rd Tier when jointly considering Frontal and Occipital Regions

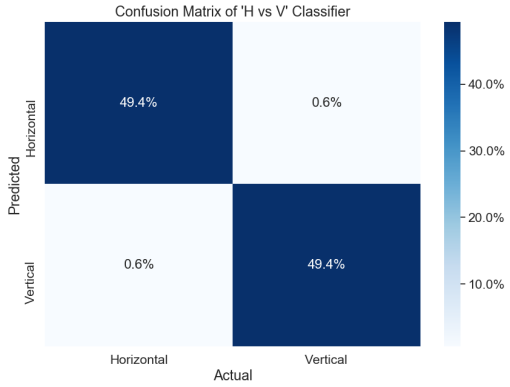

(a) Confusion Matrix of 'H vs V' Classifier

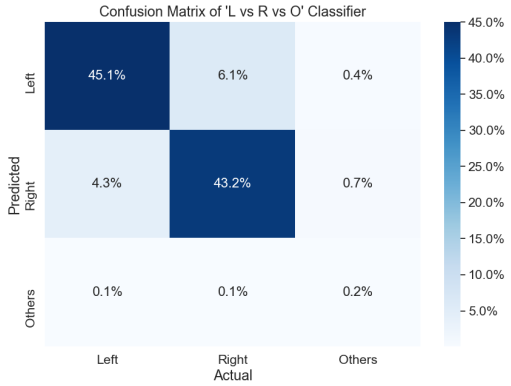

(b) Confusion Matrix of 'L vs R vs O' Classifier

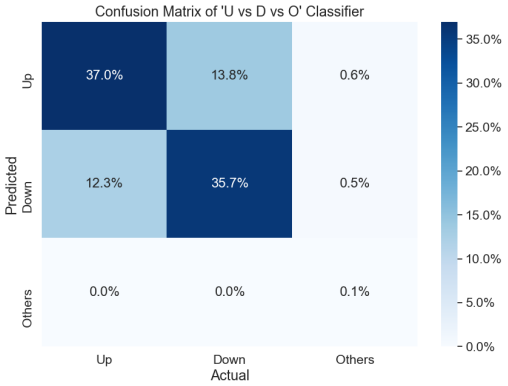

(c) Confusion Matrix of 'U vs D vs O' Classifier

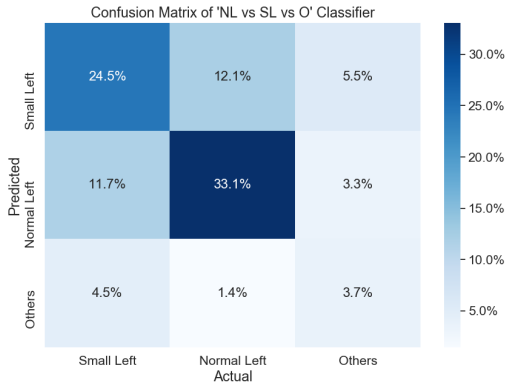

(d) Confusion Matrix of 'NL vs SL vs O' Classifier

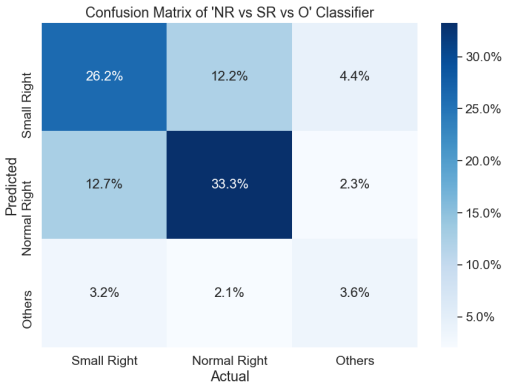

(e) Confusion Matrix of 'NR vs SR vs O' Classifier

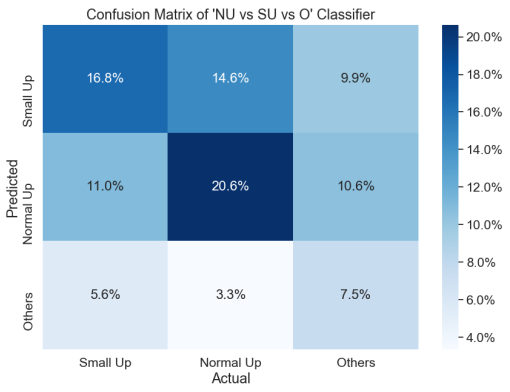

(f) Confusion Matrix of 'NU vs SU vs O' Classifier

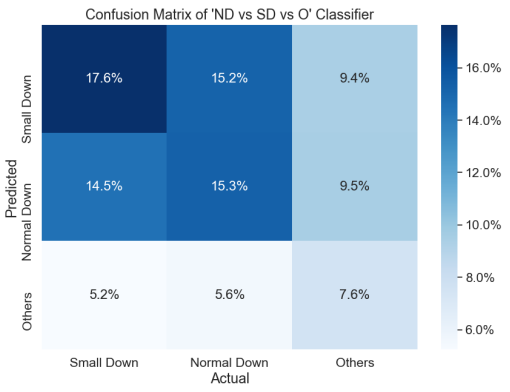

(g) Confusion Matrix of 'ND vs SD vs O' Classifier

Figure 21: Confusion Matrices of Individual Classifiers making up the Hierarchical Classifier when jointly considering Frontal and Occipital Regions

4.2.2.3 Individual Classifier and Hierarchical Classifier Analysis using only Trials with a Large Visual Angle

A similar analysis as the above was carried out considering only those trials with a large visual angle. This was done to assess whether the trials with a small visual angle, have any effect on the classification accuracy. As in this analysis we are only considering one type of visual angle, then automatically the classifiers within the third tier were excluded as the role of the third tier is only to classify between the extent of visual angle. To determine whether the trials with a small visual angle are affecting the classification accuracy in any manner, the trials with a small visual angle were omitted out of the training set. Hence the results shown in Figure 22 were obtained with only half the number of training trials used for the above analysis. The accuracy results obtained at the second tier of the hierarchical classifier are labeled under an 'L vs R vs U vs D' classifier. These results are then compared with the results portrayed in Figure 12 and Figure 19 to determine the effect of the trials with a small visual angle on the classification accuracy.

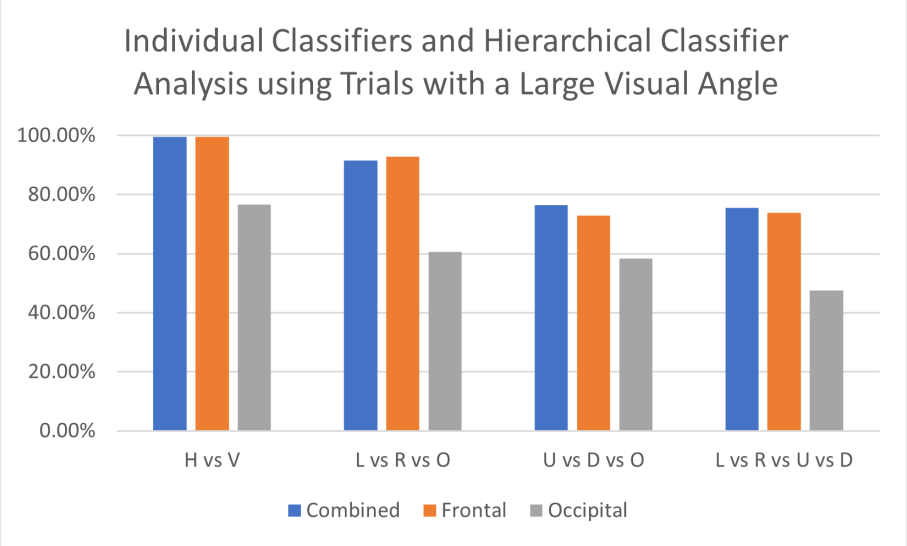

Figure 22: Classification Accuracies of Four Different Classifiers using only Trials with a Large Visual Angle

Figure 23 compares the performances of the respective classifiers shown in Figure 22 with those shown in Figures 12 and 19. It can be seen that the same performance was approximately obtained for the classifiers when considering the 'Combined' and the 'Frontal' case, despite that the results of Figure 22 were obtained with only half the number of training trials used for the other figures.

However for the 'Occipital' case, a substantial difference was found between the two methods. The method which considered only the 'Large Visual Angle' trials produced better results than the method which used trials with both small and large visual angles. Hence the subsequent analyses were carried out with trials of a large visual angle, as it either achieves the same or better performance than the other method, with just half the size of the training set.

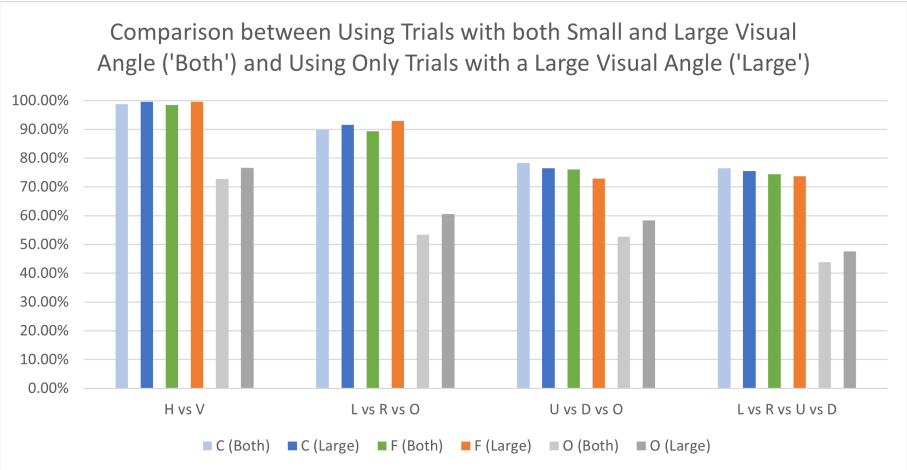

Figure 23: Comparison of the Classification Accuracies for Four Different Classifiers when using Trials with Both Small and Large Visual Angle ('Both') against using only Trials with a Large Visual Angle ('Large') for the Combined 'C', Frontal 'F' and Occipital 'O' case.

4.2.3 Results of Analysis of Frontal Channels

An analysis was carried out to investigate how the number of frontal electrodes affects the accuracy. For the purpose of this analysis, the frontal channels were omitted out, two at a time, as shown in Table 2 in Section 4.1.5.4. Figure 24 shows the results obtained for the different number of frontal channels taken into consideration.

Although this analysis concerns the frontal channels, this analysis is also extended to when the frontal and occipital are jointly considered. In this case, the electrodes within the occipital region are all kept and the frontal electrodes are reduced two at a time. Figure 25 shows the effect of the reduction in frontal channels on the accuracy.

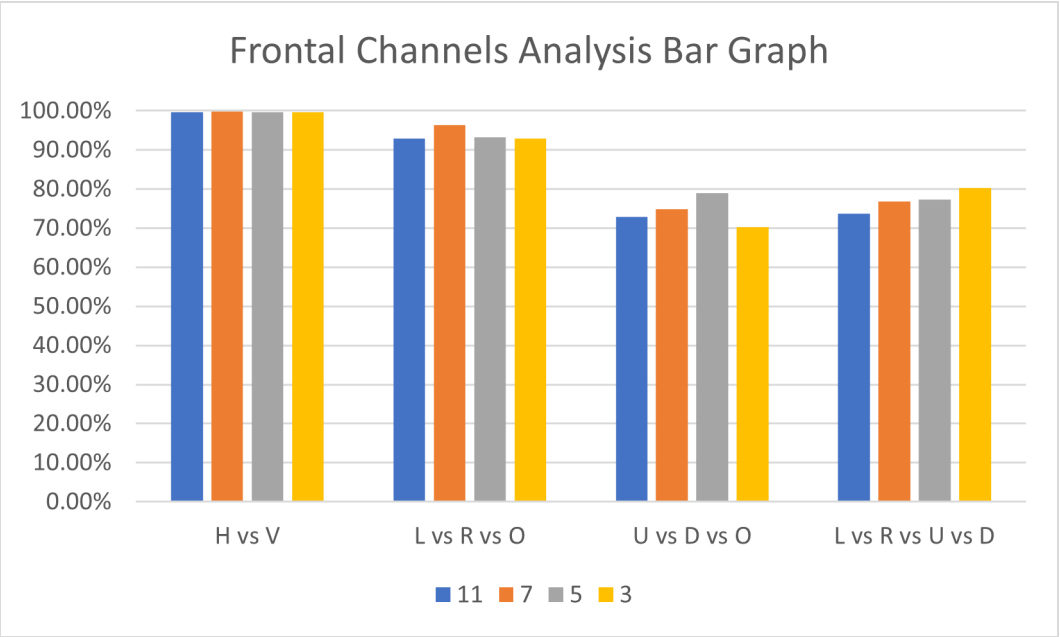

Figure 24: Classification Accuracies of Four Different Classifiers when considering 3, 5, 7, or 11 Frontal Electrodes and considering Frontal Region only

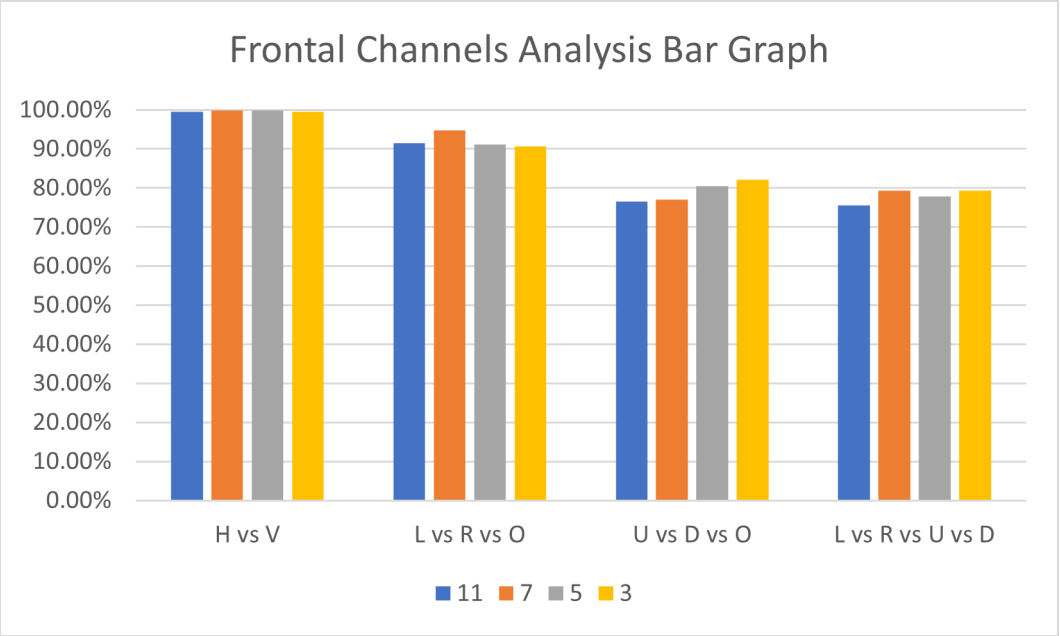

Figure 25: Classification Accuracies of Four Different Classifiers when considering 3, 5, 7, or 11 Frontal Electrodes and jointly considering Frontal and Occipital Regions

When considering only the frontal channels, a substantial difference was found in the performance of the 'U vs D vs O' classifier when the number of frontal electrodes was reduced from 11 to 5, suggesting that channels *T7, FT7, F7, F8, FT8* and *T8*, being the six channels omitted, hinder the classification of vertical saccadic eye-movements. A substantial difference in the performance of the 'U vs D vs O' classifier was also noted when using both frontal and occipital regions, with a change in performance occurring when the number of frontal electrodes was reduced from 11 to 3. Except for the 'U vs D vs O' classifier, the performances of the classifiers remain effectively the same as the number of frontal electrodes is reduced. Differences in performance of these three classifiers were not found to be significant. Therefore, a sufficiently good performance may be expected to be achieved with just three frontal electrodes placed at *AF7, Fpz* and *AF8*.

4.2.4 Results of Training Data Requirements Analysis

The purpose of this analysis is to investigate how the training set size affects accuracy. In this analysis, the performance of the classifiers was evaluated across the number of training trials used. This analysis was carried out with 16, 8 and 4 training trials/class. Figures 26a, 26b 27a and 27b illustrate how the classification accuracy of each classifier varies with the size of the training set.

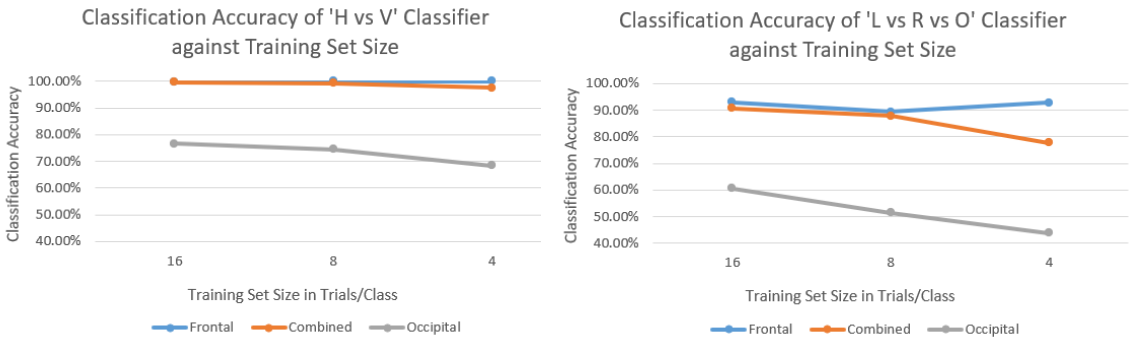

(a) 'H vs V' Classifier (b) 'L vs R vs O' Classifier

Figure 26: Classification Accuracies of 'H vs V' and 'L vs R vs O' Classifiers Against Training Set Size of 16, 8 and 4 Trials/Class

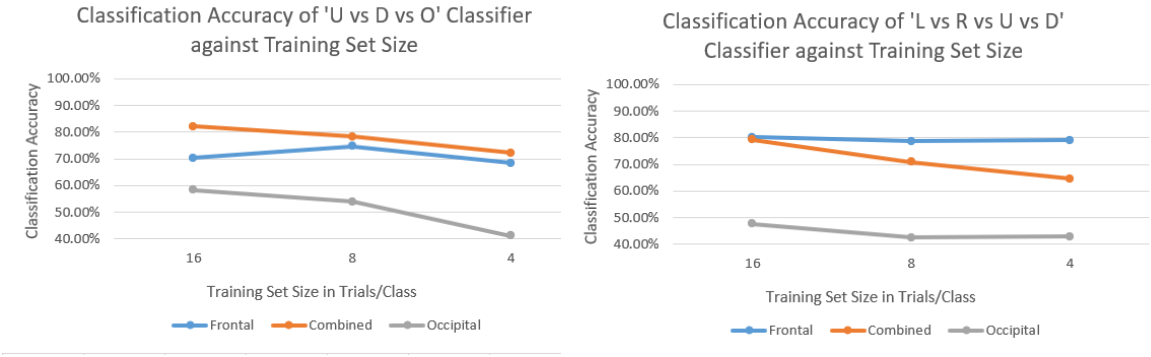

(a) 'U vs D vs O' Classifier (b) 'L vs R vs U vs D' Classifier

Figure 27: Classification Accuracies of 'U vs D vs O' and 'L vs R vs U vs D' Classifiers Against Training Set Size of 16, 8 and 4 Trials/Class

When using the frontal channels, the performances of all the classifiers remain effectively the same as the training set size is reduced, indicating that with the frontal channels, the class features are well clustered, requiring only few samples for training. Conversely, when using the occipital channels, the performances of all the classifiers monotonically decrease as the training set size is reduced, thus requiring more samples for better performance, although the best performance is very much lower than that of the frontal channel classifiers. The same decreasing trend in performance is also observed for the classifiers when using both the frontal and occipital channels, with the largest decrease in performance occurring when the number of training trials is reduced from 8 trials/class to 4 trials/class.

Therefore, best performance may be expected to be achieved with frontal channels even if few training examples per class are used. However, if only occipital channels are to be used, in view that the hybrid BCI is based on SSVEP which are optimally detected using occipital channels, then a training set of 16 trials/class would be recommended although it would typically result in a longer training time.

4.3 Conclusions drawn from the EEG-based Eye-Gaze Study

Several conclusions were drawn from the EEG-based eye-gaze offline analysis. Specifically, eye movements can be classified into horizontal or vertical eye movements with an accuracy of 98.47%. Eye movements can be further classified into four classes; leftward, rightward, upward or downward eye movements with an accuracy of 74.38%. It was also concluded that eye-movements can be classified into eight classes with an accuracy of 58.31%. The eight classes consisted of eye-movements in the four directions where each direction involved two visual angles, amounting to eight classes.

Eye movements in the same direction but having different visual angles were also concluded to be reliably classified. Leftward eye movements with a large visual angle were correctly classified from their small visual angle counterpart with an accuracy of 74.79%. Similarly, rightward eye movements can be labelled correctly with an accuracy of 73.68%. Upward and downward eye movements can be classified into two types of visual angles but with a lower accuracy of 55.56% and 50.97% respectively.

From this study it was also concluded that reliable eye-movement information can also be extracted from the occipital region alone. Eye-movement-related occipital signals can be categorised into horizontal or vertical eye movements with an accuracy of 76.67%. Furthermore, eye movements can be further labelled into left, right, up or down with an accuracy of 47.6%.

A study was also conducted to observe how the classification accuracy varies with the number of frontal channels considered and with the size of the training set. When the number of frontal channels was reduced, differences within the classification accuracies of most classifiers were found to be negligible. The size of the training set also had negligible impact on the classification accuracy when considering frontal channels only. On the other hand when considering only

occipital channels, substantial differences were found when the size of training set was varied.

4.4 Chapter Summary

This chapter detailed the signal processing methods for the EEG-based eye-gaze analysis which was aimed to identify whether different eye movements could be reliably classified using EEG signals recorded from the frontal and/or occipital brain regions.It gave a thorough description of the CSP algorithm, which was used to extract features from the EEG signals and the SVM algorithm, classifying the EEG signals upon the said features retrieved from them. It described the experimental protocols by which the EEG data was acquired and discussed the methodology by which the analyses were carried out. This chapter also presented the results of the analyses. A discussion of the results then followed, and the conclusions drawn, which will be used to construct the hybrid BCI discussed in the next chapter, were highlighted.

5 Smart Home Hybrid BCI

Based on the conclusions drawn in the previous chapter, a smart home hybrid BCI was designed and implemented. This chapter is divided in two sections; the first covers the methods used to construct the smart home hybrid BCI and the methodology by which the performance of the smart home hybrid BCI is evaluated and the second presents and discusses the results of this evaluation.

5.1 Methods and Methodology

In this section, the design of the smart home BCI application is discussed in detail. In the first part of the section, the frontend and backend of the application are explained. Algorithms used in addition to those described within Section 4.1.4 are then discussed, followed by a description of the experimental paradigms used for the comparative analysis which compared the performance of the proposed smart home hybrid BCI against a standard SSVEP-based smart home BCI.

5.1.1 System Architecture

Similar to the EEG-based eye-gaze analysis, a computer system with a 22 inch monitor, a resolution of 1920×1080 pixels and a refresh rate of 60Hz, was used. The g.USBamp from g.tec [36] was used again for EEG data acquisition. EEG data was acquired within a model compiled in SIMULINK, which was then transferred to a Python application for processing as explained in Section 5.1.1.2. Various Internet-of-Things (IOT) devices were used to create a smart home network operable from the computer system as described in the next section.

5.1.1.1 Hardware Description

The smart home system is designed as a network having a star topology. Nodes are connected to a central device, known as a hub. The hub receives requests from the nodes, processes them and relays the information and instructions accordingly to other nodes. Smart home networks can either be designed

from scratch by investing in smart home appliances, like smart TVs with internet connectivity or installed for conventional home appliances through the use of interface devices. Interface devices make conventional home appliances smart by making them operable by an alternative method other than conventional means. For this project the second method was opted for. Figure 28 illustrates the smart home network implemented for this project.

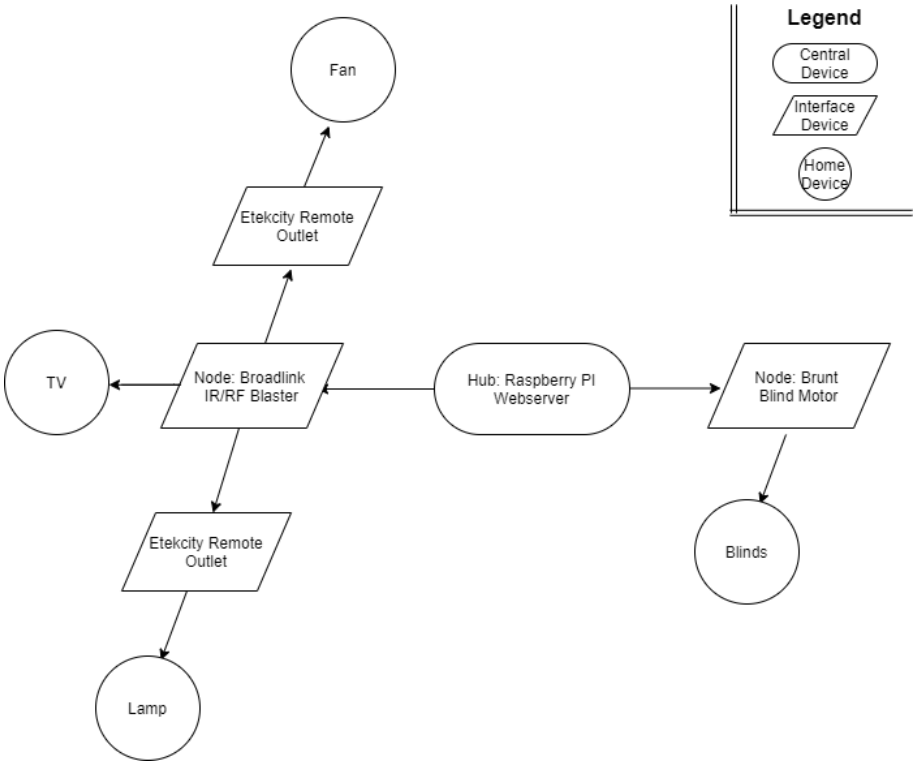

Figure 28: Hardware Infrastructure of Smart Home Network

Etekcity remote outlets [26] were used to provide remote control for power outlets within the smart home environment. Remote outlets mainly consist of a single-pole relay which connects the household powerline to the power inlet of a particular device. This relay is operated via a radiofrequency signal of 433MHz. Despite their remote operability, these can still provide a substantial amount of power to the connected load amounting to 2.4kW. For this project, two remote outlets were used. One was to switch on and off a standing fan and the other one

used to switch on and off a desk lamp.

A Universal Remote RM3 Pro from Broadlink [48] was used to operate IR and RF devices. The Broadlink IR and RF blaster learns the IR and RF codes from the remotes of the appliances and replicates the codes to control the same appliances. RF technology offers a larger coverage and is not sensitive to sensor directionality, however, it is prone to interference. On the other hand, IR technology is difficult to intercept, is much cheaper than its counterpart and offers more flexibility with its codes. Generally, audiovisual equipment makes use of IR technology while garage-door openers and motorised blinds utilise RF technology. For this project, the universal remote was used to operate the Etekcity remote outlets. It was also used to control a TV set via IR. The universal remote was programmed to execute: the power-on, volume-up, volume-down and mute commands.

The Brunt Blind Engine from Brunt [14] was used to convert the existing blinds into smart ones. This device mainly consists of a 12V DC motor with a rated speed of 41rpm and a rated torque of 1.96Nm. A gear is attached directly to the motor shaft in order to mesh with the beads of the blind, making the blind motorised. The DC motor is controlled via WiFi and hence it is directly connected to the webserver. In contrast with the Universal Remote RM3 Pro IR/RF device, Wi-Fi allows a two-way communication between the hosts and the hub. This interface device can rotate the vertical blinds to any particular angle. However for this project, the system will allow the user to rotate the blinds to either a 0° or a 90° angle.

A Raspberry Pi 3B+ was used to connect all the interface devices together, acting as the central device within the star network portrayed in Figure 28. The Raspberry Pi 3B+ can be thought of as a microcomputer as it houses a 1.4 GHz, 64-bit quad-core processor with a 2.4GHz IEEE 802.11.b/g/n/ac wireless LAN and an embedded 1GB LPDDR2 SDRAM [78]. As a central hub it acts as a

webserver for the Home Assistant platform which caters for the software side of the smart home network as described in the next section.

5.1.1.2 Software Description

The software infrastructure of the smart home network was catered for by the Home Assistant platform [64]. Home Assistant is an open-source home automation platform which runs on a Python 3 engine. The Home Assistant platform allows designers to control their IOT devices via several entities. For the purpose of this project only three such entities were used; 'switch', 'cover' and 'script'. The switch entity is used for those IOT devices whose operation is limited only to a toggle operation, that is, a switch-on or a switch off operation. Therefore, the Etekcity remote outlets, which can only toggle the power of the appliance connected to them, were configured as switch entities. The cover entity is used for those IOT devices which can either be fully open, fully closed or any position between the two extreme states. The Brunt Blind Engine which is used to operate the blinds of a window, was configured as a cover entity. The script entity provides the smart home designer with further flexibility. Script entities allow one to combine multiple commands into one. For the purpose of this project, the different TV commands available within the smart home BCI application were configured as script entities.

Frontend

A menu for the smart home BCI application was designed using PsychoPy [74] as illustrated in Figure 29. Menu options were depicted as black icons on plain white squares. White squares were used as flickering targets to evoke the SSVEP response within the user. The icons were designed with a transparent background so as not to hinder the flickering of the squares underneath. The menu options were presented in a cross configuration to utilise the eye-movement classifiers mentioned in Section 4.1.5.1. The eye-movement classifiers allow the user to halve the number of flickering stimuli by performing a horizontal or a vertical eye movement.

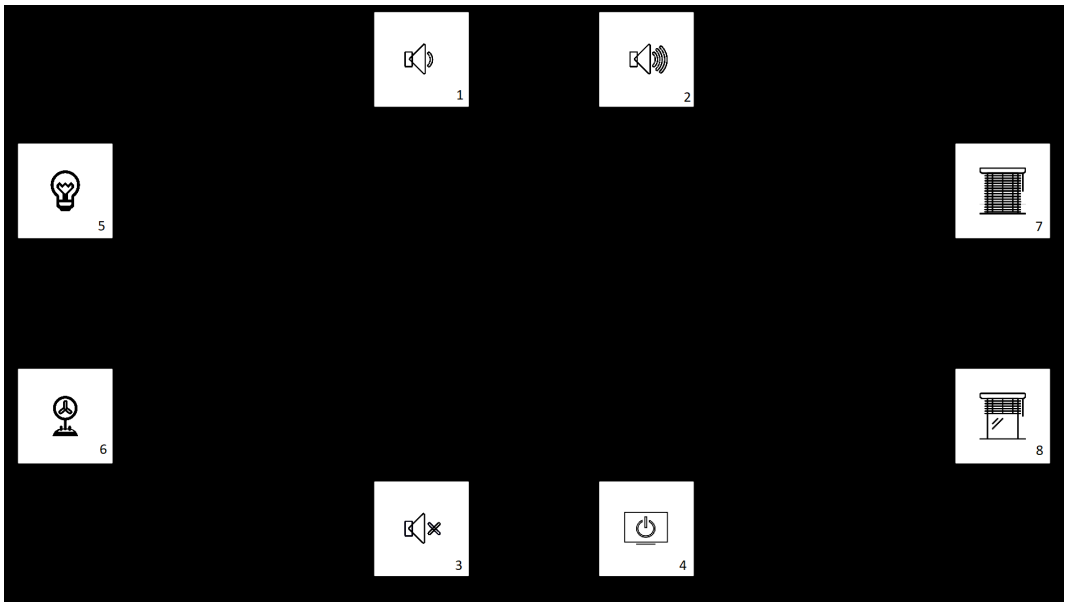

Figure 29: Menu Layout of Smart Home BCI Application

Commands associated with the TV were categorised within the vertical part of the cross. Those related to muting or powering the TV were placed in the lower part of the cross while those related to increasing or decreasing the volume were placed in the upper part. The 'Volume Increasing' button was placed on the right while the 'Volume Decreasing' was placed on the left as found within typical TV remotes. Commands associated with the blinds were placed on the right while those associated with powering the lamp and fan, were placed on the left.

In total, eight options were included within the menu. As explained later in Section 5.1.3 each option takes 4.75 or 5.5 seconds when using the SSVEP-based or hybrid system respectively. The actions performed by the menu options are explained below. For the sake of the explanation, small numbers were added to each icon within the menu portrayed in Figure 29.

1. Decrease the volume of the TV set by five bars
2. Increase the volume of the TV set by five bars
3. Mute the TV set
4. Switch on or off the TV set
5. Switch on or off a lamp
6. Switch on or off a standing fan
7. Close the window blinds
8. Open the window blinds

The fourth, fifth and sixth command execute a toggling operation of the device. Hence their corresponding icons were changed according to the status of the device. Figures 30, 31 and 32 portray how the icons were changed according to the power status of the device.

(a) TV in Off Mode (b) TV in On Mode

Figure 30: Icons for Different Statuses of the TV Set

(a) Lamp in Off Mode (b) Lamp in On Mode

Figure 31: Icons for Different Statuses of the Lamp

(a) Fan in Off Mode

(b) Fan in On Mode

Figure 32: Icons for Different Statuses of the Fan

Backend

As per the nature of BCIs, EEG data needs to be acquired from the user while he or she is focusing on selecting a menu option. Therefore, through a multiprocessing environment, two simultaneous computational processes were created in a Python script to manage the entire smart home BCI application. A parent process handles the presentation of the stimuli, the processing of the EEG data and the communication with the smart home network server, while a child process is created with the sole purpose of handling the acquisition of EEG data from the user. The EEG acquisition process was developed within a SIMULINK model, interfacing the physical EEG equipment with the code scripted in Python. A Transmission Control Protocol (TCP) socket is created to handle the transfer of EEG data from the Simulink model to the child process in Python.

Communication between the two processes is carried out using two different types of communication channels, namely, Pipe and Queue [99]. A pipe is used to send instructions from the parent process to the child process to commence the recording of the EEG data available within the TCP socket. Once the related instructions were received by the child process, EEG data is recorded for a predetermined length of time. As the recording is finished, the EEG data block is sent from the child process to the parent one via a queue. Once received by the parent process the data block is processed as explained in Section 5.1.4, and the user selection is computed. Its relevant command is communicated to the smart home network server. The communication with the network hub is being carried

out by means of an API provided by the Home Assistant platform [64]. Figure 33 illustrates the processes mentioned above in a flowchart format.

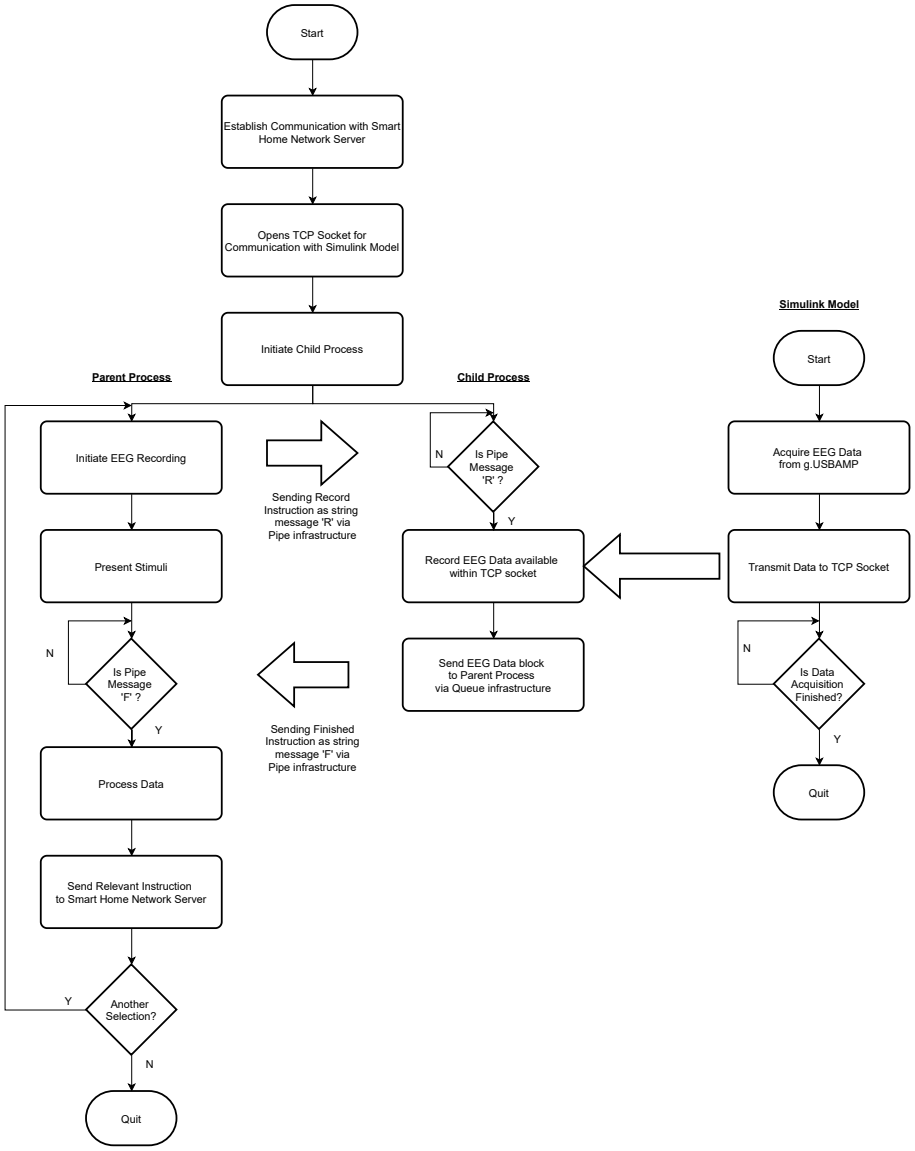

Figure 33: Software Flowchart of Smart Home BCI Application

5.1.2 Participating Subjects and Experimental Setup

Five (three male and two female) healthy subjects participated for this study. The research study was approved by the University Research Ethics Committee (UREC) of the University of Malta (UREC Code:1905). Every participant was seated in front of an LCD monitor. This was placed at approximately eye-level with the subject. Participants were also advised to limit their physical movement to avoid the coupling of EMG artifacts with the recorded data.

EEG data was recorded at a sampling frequency of 256 Hz from a total of 11 channels. Eight of these channels were in the occipital region while the rest were in the frontal region. In contrast with the eye-gaze analysis carried out in the previous chapter, only three frontal channels were used for this analysis. As explained earlier in Section 4.2.3, it was concluded that three frontal channels suffice for this hybrid BCI. Hence the final set of EEG channels consisted of O1 , Oz , O2 , PO7 , PO3 , POz , PO4 , PO8, AF7, Fpz, and AF8.

5.1.3 Experimental Paradigm for the Comparative Analysis

A comparative analysis was carried out to compare a hybrid BCI which fuses EEG-based eye-movement-potentials with SSVEPs and a conventional SSVEP-based BCI. For the purpose of this project, two different types of hBCIs were designed, namely, a sequential hybrid BCI and a mixed hybrid BCI. In the sequential hBCI, an eye-movement is first detected and classified as either horizontal or vertical. Once the eye movement is determined, the options in the application menu are halved as illustrated in Figure 34a and Figure 34b. The stimulating period then commences, and the remaining icons start flickering so that the attended icon is selected with the SSVEP detection algorithm explained in Section 5.1.4.2. The mixed hBCI functions in a similar manner, however, the attended icon is selected by a fusion of the SSVEP detection algorithm and the eye-movement detection algorithm as explained in Section 5.1.4.3. A separate HCI, which utilised only EEG-based eye-movement potentials, was also developed and compared with the SSVEP-based BCI and hybrid BCIs.

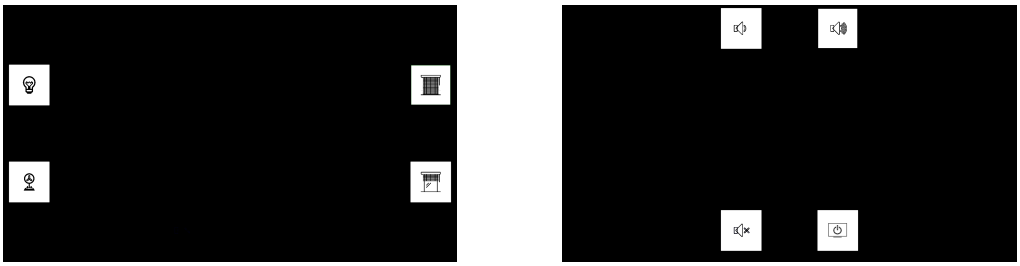

(a) Resulting Menu after a Horizontal Eye-Movement

(b) Resulting Menu after a Vertical Eye-Movement

Figure 34: Different Menus According to the type of Eye Movement Detected

The comparative analysis was first carried out offline and then online. The purpose of the offline analysis was to find an optimal stimulating window time across all the five subjects. The purpose of the online analysis was to compare and contrast the performances of the different HCIs. These include the SSVEP-based BCI, the sequential hBCI and the mixed hBCI. Although the purposes of the sessions were different, the paradigms and timings of the experiments were common throughout the two sessions.

Prior to each session, a training session of 72 seconds long was carried out. The purpose of the training session is to collect EEG-based eye-movement-potentials pertaining to four classes (Up, Down, Left and Right). Similar to the protocol for the EEG-based eye-gaze analysis described in Section 4.1.3, users were instructed to follow a white cross with their eyes as it shifts to one of four positions on the screen (Central Top, Central Bottom, Central Left or Central Right) as shown in Figure 35. Four trials were carried out for each class. Figure 36 shows the timings of one such trial. The data collected from the training session was then used to construct CSP and SVM models to classify the user's eye movements within the hBCI system. Training sessions were only required for the EEG-based eye-movement acquisition part, as the SSVEP-recognition part employed unsupervised learning techniques and hence did not require any training sessions.

Figure 35: Calibration Points Presented during the Eye-Gaze Training Session

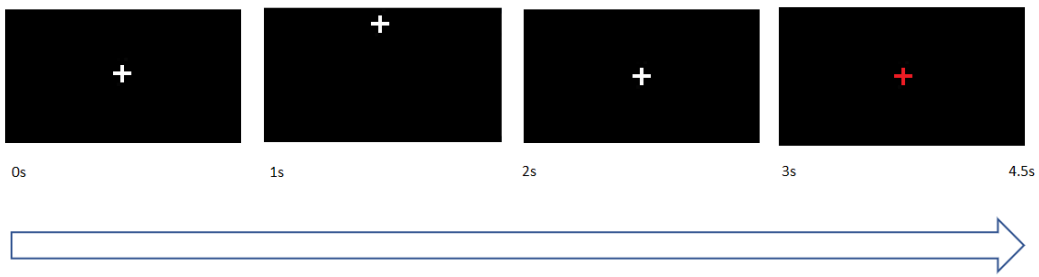

Figure 36: Timing Protocol for One Training Trial in Training Session

Following the training session, the actual experiment was conducted. For the SSVEP-based BCI, the user was allocated 0.75 seconds to shift his gaze towards the target. Another 3 seconds were allocated to the flickering of the stimuli, required to evoke the SSVEPs within the user's neurosignals. A feedback period of 2s [30] then followed to provide visual biofeedback to the user. The timings are portrayed in Figure 37 below.

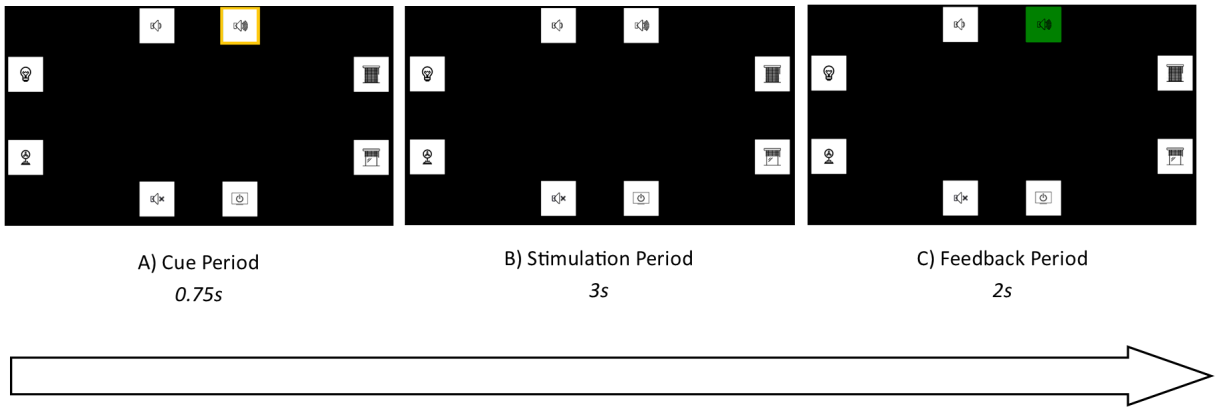

Figure 37: Timings for Execution of One Trial for SSVEP BCI

For the hybrid BCI, an additional 0.75 seconds was allocated prior to the 'gaze shift' or 'cue' period. In this short interval the user is instructed to focus on a central cross. Recentering of the user's gaze is essential for correctly classifying the user's eye movement. During the succeeding 'gaze shift period', the eye movement is detected by the system. The system then classifies the glance as either horizontal or vertical, and depending on the prediction outcome, removes half of the options. Figure 38 and Figure 39 illustrate the timings of the second experiment should the user make a horizontal selection or a vertical selection respectively.

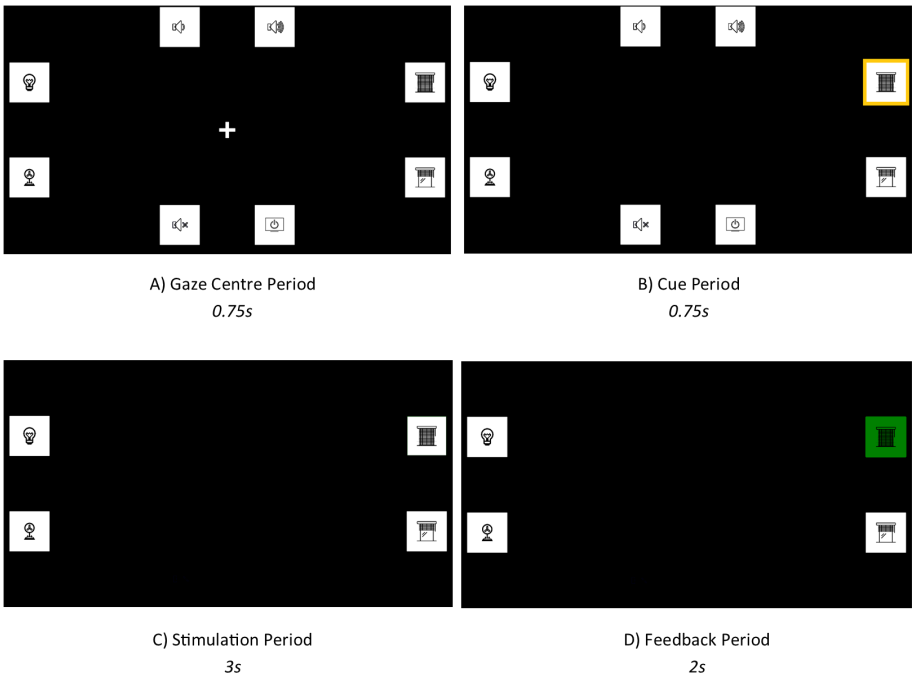

Figure 38: Timings for Execution of One Task for hybrid BCI: Horizontal Selection

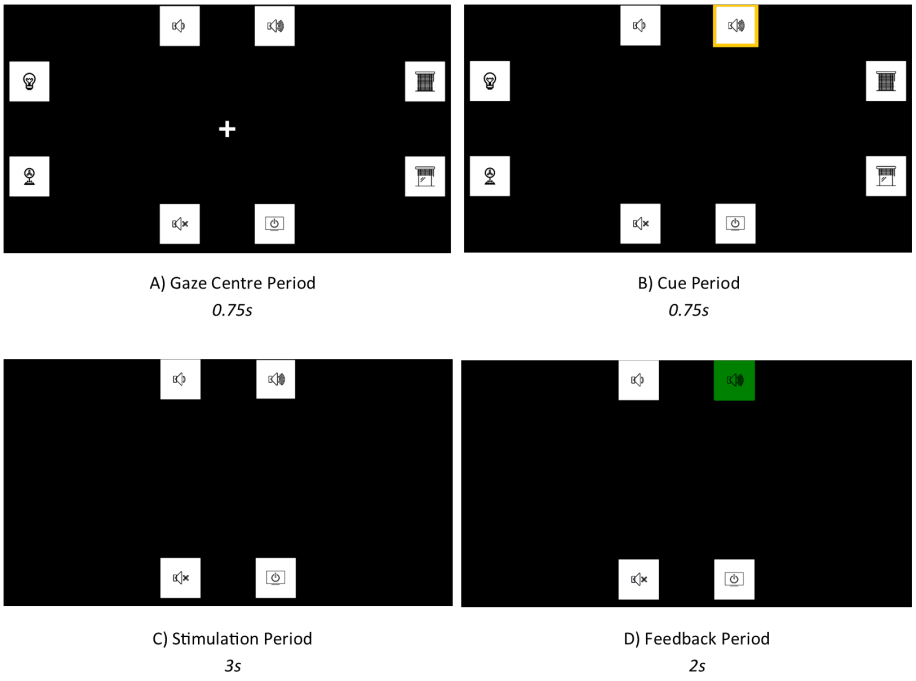

Figure 39: Timings for Execution of One Task for hybrid BCI: Vertical Selection

For the offline session, an additional HCI was taken into consideration. The additional HCI utilised only EEG-based eye-movement potentials. The performance of such a system is optimal when the layout of the menu is in the form of a cross as portrayed in Figure 40. For this HCI, the stimulation period was removed. Users were instructed to center their gaze and then shift their gaze according to the location of the target. The system then classifies the glance as one of eight classes, selecting an icon. Figure 40 illustrates the timings of the third experiment. A separate training session was conducted for this additional HCI.

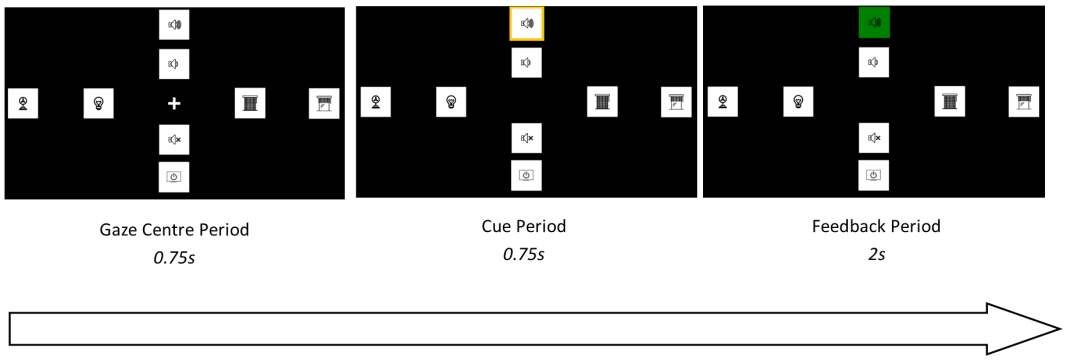

Figure 40: Timings for Execution of One Task for EEG-based Eye-Gaze HCI

The offline session consisted of three exercises, one for each different HCI architecture. Hence an exercise was carried out for:

- SSVEP-based BCI
- Hybrid BCIs
- Eye-movement EEG-based HCI

Since both hybrid BCIs share the same menu layout and paradigm, a single exercise was sufficient for both. Each exercise consisted of 24 trials. In a trial the subject was instructed to select the icon indicated by the cue. The cue was determined in such a way that each icon is selected three times in an exercise.

The online session also consisted of three exercises, one for each different BCI architecture. Hence an exercise was carried out for:

- SSVEP-based BCI
- Sequential Hybrid BCI
- Mixed Hybrid BCI

In the online session, subjects were asked to execute 3 different tasks consisting of three consecutive commands each. The three tasks were designated as follows:

1. Task 1
    (a) Switch on the TV set
    (b) Close the window blinds
    (c) Decrease the volume of the TV set
2. Task 2
    (a) Open the window blinds
    (b) Switch on the standing fan
    (c) Increase the volume of the TV set
3. Task 3
    (a) Switch on the lamp
    (b) Mute the TV set
    (c) Close the window blinds

For each command the subject was allowed three consecutive attempts to correctly select the scheduled icon. If the user did not manage to generate the necessary SSVEP and the system thus did not succeed in correctly detecting the target after three attempts, the application executed the intended command and progressed on to the following pre-defined cue.

5.1.4 Algorithms used for the Comparative Analysis

Three algorithms were needed for the comparative analysis: (i) An eye-movement classification algorithm which classifies the eye-movements detected; (ii) an SSVEP classification algorithm which processes and classifies the SSVEP response of the subject; and (iii) a fusion algorithm for the mixed hybrid BCI system which fuses the output of the eye-movement classification algorithm with the SSVEP classification algorithm.

5.1.4.1 Eye-Movement Classification Algorithm

The same algorithms used in the offline analysis described in Section 4.1.4 were used in the online experiment. The EEG trials obtained in the experiment were filtered with a 4^{th} order IIR bandpass filter having cut-off frequencies at 0.5Hz and 7Hz. The trials were then projected into CSP space. The natural logarithm was applied to the variance of the resulting signals and these were used as features to SVM classifiers. Seven pairs of CSP and SVM models, as listed below, were compiled from the training data obtained from each user prior to the experiment.

- Horizontal vs Vertical Model
- Left vs Right Model
- Left vs Other Model
- Right vs Other Model
- Up vs Down Model
- Up vs Other Model
- Down vs Other Model

The first pair classifies eye movements as either horizontal or vertical. This is used to decrease the number of options within the BCI menu. As shown in Figure 41, the other six pairs are used to either i) categorise the horizontal eye

movements as leftward or rightward eye movements ii) categorise the vertical eye movements as upward or downward eye movements or iii) through the use of the 'Others' class attempt to recover trials which are misclassified at the first tier. As shown in Figure 41, eye-movements labelled as 'Others' are passed onto the adjacent classifier within the second tier. The SVM models of these six pairs were modified with a Platt Scaling [75] as explained in the following section. With such a modification the SVM classifier is converted into a probabilistic classifier giving a probabilistic estimate of how much the EEG trial pertains to a specific class. This conversion is done to aid the SSVEP detection algorithm within the mixed hBCI as described later in Section 5.1.4.3.

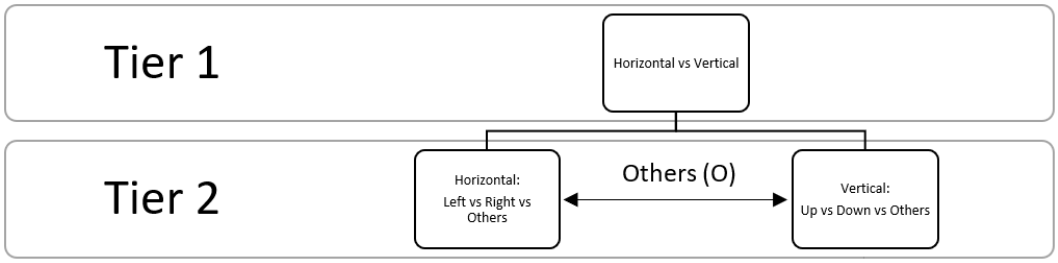

Figure 41: 2-Tiered Hierarchy for Eye-Movement Classification

Platt Scaling

From Section 4.1.4.3 the output of an SVM classifier for an i^{th} trial, x_i, is given by Equation 24:

$$y_i(x_i) = w^T \Phi(x_i) + b \tag{24}$$

The output of the SVM classifier, y_i is linearly transformed by A and B. The linearly transformed output is then passed to a sigmoid function as shown in Equation 25 [68]:

$$p_i = \frac{1}{1 + e^{Ay_i + B}} \tag{25}$$

The parameters A and B are found by minimising the binary cross-entropy cost function in Equation 26 [75].

$$(A, B) = \min_{A,B}\{-\sum_{i} \hat{t}_i log(p_i) + (1 - \hat{t}_i) log(1 - p_i)\} \tag{26}$$

$\hat{t}_i$ denotes the target variable of the i^{th} training example. Whereas for training the conventional SVM target variables had to be from the discrete set of $\{-1, 1\}$, for Platt's modification this had to be readjusted to the set $\{0, 1\}$. The rescaling is done as shown in Equation 27.

$$\hat{t}_i = \frac{t_i + 1}{2} \tag{27}$$

5.1.4.2 SSVEP Classification Algorithm

The filterbank canonical correlation analysis (FBCCA) [102] was used to process and classify the SSVEP-related EEG obtained from the user in the online experiments. The FBCCA algorithm consists of three major procedures: i) filterbank analysis; ii) CCA between SSVEP sub-band components and sinusoidal reference signals; and iii) target identification.

Filterbank Analysis

The EEG signal is decomposed into several sub-bands through the use of multiple band-pass filters with different pass-bands. Zero-phase Chebyshev type I infinite impulse response (IIR) filters were used as band-pass filters. Filtering was implemented using the 'filtfilt' method in the scipy Python package [53]. The design of the sub-bands in the filter bank was based upon a study by Chen et al. [102] since the bandwidth of stimulation frequencies used within the online experiments corresponded to that used within the study. The sub-bands covered multiple harmonic frequency bands. Each sub-band had a different lower cut-off frequency but they all shared the same upper cut-off frequency. The lower cut-off frequency of the n^{th} sub-band was set at $n\times$ 8Hz while the upper one was set at 88Hz. An additional bandwidth of 2Hz was added to both sides of the passband for each sub-band [102]. Table 5 tabulates the passband for each sub-band.

n^{th} Sub-band	Lower Cutoff Frequency, Hz	Upper Cutoff Frequency, Hz
1	6	90
2	14	90
3	22	90
4	30	90
5	38	90
6	46	90
7	54	90

Table 5: Filterbank Parameters

Canonical Correlation Analysis

A CCA is a statistical method which assesses the underlying relationship between two sets of variables [95]. The analysis seeks two sets of linear transformations, one for each set of variables, such that the correlation between the two sets of transformed variables is maximised. The transformed variables are also known as canonical variables.

Let the two sets of variables be represented as X and Y, their linear transformations denoted respectively as a^T and b^T while their respective canonical variables denoted as U and V. Their relation can be expressed mathematically in Equations 28 and 29:

$$U = a^T X \tag{28}$$

$$V = b^T Y \tag{29}$$

The objective of the CCA is to maximise the correlation between the two canonical variables by finding the appropriate linear transformations as represented in Equation 30 [42].

$$\max_{a,b} \rho(U, V) = \max_{a,b} \rho(a^T X, b^T Y) \tag{30}$$

Using theorems related to covariance and correlation [87], this can be expressed further as in Equation 31, where $\Sigma_{p,q}$ represents the covariance between p and q.

$$\max_{a,b} \rho(U,V) = \max_{a,b} \frac{a^T \Sigma_{XY} b}{\sqrt{a^T \Sigma_{XX} a}\sqrt{b^T \Sigma_{YY} b}} \tag{31}$$

For the purpose of this study, X was replaced by the EEG data obtained from a subject during a single trial, after it has been filtered by the filterbank. X was in the form of an $N_c \times T$ matrix where N_c represents the number of EEG channels making up the data and T denotes the number of samples within the epoch.

Y was replaced by reference signals. Sinusoidal and cosinusoidal signals at multiple harmonics of the target frequencies were considered as reference signals. Y was in the form of an $2N_h \times T$ matrix where N_h is the number of harmonic frequencies considered and T is the number of samples within the reference signals.

Target Identification

The CCA was executed for each target frequency present within the BCI and for each sub-band within the filterbank. The canonical correlations were stored in R, a matrix containing all the canonical correlation values for all the different target frequencies and sub-bands. R was of size $N_{sb} \times N_t$, where N_{sb} represents the number of sub-band components considered while N_t denotes the number of target frequencies present in the BCI.

A weighed sum of squares of the correlation values corresponding to all sub-band components was calculated as the feature for target identification as shown in Equation 32:

$$\tilde{\rho}_k = \sum_{n=1}^{N_{sb}} w(n) \cdot (R_{[n,k]})^2 \tag{32}$$

where n is the index of the sub-band and k is the target. According to the study carried out by Chen et al. [102], the weights for the sub-band components

were defined as in Equation 33:

$$w(n) = n^{-1.25} + 0.25 \qquad n \in [1, N_{sb}] \tag{33}$$

The predicted frequency of the SSVEPs, denoted by $\hat{k}$, is the target frequency with the maximal $\tilde{\rho}_k$.

$$\hat{k} = \arg\max_k \tilde{\rho}_k \tag{34}$$

5.1.4.3 Fusion Algorithm for the Mixed Hybrid BCI System

An algorithm was devised to fuse the predictions made by the eye-movement classification algorithm within the SSVEP-target identification algorithm for the mixed hybrid BCI. Specifically, Bayes' Theorem [55], represented as in Equation 35, was used as a basis for the fusion algorithm.

$$P(\omega_k|X) = \frac{P(X|\omega_k)P(\omega_k)}{P(X)} \tag{35}$$

X denotes the input, the EEG trial obtained from the user while ω_k denotes the class pertaining to target frequency k. By the law of total probability, $P(X)$ is further expressed as the total probability of all outcomes of X considering all possible classes/options present within the BCI, as shown in Equation 36.

$$P(X) = \sum_{j=1}^{N} P(X|\omega_j)P(\omega_j) \tag{36}$$

N denotes the total number of classes/options present within the BCI. Expressing $P(X)$ in the above form leads to the extended form of Bayes's Rule [60] as shown in Equation 37.

$$P(\omega_k|X) = \frac{P(X|\omega_k)P(\omega_k)}{\sum_{j=1}^{N} P(X|\omega_j)P(\omega_j)} \tag{37}$$

$P(\omega_k|X)$ is the posterior probability, the probability of a specific class ω_k given the input/EEG trial X. $P(X|\omega_k)$ is the class conditional distribution of X for class ω_k whereas $P(\omega_k)$ is the prior probability of class ω_k, the initial degree of belief in the class ω_k.

The prior probability is computed by the SVM classifier modified by Platt scaling. This is calculated directly from the Eye-Gaze algorithm described in Section 5.1.4.1. $P(X|\omega_k)$ is computed from the FBCCA algorithm. As stated by Equation 32 earlier, the FBCCA algorithm computes a correlation vector $\vec{\tilde{\rho}}$ of N elements quantifying the correlation between an EEG trial and the different N classes. The probability distribution of the correlation given the class is modeled to obtain a value for $P(X|\omega_k)$.

5.1.5 Performance Metrics used in Comparative Analysis

There are several measures that one may use to quantify the performance of BCI systems. The performance metrics described below are among those most commonly used [103] [12]. All of these methods have their limitations, but when combined together, they present a more complete picture. Combined together, performance metrics should be able to i) capture throughput, a combination of speed and system accuracy and ii) offer practicality, that is, providing a metric which is practicably communicable between various research groups [96].

5.1.5.1 Classification Accuracy Rate

The classification accuracy rate metric determines how often a correct selection is made by a BCI. In other words it computes the percentage of total selections that are correct. Although it is the most intuitive metric of BCI performance, this evaluation criterion does not account for speed. The classification accuracy can be computed as [89]:

$$P = \frac{N_c}{C_N} \tag{38}$$

where N_c and C_N denote the number of correct classifications and the total number of classified commands.

5.1.5.2 Information Transfer Rate

Information transfer rate (ITR), also known as bit rate, is a quantitative measure of the amount of information passing through a device or system per unit time. In addition to accuracy it takes into consideration the speed of the BCI system, giving a clearer picture of the system throughput. The ITR in bits/minute is calculated as [89]:

$$B = \log_2 N + P \log_2 P + (1 - P) \log_2 \frac{1 - P}{N - 1} \tag{39}$$

$$\text{ITR} = B \frac{C_N}{T} \tag{40}$$

where B represents the number of bits per trial and T denotes the length of the trial in minutes.

5.1.5.3 Efficiency

The efficiency metric is a measure of the efficiency of a BCI system. This evaluation criterion includes calculations for the cost of errors. The efficiency in terms of the actual time taken, t to complete a task, is calculated as [103]:

$$\eta = \frac{t_{max} - t}{t_{max} - t_{min}} \tag{41}$$

The minimum t_{min} and t_{max} time that a user could take to complete a task are computed by:

$$t_{min/max} = \kappa \times t_o \times \alpha \tag{42}$$

where κ denotes the number of commands required to complete a task, t_o represents the fixed time between two consecutive commands taken by the system to detect an SSVEP while α denotes the number of attempts taken by the user to execute the correct command.

5.2 Results and Discussion

This section presents the results of the comparative analysis of the three BCIs which were obtained as per the experimental procedures explained earlier in Section 5.1.3. Results pertaining to the offline analysis are first presented and discussed, followed by the results and discussion of the findings pertaining to the online analysis.

5.2.1 Offline Analysis

The results of the offline analysis are quantified in terms of the classification accuracy and ITR. Table 6 shows the performance across all subjects and the averaged results across all subjects. In the tabulated results, the performance of the SSVEP-based BCI, sequential hBCI and mixed hybrid BCI is compared and contrasted with each other. In addition, even though the EEG-based Eye-Gaze HCI does not utilise SSVEPs, its results are also considered within the offline comparison.

The highest classification accuracy obtained within the SSVEP-based BCI was that of 87.5% with a high ITR of 33.69 bpm. For the sequential hBCI, a high classification accuracy of 100% was achieved with a corresponding ITR of 40bpm, while for the mixed hBCI, the highest classification accuracy achieved was that of 75% with an ITR of 19.83 bpm. As for the EEG-based eye-gaze HCI, the highest performance obtained was with a classification accuracy of 41.67% and an ITR of 15.3bpm. On average, the best performance was achieved by the sequential hBCI with an average accuracy of 82.5% and an ITR of 19.06 bpm.

Method:	**SSVEP**		**Sequential Hybrid**		**Mixed Hybrid**			**EEG-based Eye-Gaze HCI**	
Metrics:	Accuracy (%)	ITR (bpm)	Accuracy (%)	ITR (bpm)	Accuracy (%)	ITR (bpm)		Accuracy (%)	ITR (bpm)
S01	83.33	30.11	91.67	31.36	75	19.83		41.67	15.3
S02	41.67	6.12	62.5	13.24	75	19.83		41.67	15.3
S03	87.5	33.69	100	40	70.83	17.47		41.67	15.3
S04	87.5	33.69	95.83	35.11	62.5	13.24		20.83	1.57
S05	45.83	7.75	62.5	13.24	37.5	3.88		16.67	0.42
Mean	**69.16**	**16.17**	**82.5**	**19.06**	**64.16**	**11.32**		**32.5**	**9.58**

Table 6: Performance Results of Offline Analysis Across all Subjects

With the exception of Subject 2, although differences in performance were noted, in general, subjects achieved their best performance when using the sequential hBCI. Conversely, Subject 2 obtained poor results with an SSVEP-based BCI and achieved their best performance when using the mixed hybrid BCI, thus emphasising the strength of this hBCI configuration when the SSVEP response of a subject is weak.

A considerable drop in performance was noted for the EEG-based Eye-Gaze HCI, indicating that the classification of EEG-based eye-movements, according to their visual angle extent, hinders the performance of an HCI system. In addition, the drop in performance attributes to the absence of SSVEP recognition techniques within the HCI.

A study was then conducted to assess how the performance of the BCIs vary with shorter stimulating periods. Figures 42, 43 and 44 portray how the classification accuracy of each BCI varies with the size of the stimulating period across subjects. As can be seen in Figure 42, in general, the classification accuracy of the SSVEP-based BCI monotonically decreases with the size of the stimulating period, reiterating that shorter stimulating periods typically result in a weaker SSVEP detection. However for the hybrid BCIs, performance was more consistent for some subjects across stimulating periods between 1.5 and 3s. Specifically, as can be seen in Figure 43, Subject 1 and Subject 3 achieved the same accuracy for the same stimulating periods when using the sequential hBCI. Similarly, as shown in Figure 44, Subject 5 achieved the same accuracy across stimulating periods between 2 and 3s when using the mixed hBCI. These results suggest that, relative to SSVEP-based BCIs, the classification accuracy of hybrid BCIs is less affected by the length of the stimulating period.

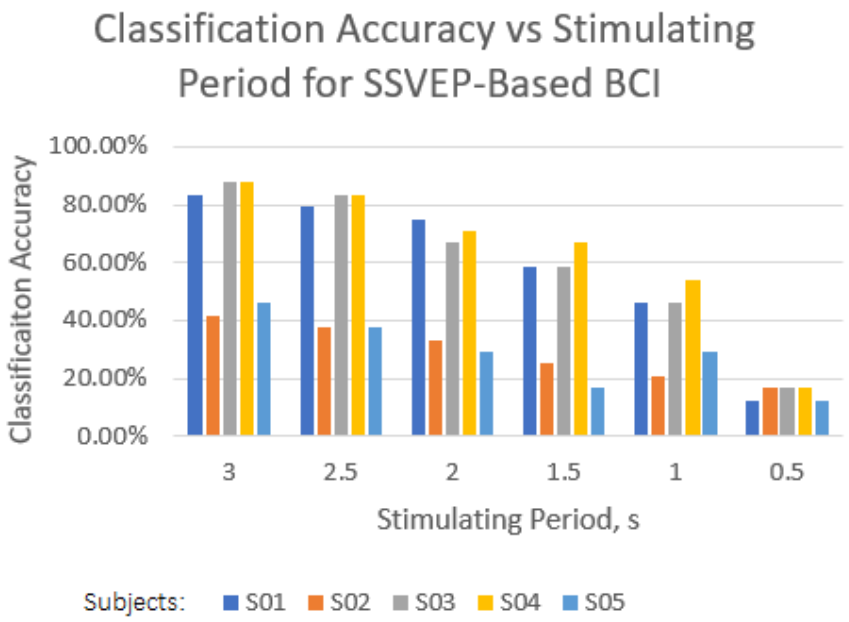

Figure 42: Classification Accuracy for Different Lengths of the Stimulating Period in the SSVEP-based BCI

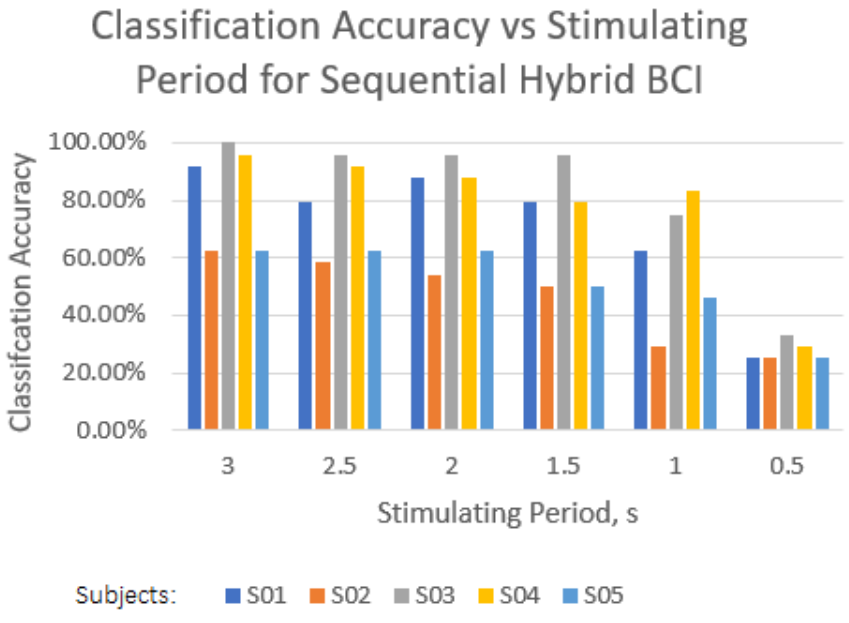

Figure 43: Classification Accuracy for Different Lengths of the Stimulating Period in the Sequential Hybrid BCI

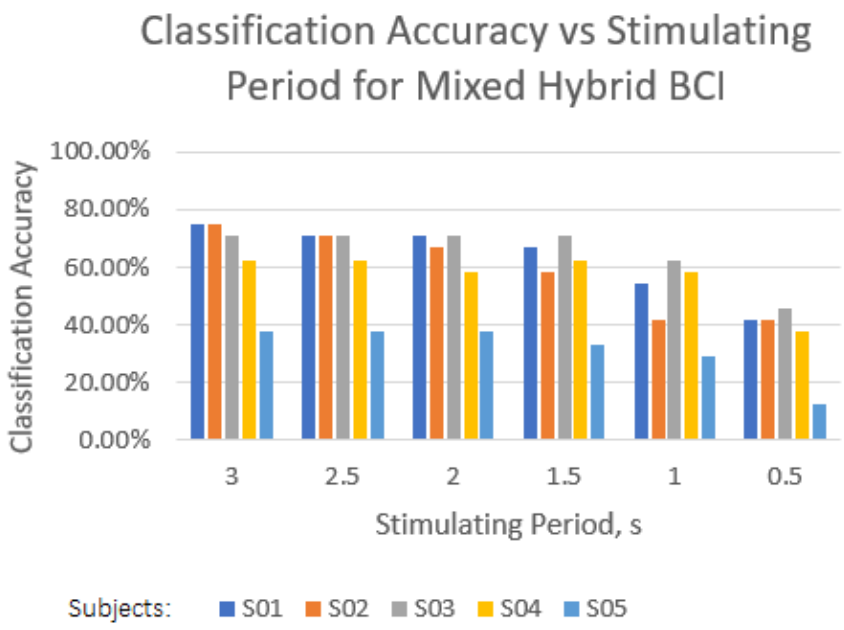

Figure 44: Classification Accuracy for Different Lengths of the Stimulating Period in the Mixed Hybrid BCI

Similarly, Figures 45, 46 and 47 illustrate how the ITR of each BCI varies with the length of the stimulating period across subjects. As for the accuracy, the ITR was also consistent for some subjects across stimulating periods, when using mixed hybrid BCIs. Specifically, as seen in Figure 47, Subject 1 and Subject 2 obtained the same performance across stimulating periods between 2.5 and 3s. As shown in Figure 46, the highest ITR was obtained by the sequential hBCI with an ITR at around 50bpm for a stimulating period of 1.5s, highlighting the advantages of this hBCI configuration at short stimulating periods.

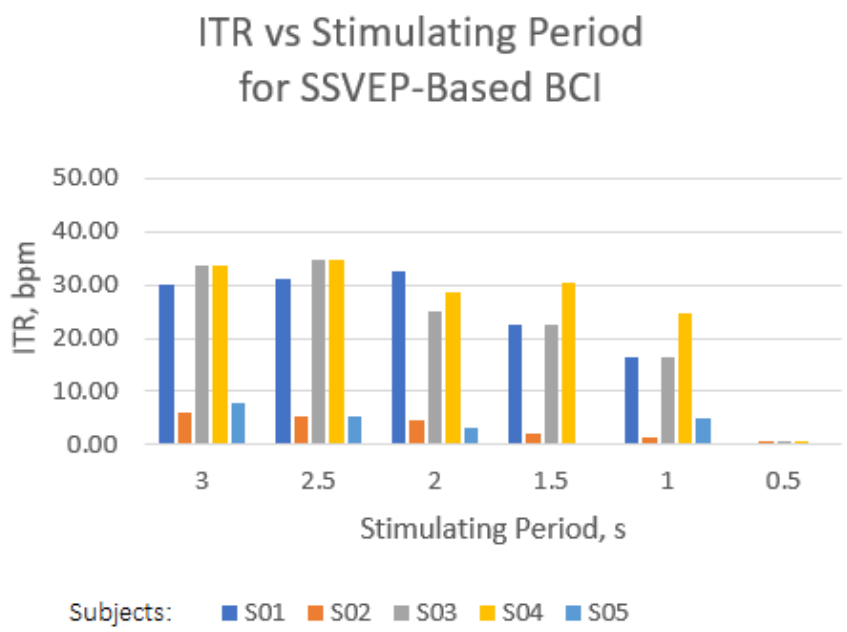

Figure 45: ITR for Different Lengths of the Stimulating Period in the SSVEP-based BCI

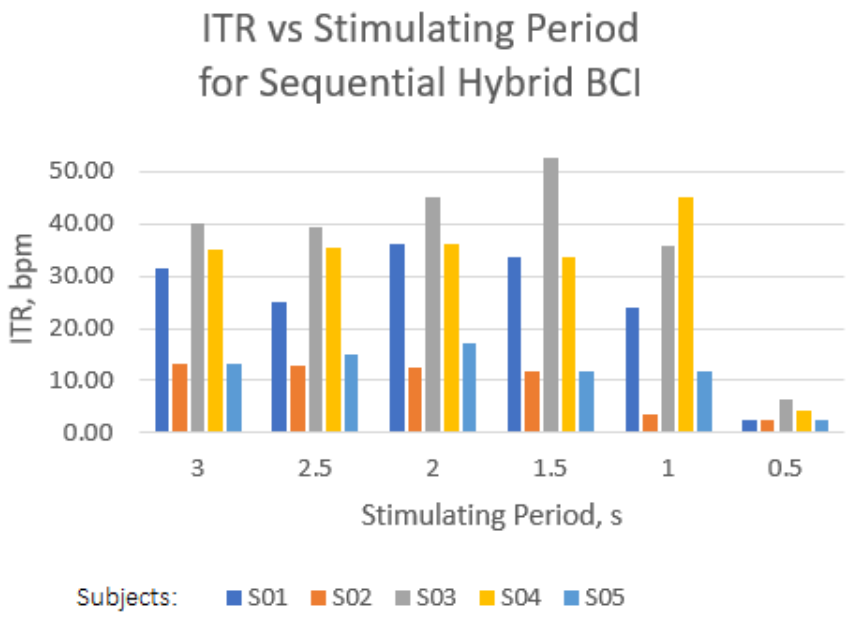

Figure 46: ITR for Different Lengths of the Stimulating Period in the Sequential Hybrid BCI

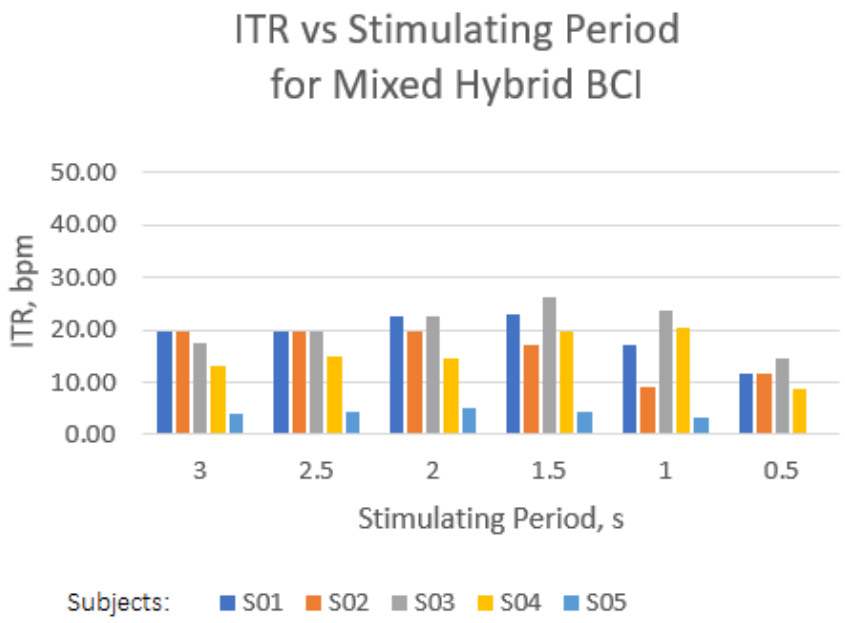

Figure 47: ITR for Different Lengths of the Stimulating Period in the Mixed Hybrid BCI

Figures 48 and 49 show the relation between the classification accuracy and ITR, respectively, and the stimulating period. As the stimulus flickering time is reduced from 3 seconds down to 1 second, the SSVEP-based BCI, the sequential hBCI and the mixed hBCI all display a reduction in accuracy, with the SSVEP-based BCI and the mixed hBCI suffering the highest and lowest reduction, respectively. It may also be noted that the sequential hBCI remains the best performing BCI throughout. With a stimulus period of 0.5s, the SSVEP is normally difficult to detect; therefore, it is not surprising that for this stimulus period, the mixed hBCI has the highest performance, albeit at around 35%, indicating that the strength of this hBCI configuration is mainly due to the separate eye-movement detection. Similarly, for this lowest stimulus period, the EEG-based Eye-Gaze HCI also outperformed the sequential hBCI and the SSVEP-based BCI.

With regard to the ITR, as the stimulus flickering time is reduced from 3 seconds down to 1 second, the performance of the SSVEP-based BCI decreases monotonically. Conversely, the ITR of the sequential hBCI and the mixed hBCI tend to remain steady, even exhibiting a slight increase, down to a stimulus period of 1.5 s, with a noticeable but small reduction at 1 s. As for the accuracy, the sequential hBCI always has the best ITR throughout. Similarly as for the accuracy, at a stimulus period of 0.5 s, both the SSVEP-based BCI and the sequential hBCI exhibit a large drop in ITR, and the mixed hBCI exhibits the highest ITR at a mere 9 bpm. The EEG-based Eye-Gaze HCI exhibits an ITR of 6bpm and, similar to the accuracy, for a stimulus period of 0.5s, the HCI outperforms the sequential hBCI and the SSVEP-based BCI.

From the classification accuracy and ITR results of the offline comparative analysis it was concluded that a stimulation period of 2s is optimal taking into consideration the performance achieved by all subjects. Hence for the online experiment, whose results are presented in the next section, the stimulating period was set to 2s.

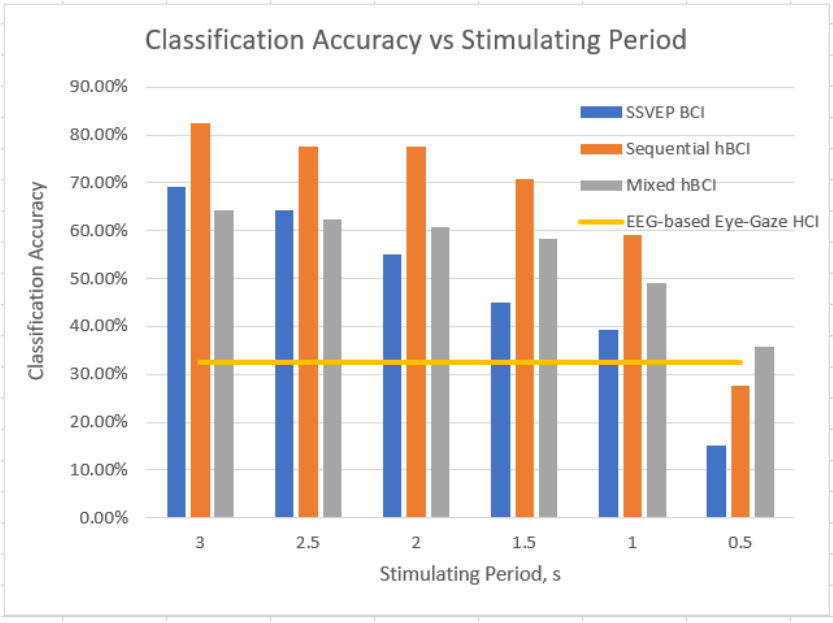

Figure 48: Classification Accuracies of Different BCI Architectures against Varying Stimulating Periods

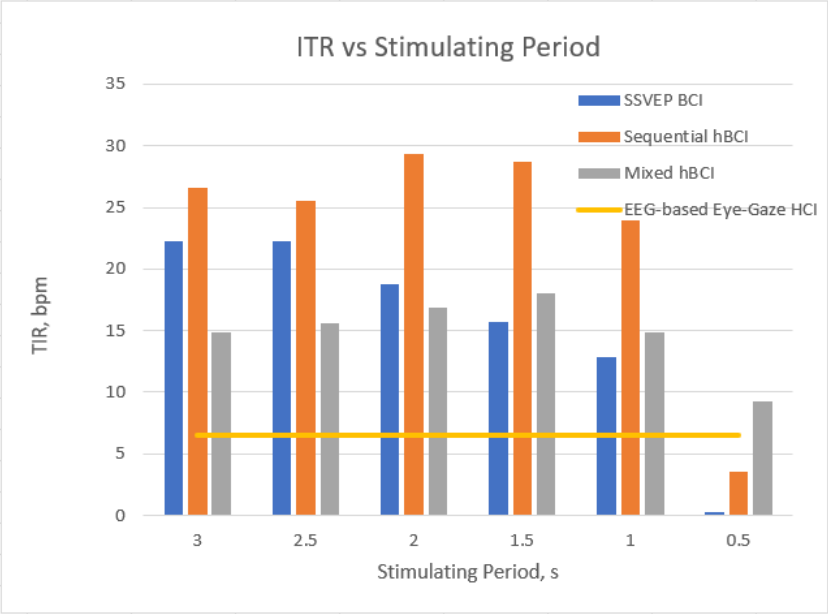

Figure 49: ITRs of Different BCI Architectures against Varying Stimulating Periods

5.2.2 Online Analysis

An online experiment was conducted to allow the subjects to operate the smart home BCI using either an SSVEP-based BCI architecture, a sequential hBCI architecture or a mixed hBCI architecture. In contrast with the offline analysis, apart from classification accuracy and ITR, the performance of the three smart home BCI systems is also quantified in terms of efficiency. As the online experiment grants each subject a number of attempts to complete a task, the efficiency evaluation criteria was introduced to take this number into consideration. Table 7 shows the performance results across all subjects and tasks and the averaged results across all subjects and tasks. A questionnaire was presented to the subjects after the experiment was conducted to obtain user feedback on the practicality of the smart home BCI.

Subject	***Task***	**SSVEP-Based BCI**			**Sequential Hybrid BCI**			**Mixed Hybrid BCI**		
		Acc. (%)	ITR (bpm)	Eff. (%)	Acc. (%)	ITR (bpm)	Eff. (%)	Acc. (%)	ITR (bpm)	Eff. (%)
S01	1	71.67	35.14	85.00	71.67	27.61	84.57	64.33	23.49	76.00
	2	60.00	19.77	75.00	91.67	42.78	95.67	45.00	9.06	54.33
	3	65.00	23.99	79.33	56.00	14.84	71.67	70.00	25.73	78.33
S02	1	19.00	1.02	36.00	50.33	12.03	62.67	19.83	1.17	35.67
	2	35.33	5.48	58.33	49.33	11.63	69.00	24.33	1.96	33.90
	3	17.50	2.51	29.33	34.67	5.39	53.67	30.00	4.21	36.37
S03	1	83.33	43.45	92.00	86.67	39.46	91.33	56.00	14.84	71.67
	2	83.33	43.45	92.00	91.67	42.78	95.67	42.00	7.51	50.00
	3	41.00	8.33	61.33	64.33	19.36	74.00	54.67	14.46	67.33
S04	1	71.67	35.14	85.00	83.33	34.14	91.33	78.33	30.82	87.00
	2	100.00	65.45	100.00	91.67	42.78	95.67	46.67	9.12	69.33
	3	91.67	54.45	96.00	75.00	29.05	82.67	54.67	14.46	67.33
S05	1	54.67	18.41	68.33	80.00	36.26	89.00	47.00	10.83	65.00
	2	65.00	23.99	79.33	86.67	39.46	91.33	27.67	2.77	47.00
	3	63.00	32.64	73.67	78.33	30.82	87.00	54.67	14.46	67.33
Mean		**61.48**	**27.55**	**74.04**	**72.76**	**28.56**	**82.35**	**47.68**	**12.32**	**60.04**

Table 7: Performance Results of Online Analysis

The highest classification accuracy obtained within the SSVEP-based smart home BCI was that of 87.8% with an ITR of 51.7 bpm and an efficiency of 93.7%. For the smart home sequential hBCI, the highest classification accuracy achieved was 82.5% while an ITR of 35.32bpm and an efficiency rating of 89.9% were obtained. For the smart home mixed hBCI, the highest classification accuracy achieved was that of 59.89%. The highest ITR was that of 19.43bpm and the highest efficiency rating was that of 74.6%. However, on average, the best performance was obtained with the smart home sequential hBCI with an average accuracy of 72.76%, an average ITR of 28.56 bpm and an efficiency rating of 82.35%.

Figure 50 portrays the results tabulated in Table 7 averaged across the tasks to illustrate the performance achieved by each subject for each BCI architecture on basis of classification accuracy, efficiency and ITR. With the exception of Subject 4, subjects achieved their best performance when using the sequential hybrid BCI. Furthermore, relative to the mixed hybird BCI, subjects achieved better results when using the SSVEP-based BCI. However, as can be seen in Figure 50a, Subject 2, who achieved poor results with an SSVEP-based BCI, achieved a slightly higher classification accuracy when using a mixed hybrid BCI, reiterating the advantages of hBCI configurations when the SSVEP response of a subject is weak.

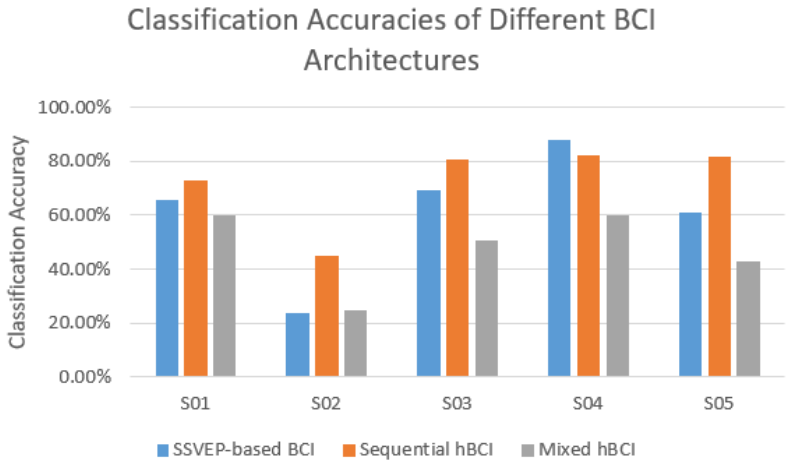

(a) Classification Accuracy for the Three Different BCI Architectures across Subjects

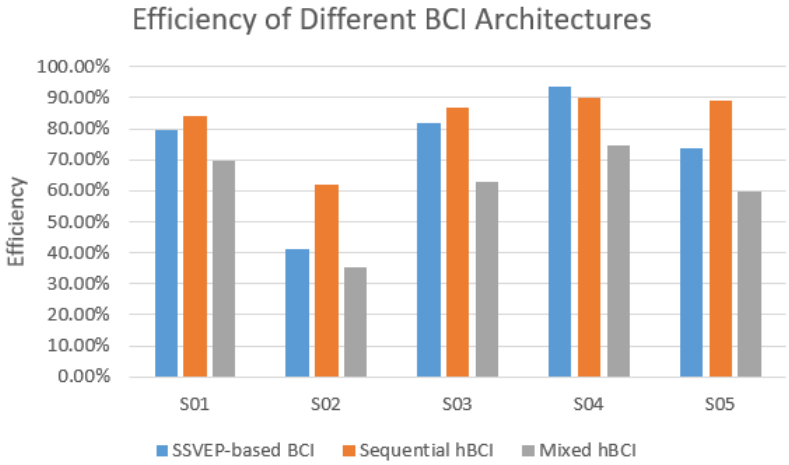

(b) Efficiency for the Three Different BCI Architectures across Subjects

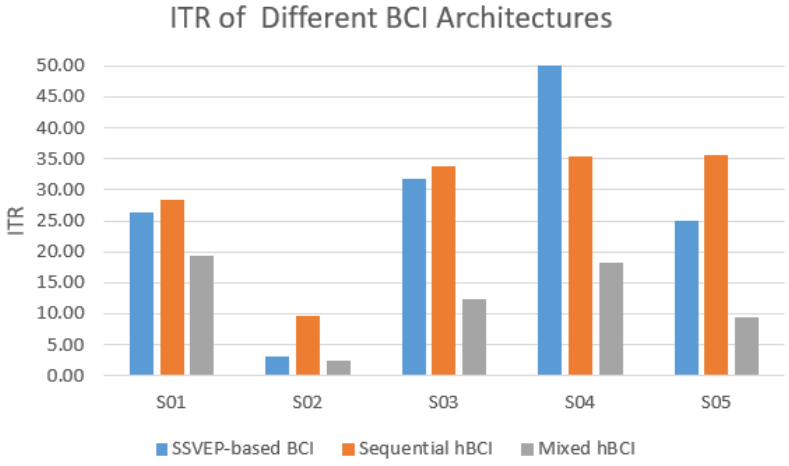

(c) ITR for the Three Different BCI Architectures across Subjects

Figure 50: Performance Metrics for the Three Different BCI Architectures across Subjects

Figures 51, 52 and 53 portray the classification accuracy, ITR and efficiency averaged across the subjects for each smart home BCI architecture. On average, the sequential hBCI outperformed the other two systems on the basis of accuracy, ITR and efficiency. The smart home sequential hBCI is 11.3% more accurate and 8.3% more efficient than the smart home SSVEP-based BCI. Pairwise t-tests were conducted and it was found that the differences between the two systems were significant (p-value < 0.01 for both metrics). In terms of ITR, a slight difference of 1bpm was found between the two, in favour of the smart home sequential hBCI. However, this was not found to be statistically significant. The smart home sequential hBCI exceeded the accuracy, efficiency and ITR of the mixed hBCI by 25.1%, 21.9% and 16.21 bpm respectively and the differences between these two smart home hybrid BCIs were also found to be statistically significant at the p < 0.01 level.

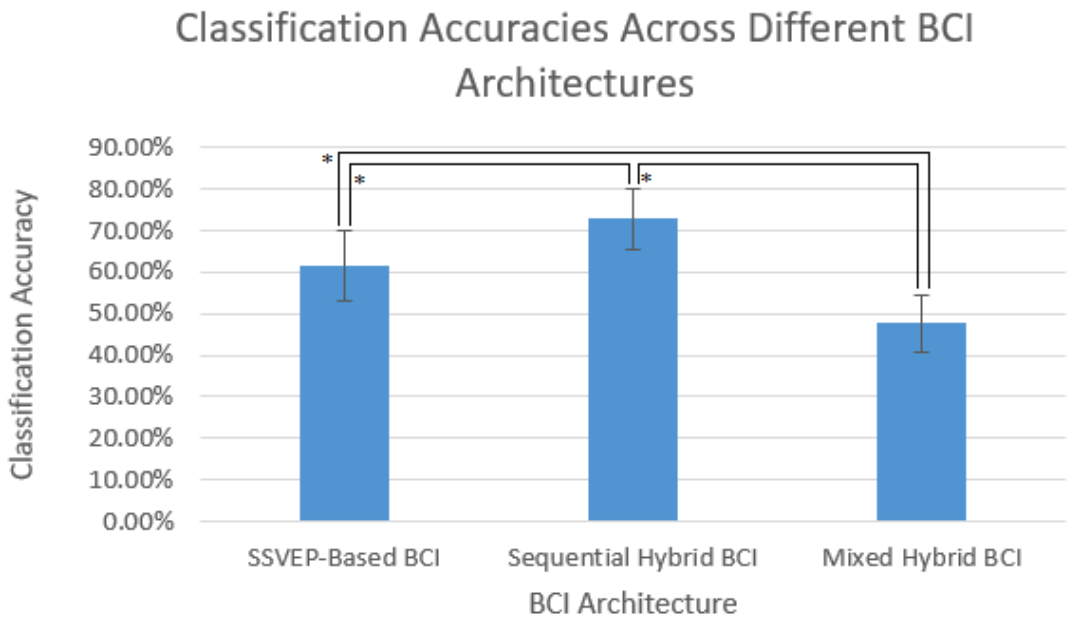

Figure 51: Averaged Classification Accuracies for the Three Different BCI Architectures. *Error bars represent a 95% confidence interval. Asterisks indicate significant difference between BCI architectures at the $p < 0.01$ level*

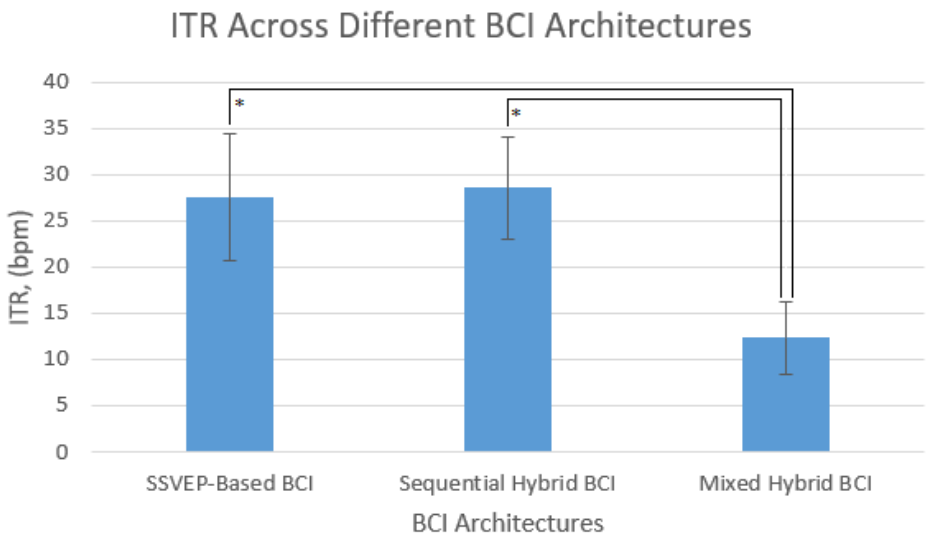

Figure 52: Averaged ITRs for the Three Different BCI Architectures. *Error bars represent a 95% confidence interval. Asterisks indicate significant difference between BCI architectures at the $p < 0.01$ level*

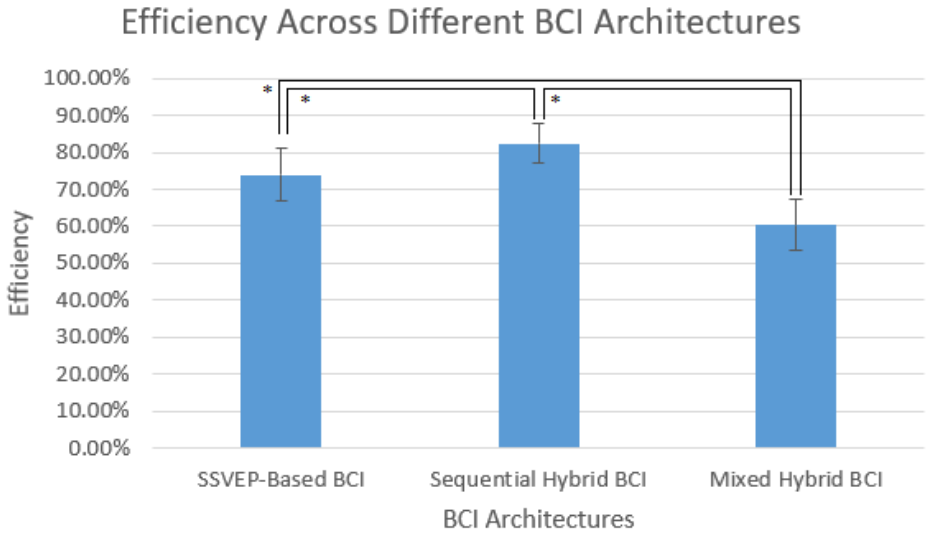

Figure 53: Averaged Efficiency Ratings for the Three Different BCI Architectures. *Error bars represent a 95% confidence interval. Asterisks indicate significant difference between BCI architectures at the $p < 0.01$ level*

5.2.2.1 User Feedback

After the online experiment, subjects were handed a brief questionnaire. These were examined to gain feedback from the experience of the subjects when using the smart home BCI application, providing a measure to compare and contrast the three systems in terms of user comfort and practicality. The first part of the questionnaire sought to find out how much the user felt in control when using the smart home BCI and whether the system was responding well to their intentions. The second part of the questionnaire investigated the user's perception of the system with regards to its annoyance factor, seeking to find to what extent, if any, did they find the system annoying, tiring or slow. The final part of the questionnaire sought to find out the user's opinion on the interface of the system and whether they found it adequate and easy to get accustomed to. The questions asked in the questionnaire were as follows:

Part 1

1. I could control the system with ease
2. I needed to concentrate significantly to control the system
3. False selections were often made by the system

Part 2

4. Flickering of the stimuli were annoying
5. Using the system is tiring
6. Time taken to make a selection is adequate

Part 3

7. The layout of the menu was adequate for easy operation of a smart home system
8. The layout of the menu was adequately organised for a smart home system
9. The Graphical User Interface (GUI) of the smart home system was easy to get used to

The first six questions were asked to the subjects three times, once for each BCI system. The last three questions were asked to the subjects once as they revolved around the design of the smart home system. A copy of the questionnaire can be found in Appendix C. For each question, the response of the subjects was measured on a Likert scale. A response of '5' indicated a strong agreement with the presented statement whereas a response of '1' indicated strong disagreement. A summary of the results observed for this questionnaire is shown in Figures 54, 55 and 56.

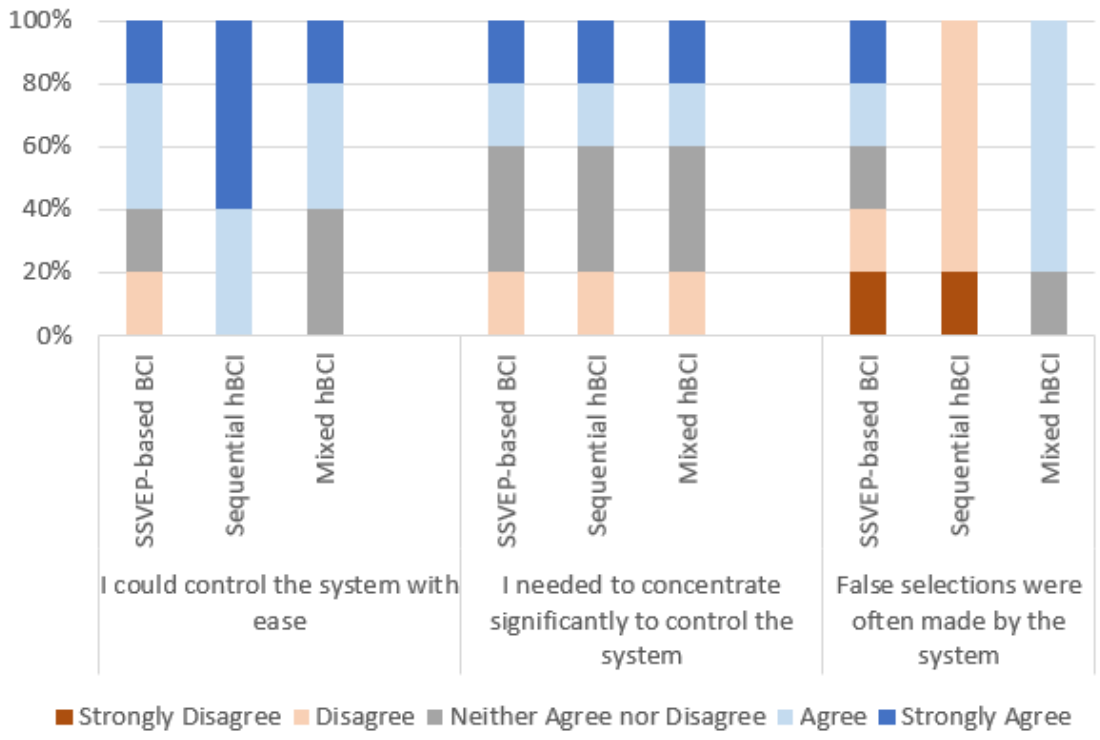

Figure 54: Summary of Questionnaire Results (Part 1)

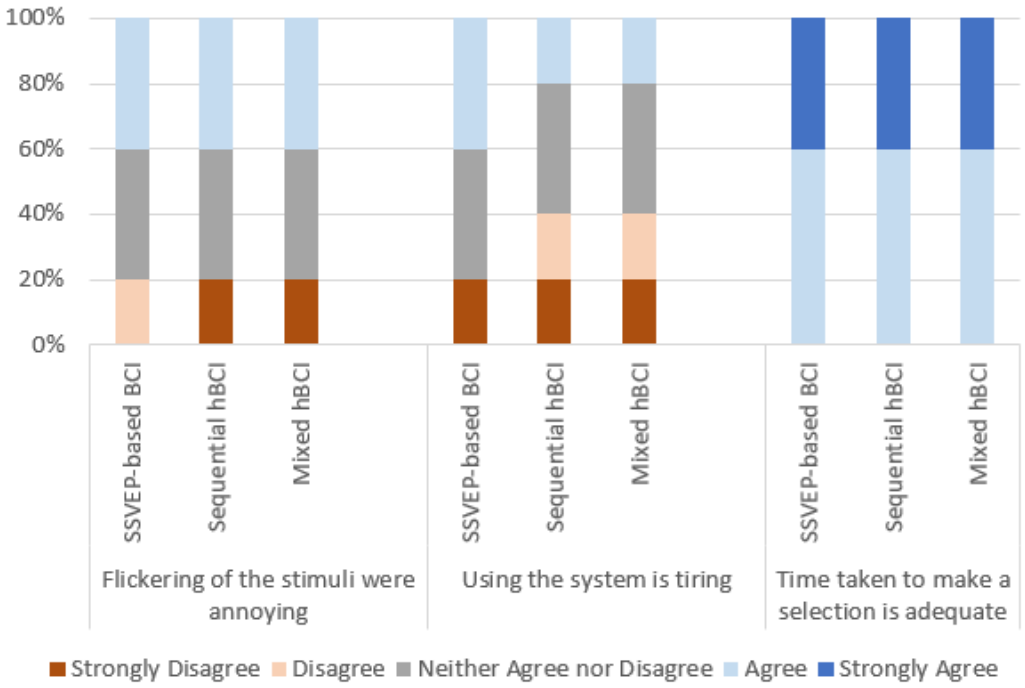

Figure 55: Summary of Questionnaire Results (Part 2)

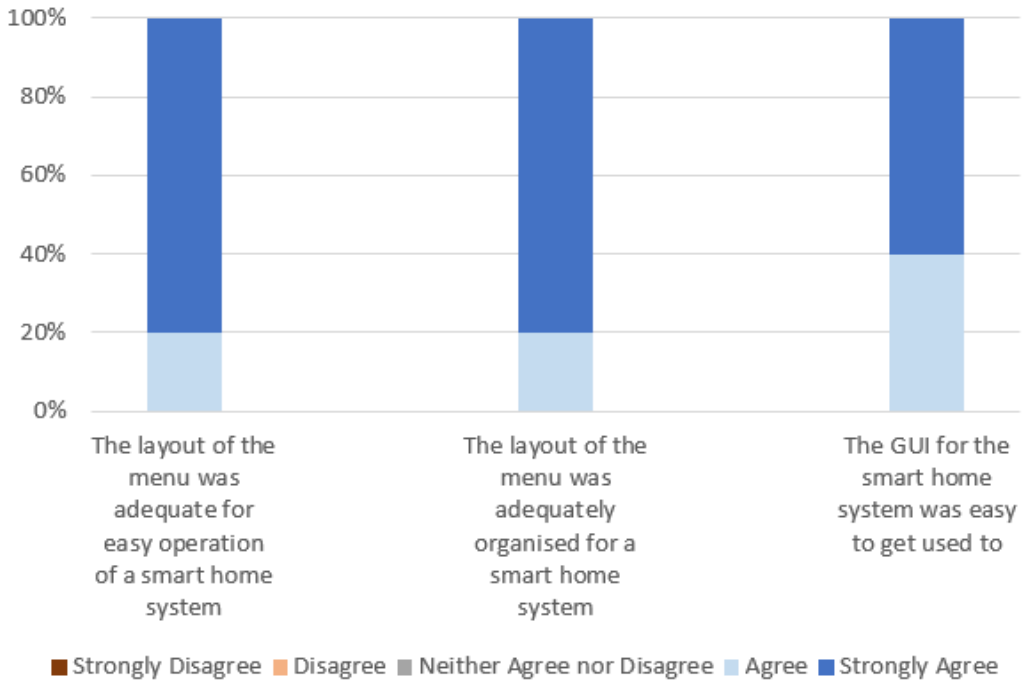

Figure 56: Summary of Questionnaire Results (Part 3)

Overall, users found the systems easy to control. The smart home sequential hBCI was reported as being the easiest to control. One user found it difficult to control the SSVEP-based BCI system and as shown within the first bar graph, disagreed with the first statement. In terms of concentration requirements, subjects found no difference between the three systems in general. Users perceived the sequential hBCI system as the least erroneous and the mixed hBCI as the most erroneous. This correlates with the quantitative results discussed earlier.

Users perceived the flickering stimuli of the hybrid systems to be less than that of the SSVEP-based BCI. This may be attributed to the fact that the hybrid systems makes use of four flickering stimuli instead of eight. In fact, users found the hybrid systems to be less tiring than the SSVEP-based BCI. Overall users agreed that the time taken to make a selection was appropriate for all systems. With regards to smart home system features, all subjects stated that the menu interface was easy to get used to and that it was adequate for a smart home system.

5.3 Chapter Summary

This chapter described the implementation of a smart home BCI specifying in detail both the hardware and software architecture of this system. The experimental protocols to test the smart home in both an SSVEP-based BCI topology and hybrid BCI topology were also described.

A comparative analysis of both the offline and online systems was presented taking into consideration the SSVEP based BCI, the sequential and mixed hybrid BCI and the EEG-based Eye-Gaze HCI. In the offline comparative analysis, performance results were obtained for varying stimulation periods and different HCI architectures. In the online analysis the performances of the different BCI architectures were compared on basis of accuracy, ITR and efficiency. Furthermore, it was concluded that a sequential hybrid BCI performs better than a conventional SSVEP-based BCI. Differences between the two systems were found to be

significant on basis of accuracy and efficiency. The results of a questionnaire also showed that the sequential hybrid BCI is better than an SSVEP-based BCI in terms of practicality and user comfort.

6 Conclusions and Future Work

The goal of this project was to design and implement a real-time smart home BCI which utilises EEG-extracted eye-movement potentials, in which the user can operate a system using neurosignals recorded non-invasively with an electroencephalogram (EEG). This chapter discusses the achievements related to this project, summarising the findings within this work. Some recommendations for future work are subsequently presented and discussed.

6.1 Achievements and Comparison with other SSVEP-based Smart Home BCI Applications

The first objective of this project was to study eye-movement detection from EEG. A thorough literature review was carried out on the extraction of eye-movement information for EEG data to explore the various electrode positions and signal processing techniques used in other studies. The literature review also focused on the processing techniques at each stage of the process including pre-processing, feature extraction and classification, where it was found out that a combination of CSP feature-extraction algorithms and SVM classifiers obtain the highest accuracy in eye-movement detection. Eye-movement-related EEG data was then acquired from five subjects in a data acquisition session. Features were extracted from the acquired data through the CSP algorithm, and fed to SVM classifiers to carry out an offline study. The study investigated into how many classes the EEG-extracted eye-movement potentials can be reliably classified. It was concluded that considering only frontal electrodes, eye movements can be classified into horizontal or vertical eye movements with an accuracy of 98.47% and also be classified into leftward, rightward, upward or downward eye movements with an accuracy of 74.38%. Furthermore, with an accuracy of 58.31% eye movements can be further classified into eight classes where the eight classes consists of leftward, rightward, upward and downward eye movements, with each direction having two visual angles. The study also determined to what extent can eye-movement information be extracted from the occipital lobe and it was shown

that eye-movement-related occipital signals can be categorised into horizontal or vertical eye movements with an accuracy of 76.67%. The study also sought to assess to what extent can eye movements in the same direction but different visual angles be classified, and it was concluded that leftward eye movements were categorised into a small or large visual angle with an accuracy of 70.83%. Similarly, rightward, upward and downward eye movements, were categorised by their visual angle with an accuracy of 68.06%, 52.5% and 50.97% respectively. The offline study also analysed how the classification accuracy varies with the number of frontal channels considered and how it varies with the size of the training set and it was concluded that three frontal channels and four training trials/class were sufficient to achieve a considerably high accuracy and hence be used within a hybrid architecture

The second objective of this project was to fuse the EEG-based eye-movement detection with an SSVEP-based BCI with the purpose of controlling a smart home environment, thus forming a real-time smart home hybrid BCI. Users of the smart home hybrid BCI could control four devices: a TV set, window blinds, a lamp and a fan. Users could toggle the power of a TV set and increase, decrease or mute the volume of the TV set. Users could also toggle the power of a fan or a lamp and could also open or close window blinds. The smart home system was based on the Home Assistant platform, an open-source home automation software, while the interface of the smart home BCI was programmed in Python. As the real-time smart home hybrid BCI was implemented from scratch, both Python and Home Assistant had to be learnt for the purpose of this project. Two hybrid architectures were designed for this project; a sequential hBCI and a mixed hBCI. User interaction with the hybrid systems was divided in two stages. In the first stage, users were first instructed to recentre their gaze and then look at the option they would like to choose. The options available to the user are then halved according to the type of eye-movement performed. In the second stage, as the remaining options/stimuli flicker, the user is instructed to focus on the icon which they had chosen previously in the first stage. The hybrid BCIs de-

veloped required a training session prior to the use of the smart home application which served to gather data to train the CSP and SVM models used to classify eye-movements. The two hybrid systems were compared with an SSVEP-based smart home BCI and the three architectures were compared on the basis of accuracy, ITR and efficiency. Best performance was obtained with the sequential hybrid BCI with an average classification accuracy of 72.76%, an average ITR of 28.56 bpm and an average efficiency of 82.35%, where the accuracy and efficiency of the SSVEP-based BCI and the sequential hBCI were found to be statistically significantly different. With regards to the other two architectures, an average classifcation accuracy of 47.68%, an average ITR of 12.32bpm and an average efficiency of 60.04% were obtained with the mixed hybrid BCI while an average classification accuracy of 61.48%, an average ITR of 27.55bpm and an efficiency of 74.04% were obtained with the SSVEP-based BCI.

In conclusion, an offline analysis was carried out to study eye-movement detection from EEG. On basis of this study, an innovative smart home brain controlled application based on SSVEPs and EEG-extracted eye-movement potentials has been developed in which the user has total control of the smart home. The conducted experimental tests showed a good and reliable performance of the smart home BCI system operating in real-time. The results also demonstrated the significant advantage of the sequential hybrid BCI over a conventional SSVEP-based BCI.

6.1.1 Comparison with Other SSVEP-based smart home BCIs

To the best of our knowledge, two other SSVEP-based smart home BCIs were found in the literature [82], [2]. The smart home BCI implemented by Saboor *et al.* [82] allows the user to control three different devices using a maximum of four simultaneously flickering stimuli. The other SSVEP-based smart home BCI implemented by Adams *et al.* [2] includes a smart home environment which is set up in a particular, fixed location and is specifically designed for a limited amount of

specific smart devices. Such a smart home environment is rigid leading to complications when installing new devices or replacing current ones. Additionally, adapting the smart home environment to a different home will also be challenging as it requires specific smart devices, resulting in a stringent number of homes eligible for such a smart home environment. Furthermore, the flickering stimuli of the system are distributed across three different screens.

The smart home BCI developed in this project has a maximum of eight simultaneously flickering stimuli all presented on one screen, allowing the user to control the smart home environment from a centralised point. Furthermore, in contrast with system implemented by Adams *et al.* [2], the smart home environment implemented in this system is designed around interface devices and not specific smart devices. Interface devices make conventional home appliances smart by making them operable by an alternative method other than conventional means. With the use of interface devices, the smart home environment facilitates the installation of new devices to the system. Furthermore, as interface devices are portable, lightweight and compatible with a wide range of conventional home appliances, the smart home environment can easily be adapted to any home.

6.2 Recommendations for Future Work

The proposed hBCI system currently entails two stages of user interaction when the system is run. First, users are expected to center their gaze and look at the option they would like to choose. The options are then halved according to the type of eye-movement performed. Then, while the remaining options/stimuli are flickering, users are expected to focus on the icon that they had previously chosen. In the first stage of user interaction, users are expected to center their gaze and look at the desired icon within a short time window of 1.5 seconds. If an eye-movement is not performed within that period, currently, the system would not recognise that no eye-movement was performed. Hence it would still attempt to process and classify the EEG recorded within the 1.5s period, producing an erroneous and invalid eye-movement classification result, and proceeding

to the second stage of user interaction where the flickering stimuli are presented unnecessarily. One future work would be to include a mechanism that checks whether an eye-movement is performed within the 1.5s period allocated for the user's eye-movement. Eye movements raise or lower the EEG potentials observed from the frontal region, and thus eye-movement-related activity can be detected by observing any spikes within the derivative of EEG signals acquired from this region. Observed spikes could then be compared against a pre-defined threshold to distinguish those induced by eye movements from those induced by other EEG artifacts. Should no eye-movement be detected, users are then instructed once again to center their gaze and perform an eye movement until an eye-movement is detected by the implemented mechanism.

One of the main challenges encountered within the design and development of BCI systems, especially when employed within a real-time scenario, is signal detection. Ideally the design and implementation of a practical BCI system should involve non-invasive sensors that are portable, wireless, relatively cheap while maintaining high signal quality, easy to set up and not susceptible to noisy environments and surroundings. The proposed smart home BCI system uses wet electrodes which requires electrolytic gel. To improve the practicality of the smart home BCI, an EEG acquisition system which uses dry electrodes and wireless headsets would be preferable. As this may result in poorer signal-to-noise ratio, the performance of the smart home BCI using such an EEG acquisition platform should be studied.

To improve the portability of the BCI system, the general purpose desktop PC or laptop would ideally be substituted by a small single-board computer. In a BCI system, a desktop PC is typically used for communicating with the EEG headset, acquiring the data from the same headset, processing it and performing a computational analysis to convert the processed neurosignals into a control signal for the application. Nowadays, single-board computers have high performance specifications given their relatively small size and can fulfill the role of the

desktop PC within a BCI system. Although single-board computers are typically not Windows-based systems, they can still communicate with EEG headsets, as most EEG headsets support communication via the LabStreamingLayer (LSL). LSL is a system used for synchronising streaming data for real-time analysis [29] and hence can be used to provide a communication link between an EEG headset like the OpenBCI system, and a single-board computer, like the Raspberry Pi. The latest model within the Raspberry Pi series includes a 1.5 GHz, quad-core 64-bit CPU endorsed with 8GB of SDRAM, all lying within a 97mm $\times$ 70mm $\times$ 25mm box. Although the performance specifications are slightly less than that of a desktop PC, the computational software of the BCI system proposed in this project can still be ported onto a single-board computer platform. A single trial within the proposed BCI system requires a computational time of 68ms when run on a 1.8GHz computer system. With a 1.5GHz computer system, it is estimated that the computational time would rise to approximately 80ms which is still an acceptable value for a real-time application [17]. This single-board computer can also be connected to two monitors, a keyboard and a mouse which can be used to program and even troubleshoot the BCI system when necessary. As it requires a 5V DC supply, this single-board computer can be battery-powered, making it more portable. In view that the proposed BCI system can be ported onto a single-board computer platform, one technological future work would be to embed the system on such a platform, as replacing the desktop PC with a single-board computer will decrease the overall cost of the BCI system by at least tenfold.

Appendix A

	Scalp Region		
	Combined	**Frontal**	**Occipital**
H vs V	98.61%	98.47%	71.11%
L vs R vs O	88.96%	89.17%	50.21%
U vs D vs O	74.40%	73.82%	53.40%
NL vs SL vs O	64.17%	70.83%	53.40%
NR vs SR vs O	65.42%	68.06%	46.25%
NU vs SU vs O	49.24%	52.50%	37.71%
ND vs SD vs O	47.78%	50.97%	37.08%

Table 8: Classification Accuracies of Seven Different Classifiers considering the Frontal and Occipital Regions Individually, as well as Both Regions Together

	Scalp Region		
	Combined	**Frontal**	**Occipital**
1st Tier	98.61%	98.47%	71.11%
2nd Tier	76.51%	74.38%	43.85%
3rd Tier	54.87%	58.31%	28.02%

Table 9: Accuracy Results at Each Tier of the Hierarhical Classifier considering the Frontal and Occipital Regions Individually, as well as Both Regions Together

	Scalp Region		
	Combined	**Frontal**	**Occipital**
H vs V	99.58%	99.58%	76.67%
L vs R vs O	91.53%	92.92%	60.56%
U vs D vs O	76.53%	72.92%	58.33%
L vs R vs U vs D	75.52%	73.75%	47.60%

Table 10: Classification Accuracies of Four Different Classifiers using only Trials with a Large Visual Angle while considering the Frontal and Occipital Regions Individually, as well as Both Regions Together

	Number of Frontal Channels Used			
	11	**7**	**5**	**3**
H vs V	99.58%	99.79%	99.58%	99.58%
L vs R vs O	92.92%	96.39%	93.19%	92.92%
U vs D vs O	72.92%	74.86%	79.03%	70.28%
L vs R vs U vs D	73.75%	76.77%	77.29%	80.21%

Table 11: Classification Accuracies of Four Different Classifiers when considering 3, 5, 7, or 11 Frontal Electrodes and considering Frontal Region only

	Amount of Frontal Channels Used			
	11	**7**	**5**	**3**
H vs V	99.58%	99.79%	99.79%	99.58%
L vs R vs O	91.53%	94.72%	91.11%	90.69%
U vs D vs O	76.53%	76.94%	80.42%	82.08%
L vs R vs U vs D	75.52%	79.27%	77.81%	79.27%

Table 12: Classification Accuracies of Four Different Classifiers when considering 3, 5, 7, or 11 Frontal Electrodes and jointly considering Frontal and Occipital Regions

	Training Trials/Class - Frontal		
	16	**8**	**4**
H vs V	99.58%	100.00%	100.00%
L vs R vs O	92.92%	89.44%	92.78%
U vs D vs O	70.28%	74.72%	68.33%
L vs R vs U vs D	80.21%	78.75%	79.17%

Table 13: Classification Accuracies of Four Different Classifiers Against Training Set Size of 16, 8 and 4 Trials/Class considering Frontal Region only

	Training Trials/Class - Combined		
	16	**8**	**4**
H vs V	99.58%	99.17%	97.50%
L vs R vs O	90.69%	87.78%	77.78%
U vs D vs O	82.08%	78.33%	72.22%
L vs R vs U vs D	79.27%	70.83%	64.58%

Table 14: Classification Accuracies of Four Different Classifiers Against Training Set Size of 16, 8 and 4 Trials/Class jointly considering Frontal and Occipital Regions

	Training Trials/Class - Occipital		
	16	**8**	**4**
H vs V	76.67%	74.58%	68.33%
L vs R vs O	60.56%	51.39%	43.89%
U vs D vs O	58.33%	53.89%	41.11%
L vs R vs U vs D	47.60%	42.50%	42.92%

Table 15: Classification Accuracies of Four Different Classifiers Against Training Set Size of 16, 8 and 4 Trials/Class considering Occipital Region only

Appendix B

Participant Consent Form

Research Study: Exploitation of EEG-Extracted Eye Movement for a Hybrid SSVEP Home Automation System

I, _____, hereby certify that I am over eighteen (18) years of age.

I give full consent to participate voluntarily in this research study entitled "Fusion of EEG-Extracted Eye Movement and SSVEP for a Home Automation System" and for the researcher, whose name and signature appear at the end of this form, to make the appropriate tests.

I understand that:

During this test session I will be asked to look at visual cues. During this time my eye movements will be recorded through electroencephalography (EEG) and an infra-red active eye gaze tracker. Electroencephalography will be acquired through EEG sensors which will either be placed around my forehead and at the back of my head using clinical gel and with an EEG cap.

The eye movement data obtained during the test session using EEG and the active eye gaze tracker will be stored, analysed, reported and/or published in a completely anonymous manner. My personal data, specifically age, sex, and type of vision, will be included with the recording of the data but since this will be anonymised there is no direct link to me. I thus understand that I will not be able to ask the researcher to remove my data from this study as it will not be known which data belongs to me.

Once this consent form is signed I will be given a copy. The original signed consent form will remain in possession of the researchers involved in this study. I can contact the researchers, whose contact details appear on this consent form, for

answers to pertinent questions about the research study and my rights as a research subject.

Clinical relevance of the eye movement data obtained is not considered pertinent to the experimental research being carried out through these tests. However, should any abnormality be detected, I understand that I will be informed.

The apparatus being used in these tests (conventional EEG setup, and eye gaze tracker) is entirely non-invasive and poses minimal risk of harm. Also, the tests that will be carried out as part of this research study are completely non-invasive and the probability and magnitude of harm or discomfort anticipated in the research are not greater than those ordinarily encountered in daily life or during the performance of routine physical or psychological examinations or tests. However, the researcher cannot be held liable for any accidental harm, physical or otherwise, that might result during the experiment.

In the event of a research-related injury, I understand that treatment will be given within the Government Health Services.

I confirm that all the details I have been instructed to provide and which will be stored with the eye gaze tracking data are, to the best of my knowledge, correct.

Since I am under no obligation to participate in this research study and am doing so voluntarily, I am free to withdraw from this research study at any time, even after having signed this consent form, without having to give any reason to the researcher involved in this research study.

Please fill in the following details in BLOCK letters where applicable:

_____	_____
Name	Surname
_____	_____
Signature of Test Subject	Date
_____	_____
Signature of Researcher	Id. No. of Researcher

Appendix C

Questionnaire

On a scale from 1 to 5 to what extent do you agree with the following statements? 1 indicates a strong disagreement and 5 indicates a strong agreement.

Smart Home SSVEP BCI (Method 1)

	1	2	3	4	5
I could control the system with ease	○	○	○	○	○
I needed to concentrate significantly to control the system	○	○	○	○	○
False selections were often made by the system	○	○	○	○	○
Flickering of the stimuli were annoying	○	○	○	○	○
Using the system is tiring	○	○	○	○	○
Time taken to make a selection is adequate	○	○	○	○	○

Smart Home Sequential Hybrid BCI (Method 2)

	1	2	3	4	5
I could control the system with ease	○	○	○	○	○
I needed to concentrate significantly to control the system	○	○	○	○	○
False selections were often made by the system	○	○	○	○	○
Flickering of the stimuli were annoying	○	○	○	○	○
Using the system is tiring	○	○	○	○	○
Time taken to make a selection is adequate	○	○	○	○	○

Smart Home Mixed Hybrid BCI (Method 3)

	1	2	3	4	5
I could control the system with ease	○	○	○	○	○
I needed to concentrate significantly to control the system	○	○	○	○	○
False selections were often made by the system	○	○	○	○	○
Flickering of the stimuli were annoying	○	○	○	○	○
Using the system is tiring	○	○	○	○	○
Time taken to make a selection is adequate	○	○	○	○	○

Smart Home Features

	1	2	3	4	5
The layout of the menu was adequate for easy operation of the system	○	○	○	○	○
The layout of the menu was adequately organised for a home automation system	○	○	○	○	○
The GUI for the home automation system was easy to get used to	○	○	○	○	○

References

[1] 10/20 System Positioning Manual. *http://chgd.umich.edu/*. Accessed: 2019-09-23.

[2] M. Adams, M. Benda, A. Saboor, A. F. Krause, A. Rezeika, F. Gembler, P. Stawicki, M. Hesse, K. Essig, S. Ben-Salem, et al. Towards an ssvep-bci controlled smart home. In *2019 IEEE International Conference on Systems, Man and Cybernetics (SMC)*, pages 2737–2742. IEEE, 2019.

[3] B. Z. Allison and J. A. Pineda. Erps evoked by different matrix sizes: implications for a brain computer interface (bci) system. *IEEE transactions on neural systems and rehabilitation engineering*, 11(2):110–113, 2003.

[4] Abdel Ilah N Alshbatat, Peter J Vial, Prashan Premaratne, and Le Chung Tran. Eeg-based brain-computer interface for automating home appliances. 2014.

[5] S. Amiri, R. Fazel-Rezai, and V. Asadpour. A review of hybrid brain-computer interface systems. *Adv. Hum. Comput. Interact.*, 2013.

[6] W. Arliss. Solving the svm: Stochastic gradient descent and hinge loss. *https://towardsdatascience.com/solving-svm-stochastic-gradient-descent-and-hinge-loss-8e8b4dd91f5b*. Accessed: 2019-10-16.

[7] M. Asadullah and A. Raza. An overview of home automation systems. In *2016 2nd International Conference on Robotics and Artificial Intelligence (ICRAI)*, pages 27–31. IEEE, 2016.

[8] C. Babiloni, V. Pizzella, C. Del Gratta, A. Ferretti, and G. Romani. Fundamentals of electroencefalography, magnetoencefalography, and functional magnetic resonance imaging. *International review of neurobiology*, 86:67–80, 2009.

[9] A.N Belkacem, H. Hirose, N. Yoshimura, D. Shin, and Y. Koike. Classification of four eye directions from eeg signals for eye-move-based commu-

nication system. *Journal of Medical and Biological Engineer*, 34:581–588, 2013.

[10] A.N. Belkacem, S. Saetia, K. Zintus-art, D. Shin, H. Kambara, N. Yoshimura, N. Berrached, and Y. Koike. Real-time control of a video game using eye-movements and two temporal eeg sensors. *Computational Intelligence and Neuroscience*, 2015.

[11] J. G. Betts. Anatomy & physiology.(2013). *Open Stax College*.

[12] G. Bin, X. Gao, Y. Wang, Y. Li, B. Hong, and S. Gao. A high-speed bci based on code modulation vep. *Journal of neural engineering*, 8(2):025015, 2011.

[13] R. Bin Sulaiman. *AI Based Chatbot: An Approach of Utilizing on Customer Service Assistance*. PhD thesis, 11 2019.

[14] Brunt. $https://www.brunt-nordic.com/en/product/bruntblindengine$. Accessed: 2020-04-09.

[15] S. R. Cherry. Fundamentals of positron emission tomography and applications in preclinical drug development. *The Journal of Clinical Pharmacology*, 41(5):482–491, 2001.

[16] H. S. Cho, J. Goo, D. Suh, K. Park, and M. Hahn. The virtual reality brain-computer interface system for ubiquitous home control. *AI 2006: Advances in Artificial Intelligence.*, pages 992–996, 01 1970.

[17] S. Choy, B. Wong, G. Simon, and C. Rosenberg. A hybrid edge-cloud architecture for reducing on-demand gaming latency. *Multimedia systems*, 20(5):503–519, 2014.

[18] Bishop C.M. *Pattern Recognition and Machine Learning*. Springer, 2006.

[19] D. Cohen. Magnetoencephalography: detection of the brain's electrical activity with a superconducting magnetometer. *Science*, 175(4022):664–666, 1972.

[20] G. G. Connell. Cursor control using eeg signals from eye movement potentials. *Suresnes, France: Les Laboratories Sevier Edition*, 2007.

[21] R. Corralejo, R. Hornero, and D. Alvarez. A domotic control system using brain-computer interface (bci). *International Work Conference on Artificial Neural Networks*, LNCS 6691:345–352, 2011.

[22] R. Corralejo, L. F Nicolás-Alonso, D. Álvarez, and R. Hornero. A p300-based brain–computer interface aimed at operating electronic devices at home for severely disabled people. *Medical & biological engineering & computing*, 52(10):861–872, 2014.

[23] D. F. Dansereau and D. D. Simpson. A picture is worth a thousand words: The case for graphic representations. *Professional Psychology: Research and Practice*, 40(1):104, 2009.

[24] D. De Venuto and G. Mezzina. User-centered ambient assisted living: Brain environment interface. *7th Mediterranean Conference on Embedded Computing*, 2018.

[25] G. Edlinger, C. Holzner, and C. Guger. A hybrid brain-computer interface for smart home control. *Hum. Comput. Interact. Interact. Tech. Environ*, 6762:417–426, 07 2011.

[26] Etekcity. *https* : *//www.etekcity.com/product/*100068. Accessed: 2020-04-09.

[27] J. Faller, G. Müller-Putz, D. Schmalstieg, and G. Pfurtscheller. An application framework for controlling an avatar in a desktop-based virtual environment via a software ssvep brain–computer interface. *Presence: teleoperators and virtual environments*, 19(1):25–34, 2010.

[28] R. Fazel-Rezai, B. Allison, C. Guger, E. Sellers, S. Kleih, and A. Kübler. P300 brain computer interface: Current challenges and emerging trends. *Frontiers in Neuroengineering*, 5:14, 2012.

[29] Swartz Center for Computational Neuroscience. Labstreaminglayer. `https://github.com/sccn/labstreaminglayer`.

[30] N. Gauci. *Phase-based SSVEPs for a Real-Time Brain Computer Interface*. PhD thesis, 09 2014.

[31] J. Gerhart. *Home Automation and Wiring*. Complete construction. McGraw-Hill, 1999.

[32] S. Geuter, M. Lindquist, and Tor D. Wager. Fundamentals of functional neuroimaging. *Cambridge Handbooks in Psychology*, 2017.

[33] A. A. Ghodake and S. D. Shelke. Brain controlled home automation system. *2016 10th International Conference on Intelligent Systems and Control (ISCO)*, pages 1–4, 2016.

[34] A. Gramfort, M. Luessi, E. Larson, D. A. Engemann, D. Strohmeier, C. Brodbeck, R. Goj, M. Jas, T. Brooks, L. Parkkonen, et al. Meg and eeg data analysis with mne-python. 7:267, 2013.

[35] A. Gramfort, M. Luessi, E. Larson, D. A. Engemann, D. Strohmeier, C. Brodbeck, L. Parkkonen, and M. S. Hämäläinen. Mne software for processing meg and eeg data. *Neuroimage*, 86:446–460, 2014.

[36] g.Tec. *http://www.gtec.at/*. Accessed: 2020-02-15.

[37] C. Guger, C. Holzner, C. Groenegress, G. Edlinger, and M. Slater. Control of a smart home with a brain-computer interface. *Brain-Computer Interface Workshop and Training Course*, 2008.

[38] S.S Gupta, S. Soman, P.G. Raj, R. Prakash, S. Sailaja, and R. Borgohain. Detecting of eye movements in eeg for controlling devices. *IEEE International Conference on Computational Intelligence and Cybernetics*, 2012.

[39] ElKamchouchi H. and ElShafee A. Design and prototype implementation of sms based home automation system. *2012 IEEE International Conference*

on Electronics Design, Systems and Applications (ICEDSA), pages 162–167, 2012.

[40] N.T. Hai, N.V. Trung, and Toi V.V. Mean threshold and arnn algorithms for identification of eye commands in an eeg-controlled wheelchair. *Scientific Research Engineering*, 5:284–291, 2013.

[41] M. R. Haji Samadi. *Eye Tracking with EEG life-style*. PhD thesis, 09 2015.

[42] N. E. Helwig. Canonical correlation analysis. *University of Minnesota (Twin Cities)*, 2017.

[43] M. J. Herrmann, E. Woidich, T. Schreppel, P. Pauli, and A. J. Fallgatter. Brain activation for alertness measured with functional near infrared spectroscopy (fnirs). *Psychophysiology*, 45(3):480–486, 2008.

[44] K. Hong and M. J. Khan. Hybrid brain-computer interface techniques for improved classification accuracy and increased number of commands: A review. *Frontiers in Neurorobotics*, 11:35, 2017.

[45] R. Hornero, R. Corralejo, D. Alvarez, and L. Martin. Design, development and assessment of a brain computer interface (bci) system applied to control domotic and electronic devices in order to improve the quality of life of people with severe disabilities. *Trauma Fund MAPFRE*, 24(2):117–125, 2013.

[46] C.H. Hsieh, H.P. Chu, and Y.H Huang. An hmm-based eye movement detection system using eeg brain-computer interface. *IEEE International Symposium on Circuits and System*, 2014.

[47] iMotions. $https://imotions.com/hardware/smi-red500/$. Accessed: 2020-02-15.

[48] Broadlink International. $https://www.ibroadlink.com/products/ir+rf$. Accessed: 2020-04-09.

[49] Arun Cyril J. and Reza M. Smart home automation security: a literature review. *SmartCR*, 5(4):269–285, 2015.

[50] A. F. Jackson and D. J. Bolger. The neurophysiological bases of eeg and eeg measurement: A review for the rest of us. *Psychophysiology*, 51(11):1061–1071, 2014.

[51] S.R.A. Jafri, T. Hamid, R. Mahmood, M.A. Alam, T. Rafi, M.Z. Ul Haque, and M.W. Munir. Wireless brain computer interface for smart home and medical system. *Springer Nature*, 2018.

[52] C. Jia, X. Gao, B. Hong, and S. Gao. Frequency and phase mixed coding in ssvep-based brain-computer interface. *IEEE Trans. Biomed. Eng*, 58:200–206, 2011.

[53] Eric Jones, Travis Oliphant, Pearu Peterson, et al. SciPy: Open source scientific tools for Python, 2001–.

[54] Shelton Jose and Kumar Gideon Praveen. Comparison between auditory and visual simple reaction times. *Neuroscience & Medicine*, 2010, 2010.

[55] J. Joyce. Bayes' Theorem. In *The Stanford Encyclopedia of Philosophy*. Metaphysics Research Lab, Stanford University, spring 2019 edition.

[56] T. Kaufmann, J. Williamson, E. Hammer, R. Murray-Smith, and A. Kübler. Visually multimodal vs. classic unimodal feedback approach for smr-bcis: a comparison study. *Int. J. Bioelectromagn*, 13:80–81, 2011.

[57] B. Kian, A.P. Bradley, and R. Cunnington. Effect of competing stimuli on ssvep-based bci. *33rd Annual International Conference of the IEEE*, 2011.

[58] N. Kosmyna, F. Tarpin-Bernard, N. Bonnefond, and B. Rivet. Feasibility of bci control in a realistic smart home environment. *Frontiers in Human Neuroscience*, 10, 2016.

[59] Nataliya Kosmyna, Franck Tarpin-Bernard, and Bertrand Rivet. Operationalization of conceptual imagery for bcis. In *2015 23rd European Signal Processing Conference (EUSIPCO)*, pages 2726–2730. IEEE, 2015.

[60] E. Kriegler. Updating under unknown unknowns: An extension of bayes' rule. *International Journal of Approximate Reasoning*, 50(4):583–596, 2009.

[61] R.Y.M Li, H.C.Y Li, C.K Mak, and T.B Tang. Sustainable smart home and home automation: Big data analytics approach. *International Journal of Smart Home*, 10(8):177–198, 2016.

[62] P. Manoilov. Eeg eye-blinking artifacts power spectrum analysis. *International Conference on Computer Systems and Technologies (CompSysTech)*, 3A:1 – 4, 2–6.

[63] M.H. Masood, M. Ahmad, M.A. Kathia, R.Z. Zafar, and A.N. Zahid. Brain computer interface based smart home control using eeg signal. *Sci.Int.(Lahore)*, 28:2219–2222, 2016.

[64] NabuCasa. $https://www.home-assistant.io$. Accessed: 2020-04-09.

[65] M. Nafea, A.A.B. Hisham, N.A. Abdul-Kadir, and F.K.C. Harun. Brainwave-controlled system for smart home applications. *2nd International Conference on BioSignal Analysis, Processing and Systems*, 2018.

[66] A. Nedaie and A. A. Najafi. Polar support vector machine: Single and multiple outputs. *Neurocomputing*, 171:118–126, 2016.

[67] Luis Fernando Nicolas-Alonso and Jaime Gomez-Gil. Brain computer interfaces, a review. *sensors*, 12(2):1211–1279, 2012.

[68] A. Niculescu-Mizil and R. Caruana. Predicting good probabilities with supervised learning. In *Proceedings of the 22nd international conference on Machine learning*, pages 625–632, 2005.

[69] A. Nijholt, D. Tan, G. Pfurtscheller, C. Brunner, J. Millán, B. Allison, B. Graimann, F. Popescu, B. Blankertz, and K. Müller. Brain-computer

interfacing for intelligent systems. *IEEE intelligent systems*, 23(3):72–79, 2008.

[70] J. Nolte. *The Human Brain in Photographs and Diagrams E-book*. Elsevier Health Sciences, 2013.

[71] R. Oostenveld and P Praamstra. The five percent electrode system for high-resolution eeg and erp measurements. *Clinical Neurophysiology*, 112:713–719.

[72] N. Padfield. *Development of a Hybrid Human Computer Interface System using SSVEPs and Eye Gaze Tracking*. PhD thesis, 09 2017.

[73] M. Pal and G. M. Foody. Feature selection for classification of hyperspectral data by svm. *IEEE Transactions on Geoscience and Remote Sensing*, 48(5):2297–2307, 2010.

[74] J. Peirce, J. R. Gray, S. Simpson, M. MacAskill, R. Höchenberger, H. Sogo, E. Kastman, and J. K. Lindeløv. Psychopy2: Experiments in behavior made easy. *Behavior research methods*, 51(1):195–203, 2019.

[75] J. Platt. Probabilistic outputs for svms and comparisons to regularized likehood methods, advances in large margin classifiers, 1999.

[76] B. Poczos. Introduction to Independent Component Analysis. *https://www.cs.cmu.edu/ bapoczos/other_presentations/ICA.pdf*. Accessed: 2019-09-23.

[77] H. Ramoser, J. Muller-Gerking, and G. Pfurtscheller. Optimal spatial filtering of single trial eeg during imagined hand movement. *IEEE transactions on rehabilitation engineering*, 8(4):441–446, 2000.

[78] RaspberryPi. *https://www.raspberrypi.org/products/raspberry − pi3B+*. Accessed: 2020-04-09.

[79] E. Ratti, S. Waninger, C. Berka, G. Ruffini, and A. Verma. Comparison of medical and consumer wireless eeg systems for use in clinical trials. *Frontiers in human neuroscience*, 11:398, 2017.

[80] D. Regan. Steady-state evoked potentials. *Journal of the Optical Society of America*, 67:1475–1489, 1977.

[81] D. Rye. My life at x10. *AV and Automation Industry*, January 1999.

[82] A. Saboor, A. Rezeika, P. Stawicki, F. Gembler, M. Benda, T. Grunenberg, and I. Volosyak. Ssvep-based bci in a smart home scenario. *Springer International Publishing AG*, (2):474–485, 2017.

[83] J. W. Salatino, K. A. Ludwig, T. D.Y. Kozai, and E. K. Purcell. Glial responses to implanted electrodes in the brain. *Nature biomedical engineering*, 1(11):862–877, 2017.

[84] Riitta Salmelin, M Hámáaláinen, M Kajola, and R Hari. Functional segregation of movement-related rhythmic activity in the human brain. *Neuroimage*, 2(4):237–243, 1995.

[85] M. Reza H. Samadi, Z. Zakeri, and N. Cooke. Vog-enhanced ica for removing blink and eye-movement artefacts from eeg. In *2016 IEEE-EMBS International Conference on Biomedical and Health informatics (BHI)*, pages 603–606. IEEE, 2016.

[86] D. Saravanakumar and M. Ramasubba Reddy. A visual keyboard system using hybrid dual frequency ssvep based brain computer interface with vog integration. 2018.

[87] G.A.F. Seber and A.J. Lee. *Linear Regression Analysis*. Wiley Series in Probability and Statistics. Wiley, 2012.

[88] C. W. Sem-Jacobsen, M. C. Petersen, H. W. Dodge Jr, J. A. Lazarte, and C. B. Holman. Electroencephalographic rhythms from the depths of the parietal, occipital and temporal lobes in man. *Electroencephalography and clinical neurophysiology*, 8(2):263–278, 1956.

[89] P. Stawicki, F. Gembler, A. Rezeika, and I. Volosyak. A novel hybrid mental spelling application based on eye tracking and ssvep-based bci. *Brain Sciences*, 4, 2017.

[90] P. Stawicki, F. Gembler, and I. Volosyak. A user-friendly dictionary-supported ssvep-based bci application. In *International Workshop on Symbiotic Interaction*, pages 168–180. Springer, 2016.

[91] M. Stein, T. R. Kaufman, Y. A.r Richarz, K. A. Tarlow, and B. C. Nesbitt. User interface for home automation system, October 31 2000. US Patent 6,140,987.

[92] W.S. Stiles and B.H. Crawford. Luminous efficiency of rays entering the eye pupil at different points. *Nature*, 139:246, 1937.

[93] S. Suleri. Using brain-computer interfaces to interact with a smart home environment. Master's thesis, 01 2017.

[94] M. Teplan. Fundamentals of eeg measurement. *Measurement science review*, 2(2):1–11, 2002.

[95] B. Thompson. Canonical correlation analysis. *Encyclopedia of statistics in behavioral science*, 2005.

[96] D. Thompson, S. Blain-Moraes, and J. Huggins. Performance assessment in brain-computer interface-based augmentative and alternative communication. *Biomedical engineering online*, 12:43, 05 2013.

[97] PD Thompson, JG Colebatch, P Brown, JC Rothwell, BL Day, JA Obeso, and CD Marsden. Voluntary stimulus-sensitive jerks and jumps mimicking myoclonus or pathological startle syndromes. *Movement disorders: official journal of the Movement Disorder Society*, 7(3):257–262, 1992.

[98] A. Ubeda, E. Ianez, J. M. Azorin, J. M. Sabater, and E. Fernandez. Classification method for bcis based on the correlation of eeg maps. *Neurocomputing*, 114:98–106, 2013.

[99] G. Van. *Python Library Reference*. 01 2006.

[100] N. Vikram, K. S. Harish, M. S. Nihaal, R. Umesh, and S. A. A. Kumar. A low cost home automation system using wi-fi based wireless sensor network incorporating internet of things (iot). *2017 IEEE 7th International Advance Computing Conference (IACC)*, pages 174–178, 2017.

[101] H. Wang and A. Bezerianos. Brain-controlled wheelchair controlled by sustained and brief motor imagery bcis. *Electronics Letters*, 53(17):1178–1180, 2017.

[102] Chen X., Wang Y., Gao S., Jung T., and Gao X. Filter bank canonical correlation analysis for implementing a high-speed SSVEP-based brain–computer interface. *Journal of Neural Engineering*, 12(4):046008, jun 2015.

[103] R. Zerafa. *SSVEP-based Brain Computer Interface (BCI) System for a Real-Time Application*. PhD thesis, 11 2013.

[104] Y. Zhang, P. Xu, T. Liu, J. Hu, R. Zhang, and D. Yao. Multiple frequencies sequential coding for ssvep-based brain-computer interface. *PLoS One*, 7, 2012.